Plasma Physics and Fusion

Todd H. Rider thor@riderinstitute.org 13 November 2019

Any suggestions for improvements would be greatly appreciated.

> Resembling fire or the sun, made of costly materials... it measured three cubits and six feet. Endued with the force of the thousand-eyed Indra's thunder... it was exceedingly terrible and destructive of all living creatures. Partha cheerfully took up that great weapon, in the shape of an arrow, which could not be resisted by the very gods... Thus sped by that mighty warrior, that shaft endued with the energy of the sun caused all the points of the compass to blaze up with light.
>
> –Karna Parva, Chapter 91

> Then Drona's son, aiming at the host of the Pandavas and the Panchalas, invoked the weapon called *Narayana*... Shafts, O king, like the very rays of the sun in a moment shrouded all the points of the compass, the sky, and the troops... That weapon became exceedingly powerful. Slaughtered by the *Narayana* weapon, as if consumed by a conflagration, the Pandava troops were exceedingly afflicted all over the field in that battle. Indeed, O lord, as fire consumes a heap of dry grass in summer, even so did that weapon consume the army of the Pandus. Beholding that weapon filling every side, seeing his own troops destroyed in large numbers, king Yudhishthira the just, O lord, became inspired with great fright.
>
> –Drona Parva, Chapter 200
> *Mahabharata* (ca. 400 B.C. - 400 A.D.)

Overview

When a gas is heated enough, its atoms acquire sufficient energy that they separate into their component nuclei (or ions) and electrons, forming a plasma. The electrically charged ions and electrons interact with each other and with external electromagnetic fields, exhibiting several categories of phenomena: individual-particle effects, diffusion or transport of a population of particles, magnetohydrodynamics, and waves. The main application of plasma physics is nuclear fusion. Small nuclei can release large amounts of energy when they fuse to form larger nuclei, but in order to overcome the Coulomb repulsion between them, they must have very high kinetic energies, or in other words form a high-temperature plasma. Fusion reactions occur naturally in stars and can also be triggered in thermonuclear explosive devices. Long-term research has striven to develop electric power plants using inertial confinement fusion (miniature thermonuclear explosions) or magnetic confinement fusion. A different application of plasma physics is designing particle accelerators.

Contents

1 Some General Properties of Plasmas **3**
1.1 Basic Equations for Modeling Plasmas . . . 3
1.2 Debye Length and Plasma Frequency . . . 5
1.3 Bremsstrahlung . . . 8
1.4 Cyclotron Motion and Related Effects . . . 9
1.5 Fusion Reactions . . . 14

2 Transport **16**
2.1 Velocity-Space Transport: Like-Particle Collisions . . . 16
2.2 Velocity-Space Transport: Unlike-Particle Collisions . . . 19
2.3 Classical Spatial Diffusion . . . 20
2.4 Neoclassical Spatial Diffusion . . . 23

3 Magnetohydrodynamics (MHD) **29**
3.1 MHD Equations . . . 29
3.2 Sausage Instability . . . 32
3.3 Kink Instability . . . 34
3.4 Rayleigh-Taylor and Flute Instabilities . . . 35

4 Waves in Plasmas **38**
4.1 Electrostatic Electron Waves . . . 38
4.2 Electrostatic Ion Waves . . . 40
4.3 Electromagnetic Electron Waves . . . 42
4.4 Electromagnetic Ion Waves . . . 46

5 Stellar Fusion **47**
5.1 Hydrostatic Equilibrium . . . 47
5.2 Energy Transport . . . 49
5.3 Fusion Reactions and Power . . . 53
5.4 Stellar Evolution . . . 56
5.5 Observational Data on Stars . . . 58

6 Inertial Confinement Fusion **61**
6.1 Basic Designs . . . 61
6.2 ICF Conditions . . . 64
6.3 Requirements for ICF Energy Gain . . . 68

7 Magnetic Confinement Fusion **71**
7.1 Open Magnetic Field Geometries . . . 71
7.2 Closed Magnetic Field Geometries . . . 73
7.3 Engineering Considerations . . . 78

8 Particle Accelerators **79**
8.1 Particle Acceleration Methods . . . 79
8.2 Particle Beam Focusing and Maintenance . . . 82

1 Some General Properties of Plasmas

This section will introduce some key equations used to model plasmas [1]-[4], then cover basic plasma phenomena such as Debye shielding, the plasma frequency, bremsstrahlung, cyclotron motion, and fusion reactions. This summary uses mks units unless otherwise noted; where equations are reduced to practical numerical values, the units of the input variables are given as subscripts.

1.1 Basic Equations for Modeling Plasmas

The simplest approach to plasma physics is to consider a typical particle with mass m, charge q, and velocity v in the plasma. From electromagnetism, an electric field $\mathbf{E}$ and magnetic field $\mathbf{B}$ will exert a Lorentz force $\mathbf{F} = q(\mathbf{E} + \mathbf{v} \times \mathbf{B})$ on the particle, so the particle's equation of motion is

$$m\frac{d\mathbf{v}}{dt} \;=\; \mathbf{F} \;=\; q(\mathbf{E} + \mathbf{v} \times \mathbf{B}) \;. \tag{1}$$

This single-particle approach will prove useful for calculating effects such as cyclotron motion.

A more general approach is to consider the plasma as a collection of particles with a distribution of positions $\mathbf{x}$ and velocities $\mathbf{v}$ given by some function $f_j(\mathbf{x}, \mathbf{v}, t)$, where j denotes the particle species. Usually only two particle species are considered–ions i and electrons e. In some cases, it is necessary to be more accurate by treating two fusion fuel ion species (e.g., deuterium and helium-3) separately or by explicitly including fusion products as additional particle species.

The total time derivative of f_j may be expressed as the sum of partial derivatives with respect to the variables t, $\mathbf{x}$, and $\mathbf{v}$ on which f_j depends:

$$\left[\frac{\partial}{\partial t} + \frac{d\mathbf{x}}{dt}\cdot\frac{\partial}{\partial \mathbf{x}} + \frac{d\mathbf{v}}{dt}\cdot\frac{\partial}{\partial \mathbf{v}}\right] f_j \quad = \quad \frac{df_j}{dt} \;, \quad \text{or}$$

$$\left[\frac{\partial}{\partial t} + \mathbf{v}\cdot\frac{\partial}{\partial \mathbf{x}} + \mathbf{a}\cdot\frac{\partial}{\partial \mathbf{v}}\right] f_j \quad = \quad \left(\frac{\partial f_j}{\partial t}\right)_{\text{col}} \qquad \textbf{Fokker-Planck equation}, \tag{2}$$

$$\text{where} \quad \mathbf{a} \;\equiv\; \frac{q}{m}(\mathbf{E} + \mathbf{v} \times \mathbf{B}) \quad \text{from Eq. (1).}$$

Equation (2) is called the Boltzmann equation by everyone except plasma physicists, who call it the Fokker-Planck equation just be different. The left side of Eq. (2) accounts for all effects except collisions between the particles, so collisions are the only thing that can affect the total time derivative on the right side. The collision operator $(\partial f_j/\partial t)_{\text{col}}$ accounts for both collisions among the same particle species j and collisions with the other species. It may be explicitly written as a complicated integral involving the particle distributions, but calculations with it are very nasty [5, 6, 7]. If collisions may be neglected, $(\partial f_j/\partial t)_{\text{col}} = 0$, Eq. (2) is called the **Vlasov equation**.

As will be shown in Section 2, collisions within a particle species have a much stronger effect on the particle distributions than collisions between different particle species. Like-particle collisions create a velocity distribution that is in thermal equilibrium, so from statistical physics:

$$f_j \;\propto\; \exp\left(-\frac{E_j}{k_B T_j}\right) \;\propto\; \exp\left(-\frac{m_j v_j^2}{2k_B T_j}\right) \;, \quad \text{or}$$

$$f_j(\mathbf{v}) \;=\; \frac{n}{(\sqrt{2\pi} v_{tj})^3}\; \exp\left[-\frac{(\mathbf{v} - \mathbf{v_{oj}})^2}{2v_{tj}^2}\right] \qquad \textbf{Maxwellian velocity distribution (see Fig. 1)} \tag{3}$$

E_j is the average particle energy, $k_B = 1.3807 \times 10^{-23}$ J/^{o}K is the Boltzmann constant, T_j is the temperature, and $v_{tj} \equiv \sqrt{k_B T_j/m_j}$ is the **thermal velocity**. (Note that some other authors include a $\sqrt{2}$ in the definition of v_t.) In Eq. (3), the distribution has been generalized in case the particle velocities are centered about a nonzero average velocity $\mathbf{v_{oj}}$. The distribution has also been normalized so that integration over all velocities yields the particle density n.

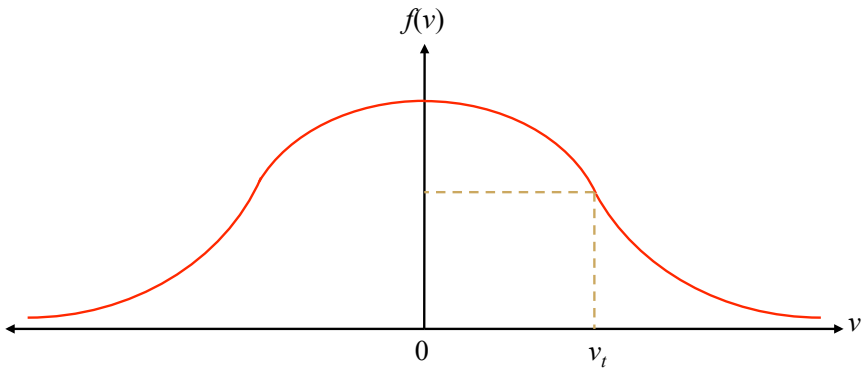

Figure 1. Maxwellian velocity distribution. In a Maxwellian plasma, the velocities of the particles in the plasma fit a Gaussian (bell curve) distribution centered around v_0, which is taken here to be zero. The thermal velocity $v_t \equiv \sqrt{k_B T/m}$ corresponds to the standard deviation of the Gaussian, or the point where the distribution f has fallen to $e^{-1/2} \approx 0.607$ of its peak central value $f(0)$.

The thermal velocities of electrons and ions are

$$v_{te} \equiv \sqrt{\frac{k_B T_e}{m_e}} = 1.32 \times 10^7 \sqrt{T_{e,\,keV}} \ \frac{\text{m}}{\text{sec}} \qquad \textbf{Electron thermal velocity} \qquad (4)$$

$$v_{ti} \equiv \sqrt{\frac{k_B T_i}{m_i}} = 3.09 \times 10^5 \sqrt{\frac{m_p}{m_i}} \sqrt{T_{i,\,keV}} \ \frac{\text{m}}{\text{sec}} \qquad \textbf{Ion thermal velocity} \qquad (5)$$

The ion mass has been expressed relative to the proton mass m_p. As is common in plasma physics, Eqs. (4) and (5) have converted the temperature T to its equivalent thermal energy $k_B T$ in kilo-electron volts (keV). The typical temperatures of plasmas are so high that it is more manageable to express the numbers in keV than in degrees Kelvin. The equivalency is

$$1 \text{ keV} = 1.16 \times 10^7 \ ^o\text{K} \qquad (6)$$

Because collisions very quickly create Maxwellian velocity distributions (see Section 2.1), the electrons and ions are generally assumed to be Maxwellian unless there is a reason to believe otherwise. The details of the velocity distribution can then be ignored, and one can treat the ions and electrons as two interpenetrating fluids, each with some spatial distribution $n_j(\mathbf{x})$ and net velocity $\mathbf{v_{oj}}$ or simply $\mathbf{v_j}$. The thermal velocity v_{tj} can also be invoked whenever necessary for certain calculations.

Neglecting particles lost to nuclear reactions, conservation of species j particles may be expressed as the usual continuity equation (see the mathematics summary for more details):

$$\frac{\partial n_j}{\partial t} + \nabla\cdot(n_j \mathbf{v_j}) = 0 \qquad \textbf{Conservation of particles} \qquad (7)$$

Treating species j (electrons or ions) as a fluid, Newton's second law for conservation of momentum may be written as

$$\overbrace{n_j m_j \left(\frac{\partial}{\partial t} + \mathbf{v_j}\cdot\nabla\right)\mathbf{v_j}}^{\text{Mass} \times \text{acceleration}} = \overbrace{n_j q_j(\mathbf{E} + \mathbf{v_j} \times \mathbf{B})}^{\text{Lorentz force}} \ \overbrace{-\nabla p}^{\text{Pressure force}} + \overbrace{\mathbf{P_{jl}}}^{\text{Force from collisions with other species}} \qquad \textbf{Momentum equation} \qquad (8)$$

Because they are written in terms of the density n_j, the quantities on the left and right sides of Eq. (8) are per volume. Equation (8) is really just the Navier-Stokes equation from fluid mechanics. The collision term $\mathbf{P_{jl}}$ is scary to actually calculate and can usually be ignored anyway.

As explained in the fluid mechanics summary, the term $(\partial/\partial t + \mathbf{v}\cdot\nabla) \equiv d/dt$ is called the **convective derivative**. The $\partial/\partial t$ represents actual variation with time, and the $\mathbf{v}\cdot\nabla$ accounts for apparent time variation of a quantity due to moving along a spatial gradient ∇ of the quantity at velocity $\mathbf{v}$. Often the $\mathbf{v}\cdot\nabla$ term can be neglected in actual calculations.

The total pressure p is the sum of the partial pressures p_j of each particle species j, which are usually found from the ideal gas law:

$$p_j \;=\; n_j k_B T_j \qquad\qquad \textbf{Ideal gas law} \tag{9}$$

When ions or electrons are compressed, the compression is usually assumed to be adiabatic:

$$\frac{p_j}{n_j^\gamma} \;=\; \text{constant} \qquad \Longrightarrow \qquad dp_j \;=\; \gamma\,\frac{p_j}{n_j}\,dn_j \qquad\qquad \textbf{Adiabatic relation} \tag{10}$$

From *Statistical Physics* ?.?, for adiabatic compression in D dimensions $\gamma = (D+2)/D$. Thus $\gamma = 3$ for 1D compression, 2 for 2D, and 5/3 for 3D. For isothermal compression, Eq. (10) may still be used but with $\gamma = 1$, as may be seen from Eq. (9) with T_j held constant.

Instead of treating electrons and ions as separate interpenetrating fluids, under certain circumstances they can be lumped together and treated as a single fluid. This approach is called **magnetohydrodynamics** and is discussed in Section 3.

1.2 Debye Length and Plasma Frequency

An important property of plasmas is their ability to screen out electric or electromagnetic fields. The Debye length and the plasma frequency are two different measures of this screening ability.

Debye Length

Consider a positive test charge Q at position $\mathbf{r} = 0$ in a plasma, as shown in Fig. 2(a). It will repel ions and attract electrons from the plasma, thereby surrounding itself with a cloud of negative charge. This negative charge screens out the positive charge Q beyond a certain distance, the **Debye length** λ_D, which can be calculated.

Using Poisson's equation from electromagnetism, the electric potential surrounding Q depends on the electron and ion densities ($Z = 1$ is assumed here for simplicity):

$$\nabla^2\phi \;=\; \frac{e}{\epsilon_o}(n_e - n_i) - \frac{Q}{\epsilon_o}\delta(\mathbf{r})\;. \tag{11}$$

Yet from statistical physics, the electron and ion densities also depend on the potential:

$$n_e \;=\; n_o \exp\left(\frac{e\phi}{k_{_B}T_e}\right) \;\approx\; n_o\left(1 + \frac{e\phi}{k_{_B}T_e}\right) \tag{12}$$

$$n_i \;=\; n_o \exp\left(-\frac{e\phi}{k_{_B}T_i}\right) \;\approx\; n_o\left(1 - \frac{e\phi}{k_{_B}T_i}\right)\;, \tag{13}$$

in which n_o is the equilibrium density required for strict electrical neutrality, $n_e = n_i = n_o$, and Taylor expansions have been made assuming the electric potential is relatively weak ($e\phi \ll k_{_B}T$).

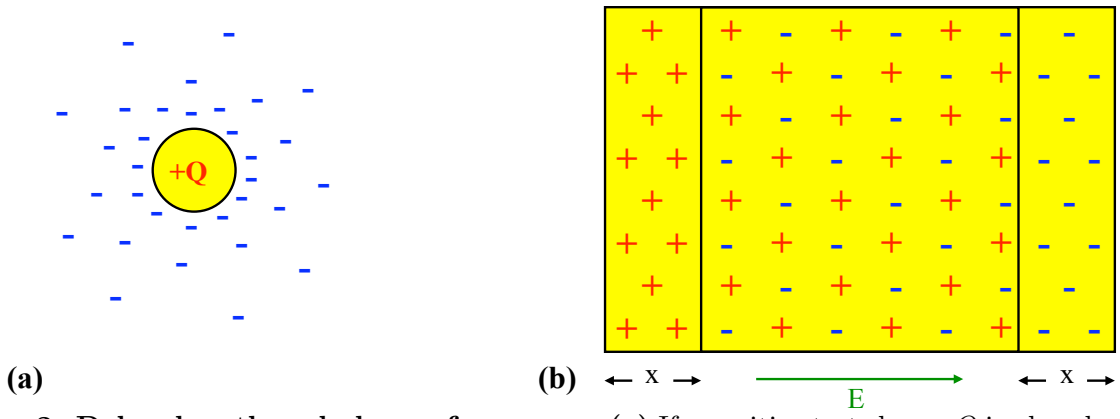

Figure 2. Debye length and plasma frequency. **(a)** If a positive test charge Q is placed within a plasma, it will attract electrons and repel ions from its vicinity, thereby surrounding itself with a cloud of negative charge. This cloud effectively screens out electric charges (or electric potentials) at distances greater than the Debye length λ_D. **(b)** Charges (especially electrons) within a plasma can slosh back and forth, leaving regions of excess negative charge and unneutralized positive charge. The charged regions produce electric fields that drag the charges back the other way, but the charges overshoot and keep oscillating back and forth. The natural frequency of this sloshing is called the plasma frequency ω_p. Applied electromagnetic fields with frequencies less than ω_p cannot propagate into a plasma, because the plasma's charges can oscillate quickly enough to cancel out the applied field.

Inserting Eqs. (12) and (13) into Eq. (11) produces

$$\nabla^2\phi \;=\; \frac{1}{\lambda_D^2}\phi - \frac{Q}{\epsilon_o}\delta(\mathbf{r})\;, \tag{14}$$

in which the Debye length λ_D has been defined as

$$\frac{1}{\lambda_D^2} \;\equiv\; \frac{1}{\lambda_{De}^2} + \frac{1}{\lambda_{Di}^2} \qquad \textbf{Total Debye length } \lambda_D \tag{15}$$

$$\lambda_{De} \;\equiv\; \sqrt{\frac{\epsilon_o k_B T_e}{n_e e^2}} \;=\; 235\sqrt{\frac{T_{e,\,keV}}{n_{e,\,cm^{-3}}}}\ \text{m} \qquad \textbf{Electron Debye length} \tag{16}$$

$$\lambda_{Di} \;\equiv\; \sqrt{\frac{\epsilon_o k_B T_i}{n_i Z^2 e^2}} \;=\; \frac{235}{Z}\sqrt{\frac{T_{i,\,keV}}{n_{i,\,cm^{-3}}}}\ \text{m} \qquad \textbf{Ion Debye length} \tag{17}$$

The ion charge Z has been restored in Eq. (17) for generality.

The solution of Eq. (14) is

$$\phi \;=\; \frac{Q}{4\pi\epsilon_o r}\exp\left(-\frac{r}{\lambda_D}\right)\;. \tag{18}$$

This result is the usual Coulomb potential around a point charge, except for the exponential factor. As predicted, the plasma screens out the test charge beyond a distance $\sim \lambda_D$. More generally, a plasma efficiently screens out almost any applied electric potential. Incidentally, Eq. (18) has the same form as the Yukawa potential that describes strong force interactions mediated by pions.

Plasma Frequency

Plasmas can respond to oscillating as well as static electric fields. Figure 2(b) shows a slab of plasma, which can be treated as a simple one-dimensional problem. In an oscillating electric field, the electrons slosh back and forth but the ions remain relatively motionless due to their much larger mass. As the electrons move back and forth, they create a negative surface charge Σ of excess electrons on one side of the slab and a positive surface charge of the same magnitude of unneutralized ions on the other side. That produces an electric field that drags the electrons back the other way, but they overshoot in the other direction and thus oscillate. This closes the cycle–the oscillating electrons create the time-varying electric field, and the electric field causes the electrons to oscillate. The resonant frequency of these natural oscillations is called the **plasma frequency**.

Applying Poisson's equation $\nabla \cdot \mathbf{E} = \rho_{\text{charge}}/\epsilon_o$ to the slab (defining ρ_{charge} as the charge density and x as the thickness of the unneutralized charge layers) yields the electric field E in the slab:

$$E \;=\; \frac{\Sigma}{\epsilon_o} \;=\; \frac{e n_e x}{\epsilon_o}\,. \tag{19}$$

The electric field creates a restoring force F on the electrons,

$$F \;=\; -eE \;=\; -\,\frac{e^2 n_e}{\epsilon_o}\,x \tag{20}$$

Using this restoring force, Newton's second law $F = m_e\, d^2x/dt^2$ for the electrons becomes

$$0 \;=\; \frac{d^2x}{dt^2} \;+\; \frac{e^2 n_e}{\epsilon_o m_e}\,x \;=\; \frac{d^2x}{dt^2} \;+\; \omega_{pe}^2 x \tag{21}$$

According to Eq. (21), the electrons thus behave like a simple harmonic oscillator with frequency

$$\omega_{pe} \;\equiv\; \sqrt{\frac{e^2 n_e}{\epsilon_o m_e}} \qquad \textbf{Angular electron plasma frequency} \tag{22}$$

Although the more massive ions do not slosh as well, it is convenient to define an analogous ion plasma frequency to be used in calculations of ion waves in Section 4:

$$\omega_{pi} \;\equiv\; \sqrt{\frac{Z^2 e^2 n_i}{\epsilon_o m_i}} \qquad \textbf{Angular ion plasma frequency} \tag{23}$$

The corresponding frequencies $f_p = \omega_p/2\pi$ for electrons and ions are

$$f_{pe} \;=\; \frac{1}{2\pi}\sqrt{\frac{e^2 n_e}{\epsilon_o m_e}} \;=\; 8980\sqrt{n_{e,\,cm^{-3}}}\ \text{Hz} \qquad \textbf{Electron plasma frequency} \tag{24}$$

$$f_{pi} \;=\; \frac{1}{2\pi}\sqrt{\frac{Z^2 e^2 n_i}{\epsilon_o m_i}} \;=\; 210\,Z\sqrt{\frac{m_p}{m_i}}\,\sqrt{n_{i,\,cm^{-3}}}\ \text{Hz} \qquad \textbf{Ion plasma frequency} \tag{25}$$

It is worth noting the relations

$$\omega_{pe} \;=\; \frac{v_{te}}{\lambda_{De}} \qquad\qquad \omega_{pi} \;=\; \frac{v_{ti}}{\lambda_{Di}} \tag{26}$$

These relations may be interpreted as meaning that the electrons or ions, moving at their thermal velocity, can travel approximately one Debye shielding length during one plasma oscillation. In other words, the plasma particles can move quickly enough to provide full (at least one Debye length) screening of an applied electric or electromagnetic field if the field is oscillating at a frequency no greater than the plasma frequency. Section 4 will analyze in more detail the ability of plasmas to screen out electromagnetic waves with frequencies below the plasma frequency.

1.3 Bremsstrahlung

When electrons collide with ions, they convert some of their kinetic energy into electromagnetic radiation, termed **bremsstrahlung** (German for "braking radiation"). This radiation is one of the most important power loss mechanisms in fusion plasmas, and it is also useful as a diagnostic to measure the electron temperature. A rigorous derivation of bremsstrahlung requires quantum electrodynamics (QED) and is very nasty, even by the standards of QED. The derivation that follows is a crude physical argument that arrives at the correct answer.

When an electron encounters an ion with impact parameter b [Fig. 3(a)], the electron's maximum acceleration a may be estimated by applying Newton's second law to the Coulomb force F:

$$m_e a \;=\; F \;\approx\; \frac{Z_i e^2}{4\pi\epsilon_o b^2}\;. \tag{27}$$

Figure 3. Bremsstrahlung radiation. (a) Due to attraction by an ion, an electron is deflected from its original trajectory to a new trajectory. If the impact parameter of the original trajectory is b, the distance of closest approach may be approximated as $\sim b$, and the path length over which the acceleration (trajectory deflection) occurs may be taken as $\sim 2b$. The acceleration causes the electron to emit bremsstrahlung radiation. **(b)** Acceleration of an electron by all ions may be taken into account by considering the ion density and integrating over all impact parameters.

From electromagnetism, the electromagnetic power radiated by the accelerated electron is

$$P_e \;=\; \frac{e^2 a^2}{6\pi\epsilon_o c^3} \qquad \textbf{Power radiated by accelerated electron} \tag{28}$$

$$\;=\; \frac{Z_i^2 e^6}{96\pi^3\epsilon_o^3 c^3 m_e^2 b^4} \qquad \text{using Eq. (27)}\;. \tag{29}$$

The acceleration and hence bremsstrahlung emission lasts for a time $\sim 2b/v_{te}$, so the total energy emitted during the encounter is

$$E_e \;=\; \frac{2b}{v_{te}} P_e \;=\; \frac{Z_i^2 e^6}{48\pi^3\epsilon_o^3 c^3 b^3 m_e^2 v_{te}}\;. \tag{30}$$

The average power emitted by one electron encountering multiple ions [Fig. 2(b)] is

$$P_{\rm mult} \;=\; \overbrace{\int_{b_{\rm min}}^{\infty} (2\pi b\, db)\,(n_i v_{te})}^{\text{Rate of encounters with ions}} \overbrace{E_e}^{\text{Energy emitted per encounter}}$$

$$\;=\; \frac{e^6 \sum_i (Z_i^2 n_i)}{24\pi^2\epsilon_o^3 c^3 m_e^2} \int_{b_{\rm min}}^{\infty} \frac{db}{b^2} \;=\; \frac{e^6 \sum_i (Z_i^2 n_i)}{24\pi^2\epsilon_o^3 c^3 m_e^2 b_{\rm min}} \tag{31}$$

If the minimum possible impact parameter were $b_{\min} = 0$, the bremsstrahlung power would be infinite. Quantum physics spares us from that nonsensical result by supplying a nonzero minimum impact parameter. At such small distances, the electron behaves quantum mechanically and obeys the Heisenberg uncertainty principle, $(\Delta x)(\Delta p) \approx h/2\pi$, where h is Planck's constant. Assuming $\Delta p \approx m_e v_{te}$, the minimum impact parameter is simply the DeBroglie wavelength of the electron:

$$b_{\min} \;\approx\; \Delta x \;\approx\; \lambda_{\text{DeBroglie}} \;\equiv\; \frac{h}{2\pi m_e v_{te}} \;=\; \frac{h}{2\pi\sqrt{m_e k_B T_e}}\,. \tag{32}$$

Using Eqs. (31) and (32), the bremsstrahlung power from all the electrons within a volume is

$$\frac{P_{\text{brem}}}{\text{vol.}} = n_e P_{\text{mult}} = \frac{\sum_i (Z_i^2 n_i) e^6 n_e \sqrt{k_B T_e}}{12\pi\epsilon_o^3 c^3 m_e^{3/2} h} \approx 5.34\times10^{-31} \sum_i (Z_i^2 n_{i,\,cm^{-3}}) n_{e,\,cm^{-3}} \sqrt{T_{e,\,keV}}\;\frac{\text{Watts}}{\text{cm}^3} \tag{33}$$

It is important to minimize the Z of the ion species in the plasma. Thus fuel ions should have very low Z, and fusion products like ^{4}He should be quickly removed. Likewise, the first wall surrounding the plasma should be made of very low-Z material that ablates very little into the plasma.

To lowest order, collisions between electrons do not produce radiation, because the acceleration of one electron is equal but opposite that of the other, or in other words, the electromagnetic waves from each electron cancel out. At high electron energies, relativistic effects can produce unequal accelerations and thus some electron-electron bremsstrahlung. Relativistic corrections are of the order $T_e/m_e c^2$ and therefore are generally only important for $T_e > 100$ keV. For more information, see [5]. Bremsstrahlung from ions is negligible due to their large masses and small accelerations.

1.4 Cyclotron Motion and Related Effects

A magnetic field causes charged particles to move in circles perpendicular to the field. Because this principle is used to make circular particle accelerators (see Section 8.1), it is termed cyclotron or synchrotron (or sometimes Larmor) motion. The centripetal acceleration of the charged particles makes them emit electromagnetic cyclotron radiation. As will be shown, variations in the magnetic field or the presence of additional fields can cause a net drift velocity for the spiraling particles. Cyclotron motion can also be used to trap particles in a magnetic mirror field.

Cyclotron Motion

For a charged particle moving in the presence of a static magnetic field $\mathbf{B}$, Eq. (1) becomes

$$m\frac{d\mathbf{v}}{dt} \;=\; q\mathbf{v}\times\mathbf{B} \qquad\Longrightarrow\qquad \frac{d\mathbf{v}}{dt} \;=\; \omega_c(\mathbf{v}\times\hat{\mathbf{b}})\,, \tag{34}$$

where $\hat{\mathbf{b}}$ is a unit vector along the magnetic field's direction and the angular cyclotron frequency is

$$\omega_c \;\equiv\; \frac{qB}{m} \qquad\qquad \textbf{Angular cyclotron frequency} \tag{35}$$

Equation (34) shows that the charged particle moves in a circle perpendicular to the magnetic field with angular frequency ω_c [Fig. 4(a)]. The direction of rotation depends on the sign of the particle's charge. For electrons or ions, the corresponding frequency $f_c = \omega_c/2\pi$ is

$$f_{ce} \;\equiv\; \frac{eB}{2\pi m_e} \;=\; 28.0\,B_T\ \text{GHz} \qquad \textbf{Electron cyclotron frequency} \tag{36}$$

$$f_{ci} \;\equiv\; \frac{ZeB}{2\pi m_i} \;=\; 15.2\,Z\left(\frac{m_p}{m_i}\right)B_T\ \text{MHz} \qquad \textbf{Ion cyclotron frequency} \tag{37}$$

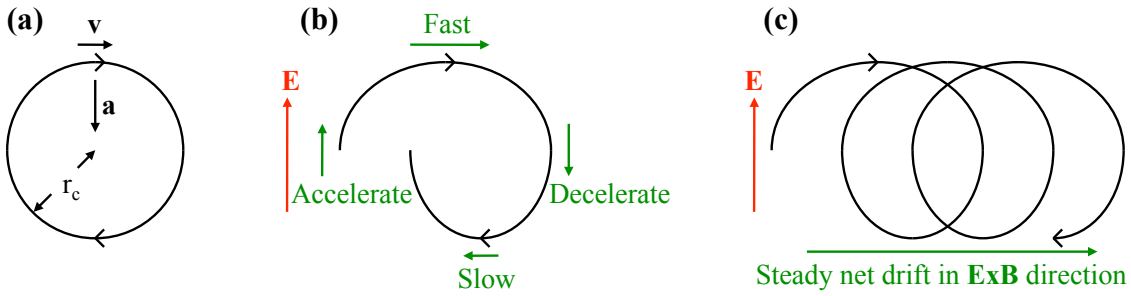

Figure 4. Cyclotron motion and E×B drift. **(a)** The **v**×**B** force due to a magnetic field pointing out of the page creates a centripetal acceleration a that bends a positively charged particle's trajectory into a circular cyclotron orbit with radius r_c as shown. A negative particle would orbit in the other direction. **(b)** If an upward electric field is added, it will accelerate a positive particle when it is going upward on the left side of the orbit and decelerate the particle when it is moving downward on the right. The particle goes faster when moving to the right than when moving to the left, displacing the particle orbit to the right. A negative particle orbits in the opposite direction and is accelerated downward by the electric field, so its orbit is also displaced to the right. **(c)** Therefore, the cyclotron orbits of both positive and negative particles experience a steady net drift in the **E**×**B** direction.

If a particle has an average thermal energy $\frac{1}{2}k_B T$ per degree of freedom, its kinetic energy and hence velocity in the plane perpendicular to the magnetic field are

$$\frac{1}{2}mv_\perp^2 \;=\; k_B T \qquad \Longrightarrow \qquad v_\perp \;=\; \sqrt{\frac{2k_B T}{m}} \;=\; \sqrt{2}v_t \tag{38}$$

The cyclotron radius of the particle's orbit is simply $r_c = v_\perp/\omega_c$, or

$$r_{ce} \;\equiv\; \frac{\sqrt{2k_B T_e m_e}}{eB} \;=\; 0.106\frac{\sqrt{T_{e,\,keV}}}{B_T}\ \text{mm} \qquad \textbf{Electron cyclotron radius} \tag{39}$$

$$r_{ci} \;\equiv\; \frac{\sqrt{2k_B T_i m_i}}{ZeB} \;=\; 4.56\frac{\sqrt{T_{i,\,keV}}}{ZB_T}\sqrt{\frac{m_i}{m_p}}\ \text{mm} \qquad \textbf{Ion cyclotron radius} \tag{40}$$

Some authors define the cyclotron radius without the above factor of $\sqrt{2}$. For a typical fusion plasma with $T \sim 10-20$ keV and $B \sim 1-10$ T, r_{ce} and r_{ci} are much smaller than the dimensions of most plasma containment vessels, so particles spiral tightly about the magnetic field lines. Particle motion along the field lines is not affected by any $\mathbf{v}\times\mathbf{B}$ magnetic forces. To a first approximation, particles may thus be regarded as closely following the magnetic field lines.

Cyclotron Radiation

From Eq. (34), electrons undergoing cyclotron motion experience a centripetal acceleration $a = eBv_\perp/m_e$. Using this acceleration in Eq. (28) yields the electromagnetic power radiated by each gyrating electron:

$$P_e \;=\; \frac{e^4}{6\pi\epsilon_o c^3 m_e^2}B^2 v_\perp^2 \;=\; \frac{e^4}{3\pi\epsilon_o c^3 m_e^3}B^2 k_B T_e\ . \tag{41}$$

The cyclotron power radiated by all electrons within a given volume is just $n_e P_e$, or

$$\frac{P_{\rm cycl}}{\rm volume} \;=\; \frac{e^4}{3\pi\epsilon_o c^3 m_e^3}B^2 n_e k_B T_e \;=\; 6.21\times10^{-17}B_T^2\, n_{e,\,cm^{-3}}\, T_{e,\,keV}\ \frac{\rm Watts}{\rm cm^3} \tag{42}$$

This power is radiated at the electron cyclotron frequency f_{ce} and higher harmonics. To minimize power losses due to cyclotron radiation, the magnetic field inside a fusion plasma can be kept as small as possible. Fortunately, cyclotron radiation is also in a frequency range that can be reflected back into the plasma and reabsorbed with a relatively good efficiency. The cyclotron radiation from ions is smaller than that from electrons by a factor of $(m_e/m_i)^3$ and thus may be neglected.

Drift of Cyclotron Orbit Due to Electric Field or Other Force

As shown in Fig. 4(b), an upward electric field (or other force) causes a particle orbiting in a perpendicular magnetic field to accelerate while moving upward and decelerate while moving downward. The particle's motion to the right during the upper part of the orbit then exceeds its motion to the left during the lower part, inducing a net drift of the orbit [Fig. 4(c)]. The particle velocity is a purely circular cyclotron motion $\mathbf{v}_{\rm cycl}$ plus a constant linear drift velocity $\mathbf{v}_{\rm drift}$ induced by the electric field:

$$\mathbf{v} \;=\; \mathbf{v}_{\rm cycl} + \mathbf{v}_{\rm drift} \;, \qquad \text{where} \quad \frac{d\mathbf{v}_{\rm drift}}{dt} \;=\; 0 \tag{43}$$

Equation (43) may be substituted into Eq. (1). Removing the terms that involve $\mathbf{v}_{\rm cycl}$ and correspond to Eq. (34) leaves only the drift terms

$$0 \;=\; \mathbf{E} + \mathbf{v}_{\rm drift}\times\mathbf{B} \tag{44}$$

The drift velocity is perpendicular to both $\mathbf{E}$ and $\mathbf{B}$, so it must take the form

$$\mathbf{v}_{\rm drift} = \alpha\mathbf{E}\times\mathbf{B} \;, \tag{45}$$

where α is some function of the fields. Substituting Eq. (45) into Eq. (44) shows what α must be:

$$0 \;=\; \mathbf{E} + \alpha(\mathbf{E}\times\mathbf{B})\times\mathbf{B} \;=\; \mathbf{E} - \alpha B^2\mathbf{E} \qquad \Longrightarrow \qquad \alpha \;=\; \frac{1}{B^2} \;. \tag{46}$$

Thus the drift due to the electric field is

$$(\mathbf{v}_{\rm drift})_{\rm electric} \;=\; \frac{\mathbf{E}\times\mathbf{B}}{B^2} \tag{47}$$

The drift due to a more general force $\mathbf{F}$ may be found by substituting $q\mathbf{E} \to \mathbf{F}$ in Eq. (47)

$$(\mathbf{v}_{\rm drift})_F \;=\; \frac{\mathbf{F}\times\mathbf{B}}{qB^2} \tag{48}$$

The drift direction due to $\mathbf{F}$ depends on the sign of q, since charges of opposite sign orbit in opposite directions. However, the electric-field-induced drift does not depend on q; reversing the charge's sign reverses both the orbital direction and the force $q\mathbf{E}$, leaving the drift direction unchanged.

Drift Due to Curved Magnetic Field Lines

If magnetic field lines bend with a radius of curvature $\mathbf{R}$ as in Fig. 5(a), particles moving along those lines will experience a centrifugal force $mv_\parallel^2\mathbf{R}/R^2$. From Eq. (48), this causes a drift velocity

$$(\mathbf{v}_{\rm drift})_{\rm curvature} \;=\; \frac{mv_\parallel^2}{q}\,\frac{\mathbf{R}\times\mathbf{B}}{R^2B^2} \tag{49}$$

Drift Due to Gradient in Magnetic Field Strength

If $\mathbf{B}$ differs at different points in a particle's orbit, the particle will experience a net drift. As a simple yet illustrative example, Fig. 5(b) shows that if the magnetic field in the left half of a particle orbit is stronger than that in the right half, the cyclotron radius will change during the orbit and the particle will drift downward. Another way to view this phenomenon is that the Lorentz force $q\mathbf{v}\times\mathbf{B}$ averaged over a complete orbit is zero for a uniform magnetic field but nonzero if the field varies with position. A spatially varying magnetic field exerts a net sideways force:

$$\begin{aligned}\mathbf{F}_{\rm net} \;&=\; q\,\langle\mathbf{v}\times\mathbf{B}\rangle_{\rm cycle} \;=\; -q\,\langle(v_\perp\cos\omega_c t)(\nabla B r_c\cos\omega_c t)\rangle_{\rm cycle} \\ &=\; -qv_\perp r_c\nabla B\left\langle\cos^2\omega_c t\right\rangle_{\rm cycle} \;=\; -\frac{1}{2}qv_\perp r_c\nabla B\end{aligned} \tag{50}$$

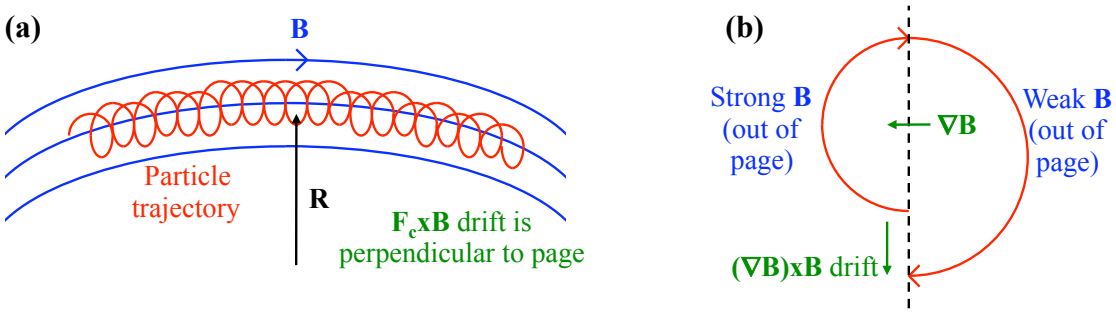

Figure 5. Curvature and ∇B drifts. **(a)** Magnetic field lines with a radius of curvature R cause particles spiraling along them to feel an outward centrifugal force $F_c \parallel R$. This creates an $F_c \times B$ drift, with positive particles moving into the page and negative particles moving out of the page. **(b)** If a magnetic field coming out of the page is stronger on the left side and weaker on the right, a particle will have a smaller cyclotron orbital radius on the left side than the right. This difference causes a drift downward [in the $(\nabla B) \times B$ direction] for positive particles and upward for negative ones.

Using this force in Eq. (48) gives the drift velocity

$$(\mathbf{v}_{\text{drift}})_{\nabla B} \;=\; \frac{1}{2} v_\perp r_c \frac{\mathbf{B}\times(\nabla B)}{B^2} \tag{51}$$

Magnetic Mirror Effect

If plasma particles are spiralling along magnetic field lines and the field lines become stronger (closer together) at opposite ends of the plasma, the particles will bounce back and forth between the ends and be trapped. This **magnetic mirror effect** is illustrated in Fig. 6. It has been considered as a method to confine fusion plasmas, as will be discussed in Section 7.1.

The mirror effect requires that the strength of the magnetic field increase along the field lines ($\nabla \mathbf{B}$ parallel to $\mathbf{B}$, as opposed to $\nabla \mathbf{B}$ perpendicular to $\mathbf{B}$, which causes the gradient drift derived above). One can begin this analysis by finding the effect of changing B on the cyclotron motion of a particle. Because the magnetic force on an orbiting particle is purely radial with respect to the orbit (ie., it has no torque), the particle's angular momentum L remains constant:

$$\begin{aligned} \text{Constant} \;=\; L \;&=\; m v_\perp r_c \;=\; \frac{m v_\perp^2}{\omega_c} \;=\; \frac{m^2}{q}\,\frac{v_\perp^2}{B} \\ \Longrightarrow\quad \frac{v_\perp^2}{B} \;&=\; \text{constant} \end{aligned} \tag{52}$$

Equation (52) can also be derived using the magnetic moment of the orbiting particle.

Consider a particle traveling from the midpoint o of the magnetic field shown in Fig. 6(a) to the mirror point m on one end. Conservation of the particle's kinetic energy $m(v_\parallel^2 + v_\perp^2)/2$ dictates

$$v_{\parallel o}^2 + v_{\perp o}^2 \;=\; v_{\parallel m}^2 + v_{\perp m}^2 \,. \tag{53}$$

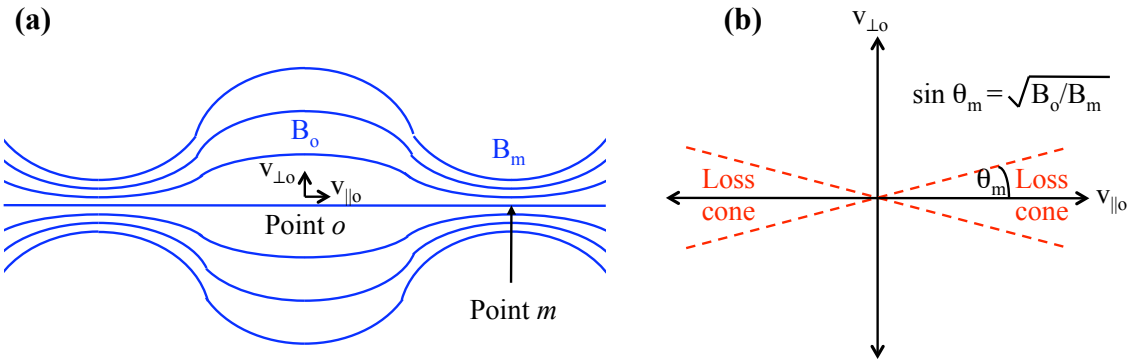

Figure 6. Magnetic mirror effect. (a) A magnetic mirror field is stronger (the magnetic field lines are closer together) at the mirror endpoint m than at the central point o. A particle's velocity may be separated into the components parallel ($v_\parallel$) and perpendicular ($v_\perp$) to the magnetic field direction. **(b)** The velocity components of particles at the central point o are plotted. If a particle's velocity lies within the loss cone, it will be able to escape when it comes to the end of the mirror. All other particles are reflected back and forth between the ends of the mirror field.

Using Eq. (52) to write $v_{\perp m}^2 = v_{\perp o}^2 B_m / B_o$ and substituting this into Eq. (53) yields

$$v_{\parallel m}^2 \;=\; v_{\parallel o}^2 + v_{\perp o}^2 - \frac{B_m}{B_o}\, v_{\perp o}^2 \tag{54}$$

The particle will come to a stop at the mirror point m and reflect back in the other direction if $v_{\parallel m} = 0$. From Eq. (55), this requires

$$\frac{B_o}{B_m} \;=\; \frac{v_{\perp o}^2}{v_{\parallel o}^2 + v_{\perp o}^2} \;\equiv\; \sin^2\theta_m \;, \tag{55}$$

in which θ is defined as the mirror angle. Figure 6(b) plots the parallel $v_{\parallel o}$ and perpendicular $v_{\perp o}$ components of the velocities of particles at the central point o in the system. θ_m is the half-angle of a cone-shaped region in that velocity space. Particles within this **loss cone** have too much $v_\parallel$ (or not enough $v_\perp$) to be reflected at the ends of the mirror field, so they will be lost out the ends of the system. All of the other particles in velocity space are trapped by the mirror field. However, as will be shown in Section 7.1, collisions between trapped particles can change their velocities and scatter them into the loss cone, leading to a continual loss of particles from the mirror field.

Due to the magnetic mirror effect, the earth's magnetic field traps charged particles in the space surrounding the earth, creating the **Van Allen radiation belts**. The earth's magnetic field exits the north pole, arcs out into space over the equator, and re-enters the south pole. Ions and electrons ejected from the sun as part of the solar wind are trapped by the earth's field, traveling along the field lines in tight spirals. Since the field is stronger (the field lines are closer together) at the earth's poles than over the equator, the particles mirror-reflect above each pole, bouncing back and forth along the field lines in space. Particles in the velocity-space loss cone are not reflected and instead hit the upper atmosphere, causing colorful atmospheric auroras near the earth's poles. This effect is especially pronounced when fresh high-energy charged particles are added during solar storms.

1.5 Fusion Reactions

For a detailed introduction to fusion reactions, see *Nuclear Physics* 3.2. Certain small nuclei release lots of energy when they fuse together, but they must collide at high energies to overcome their mutual electric repulsion. If ion beams with the optimum energies collide, much more scattering than fusion occurs (Section 2.1 and [5]) and the ions are lost, along with the input energy invested in them. Ion beams striking solid fusion targets are dissipated by both scattering and ionization of the target [2]. Therefore, high-energy ions must be confined so they can collide and scatter repeatedly until they finally fuse. The scattering creates Maxwellian ion velocity distributions (Section 2.1). Although electrons steal energy from the ions and waste it via bremsstrahlung and cyclotron radiation, they must be included to neutralize the ions' charge and reach high ion densities and fusion rates. Thus fusion requires a thermal ion-electron plasma.

Below are the main fusion reactions, where p stands for proton, n for neutron, D for deuterium nucleus, T for tritium nucleus, and ^{4}He or α for helium-4 nucleus. Fusion energy is released as kinetic energy of the reaction products, listed below in MeV, millions of electron volts.

$$\mathrm{D} \;+\; \mathrm{T} \;\rightarrow\; {}^4\mathrm{He}\ (3.5\ \mathrm{MeV}) \;+\; \mathrm{n}\ (14.1\ \mathrm{MeV}) \tag{56}$$

The D+T reaction, Eq. (56), is the easiest fusion reaction to carry out, having the largest reaction rate at the lowest temperature. Unfortunately it requires radioactive tritium and produces high-energy neutrons, which can **activate** (induce radioactivity in) surrounding materials in a reactor.

$$\mathrm{D} \;+\; \mathrm{D} \;\rightarrow\; \begin{cases} \mathrm{T}\ (1.01\ \mathrm{MeV}) \;+\; \mathrm{p}\ (3.02\ \mathrm{MeV}) & [50\%] \\ {}^3\mathrm{He}\ (0.82\ \mathrm{MeV}) \;+\; \mathrm{n}\ (2.45\ \mathrm{MeV}) & [50\%] \end{cases} \tag{57}$$

The D+D reaction (57) can produce either tritium or ^{3}He. If those products fuse with additional deuterium, the overall fusion energy increases to 21.6 MeV per initial D+D reaction. Note that neutrons are still produced, both by initial D+D reactions and by subsequent D+T reactions.

$$\mathrm{D} \;+\; {}^3\mathrm{He} \;\rightarrow\; {}^4\mathrm{He}\ (3.6\ \mathrm{MeV}) \;+\; \mathrm{p}\ (14.7\ \mathrm{MeV}) \tag{58}$$

D+^{3}He is more attractive, as it yields no neutrons and charged products carry all its fusion energy, potentially permitting direct conversion to electricity at high efficiencies. However, D+^{3}He is harder to burn than D+T, and some neutrons are still produced by (lower probability) D+D side reactions.

$$\mathrm{T} \;\rightarrow\; {}^3\mathrm{He} \;+\; \mathrm{e}^-\ (18.6\ \mathrm{keV}) \quad [12.3\text{-year half-life}] \tag{59}$$

As shown in Eq. (59), tritium is radioactive, decaying into ^{3}He with a half-life of 12.3 years. Therefore there is virtually no naturally occuring tritium; tritium must be created if required. If tritium is available and ^{3}He is desired, the tritium can simply be allowed to decay.

$$\mathrm{n} \;+\; {}^6\mathrm{Li} \;\rightarrow\; {}^4\mathrm{He}\ (2.1\ \mathrm{MeV}) \;+\; \mathrm{T}\ (2.7\ \mathrm{MeV}) \tag{60}$$

Reaction (60) is the most common method of producing tritium. In a fusion reactor, a blanket containing ^{6}Li might surround the plasma. Fusion neutrons produced in the plasma would breed fresh tritium in the blanket, which could be extracted and used in further rounds of fusion reactions.

Fusion power P_{fus} per volume is the fusion reaction rate times the energy E_{fus} produced per reaction:

$$\frac{P_{\mathrm{fus}}}{\mathrm{volume}} \;=\; n_{i1} n_{i2} \langle \sigma v \rangle E_{\mathrm{fus}} \;=\; 1.602 \times 10^{-13}\, n_{i1,\,\mathrm{cm}^{-3}}\, n_{i2,\,\mathrm{cm}^{-3}}\, \langle \sigma v \rangle_{\mathrm{cm}^3/\mathrm{sec}}\, E_{\mathrm{fus,\,MeV}}\, \frac{\mathrm{Watts}}{\mathrm{cm}^3}\ , \tag{61}$$

in which n_{i1} and n_{i2} are the densities of the fuel ion species. For reactions like D+D with only one ion species, one should change $n_{i1} n_{i2} \rightarrow n_i^2/2$ in Eq. (61); dividing by 2 prevents double-counting ions. v is the collision velocity between the ions. The reaction cross section σ (gauging how easily the reaction can happen) is a function of v. Generally the fuel ion species have Maxwellian velocity distributions with the same temperature T_i, so $\langle \sigma v \rangle$ is averaged over the Maxwellians, becoming simply a function of T_i (*Nuclear Physics* 3.2). Fusion consumes most of the ions on a timescale

$$\tau_{\mathrm{fus}} \;\equiv\; \frac{1}{n_i \langle \sigma v \rangle} \qquad \textbf{Fusion time} \tag{62}$$

As discussed in Section 1.3, bremsstrahlung power losses are important, since the radiation cannot be reflected back into the plasma and does not depend on the fusion reactor's geometry. If the bremsstrahlung losses exceed the power produced by a fusion reaction, that reaction cannot produce net power in a reactor. Using Eqs. (33) and (61) with $n_{i1} = n_{i2} = n_i/2$ for simplicity, one finds

$$\frac{P_{\rm brem}}{P_{\rm fus}} \;=\; 3.33 \times 10^{-18} (Z_{i1}^2 + Z_{i2}^2)(Z_{i1} + Z_{i2}) \frac{\sqrt{T_{e,\,\rm keV}}}{\langle \sigma v \rangle_{\rm cm^3/sec}\, E_{\rm fus,\,MeV}} \; . \tag{63}$$

If there is only one species of ions, one should change $(Z_{i1}^2 + Z_{i2}^2)(Z_{i1} + Z_{i2}) \rightarrow 2Z_i^3$ in Eq. (63). Bremsstrahlung and fusion are both two-body collisional processes and hence vary like $n^2 \times$ (volume), so their ratio, given in Table 1, is independent of the plasma density and volume:

Reaction	T	$\langle \sigma v \rangle$	E_{fus}	P_{brem}/P_{fus}
D+T	20 keV	4.2×10^{-16} cm^3/sec	17.6 MeV	0.0081
D+D	50 keV	2.1×10^{-17} cm^3/sec	21.6 MeV	0.10
D+^{3}He	100 keV	1.6×10^{-16} cm^3/sec	18.3 MeV	0.17

Table 1. Bremsstrahlung power loss fractions for different fusion reactions.

Here $T_i = T_e \equiv T$ was assumed for simplicity. The conditions are nearly optimum for each fuel; for more information on optimization, see [5]. As shown in Table 1, the bremsstrahlung loss is insignificant for D+T and significant but manageable for D+D and D+^{3}He at typical reactor conditions. The precise maximum tolerable limit on the ratio $P_{\rm brem}/P_{\rm fus}$ depends on the fractions of $P_{\rm brem}$ and $P_{\rm fus}$ that can be converted to electricity and the severity of other power loss mechanisms.

Alternative fusion reactions such as the following have been proposed:

$$\mathrm{p} \;+\; {}^{11}\mathrm{B} \;\rightarrow\; 3\,{}^4\mathrm{He} \;+\; 8.7\,\mathrm{MeV} \qquad (\text{requires } T_i \approx 300 \text{ keV}) \tag{64}$$

$${}^3\mathrm{He} \;+\; {}^3\mathrm{He} \;\rightarrow\; {}^4\mathrm{He} \;+\; 2\,\mathrm{p} \;+\; 12.3\,\mathrm{MeV} \qquad (\text{requires } T_i \approx 1 \text{ MeV}) \tag{65}$$

These reactions would produce no neutrons directly and very few neutrons indirectly. Unfortunately, because of the large Z, high temperature, and relatively low energy output per reaction, the bremsstrahlung loss exceeds the fusion power even under the best of circumstances [5].

The power loss $P_{\rm escape}$ due to bremsstrahlung, escaping energetic particles, and other losses may be written in terms of the time τ required to lose the entire thermal energy of the ions and electrons:

$$\frac{P_{\rm losses}}{\rm volume} \;=\; \frac{\frac{3}{2} k_B (n_i T_i + n_e T_e)}{\tau} \; . \tag{66}$$

After converting fusion power to electricity at efficiency η, there must still be enough power to compensate for the losses (using $T_i = T_e \equiv T$, $n_{i1} = n_{i2} = n_i/2$, and $n_e \equiv Z_{\rm avg} n_i$ for simplicity):

$$\begin{aligned} P_{\rm fus}\eta \;>\; P_{\rm losses} \quad &\Longrightarrow \quad \frac{1}{4} n_i^2 \, \langle \sigma v \rangle \, E_{\rm fus} \eta \;>\; \frac{\frac{3}{2} n_i (1 + Z_{\rm avg}) k_B T}{\tau} \\ &\Longrightarrow \quad n_i \tau \;>\; \frac{6(1 + Z_{\rm avg})}{\eta} \, \frac{k_B T}{E_{\rm fus}} \, \frac{1}{\langle \sigma v \rangle} \quad \textbf{Lawson criterion} \end{aligned} \tag{67}$$

For like-particle reactions such as D+D, the coefficient 6 in Eq. (67) should be replaced by a 3. Using Table 1 and a thermal conversion efficiency $\eta = 0.4$ yields

$$n_i \tau \;>\; \begin{cases} 8 \times 10^{13} \;\; \mathrm{sec/cm^3} & \text{for D+T} \\ 2 \times 10^{15} \;\; \mathrm{sec/cm^3} & \text{for D+D} \\ 1 \times 10^{15} \;\; \mathrm{sec/cm^3} & \text{for D+}^3\mathrm{He} \end{cases} \tag{68}$$

Again, D+T is easier to burn that D+D and D+^{3}He. As Section 5 will show, stars are so large that they efficiently trap radiation and particles within their plasma and thus can generate power from very difficult fusion reactions such as p+p that could not be exploited in a man-made reactor.

2 Transport

Collisions between charged ions can result in Coulomb scattering instead of fusion, so one must consider ion-ion Coulomb collisions. Ion-electron and electron-electron collisions are also important, due to their critical roles in energy transport within the plasma. This section will analyze the effect of collisions on particle diffusion in both velocity-space and actual physical space. Danger Will Robinson: many transport properties vary by a factor of 2 or so among various plasma textbooks.

2.1 Velocity-Space Transport: Like-Particle Collisions

Collision Times

The characteristic times over which like-particle (ion-ion or electron-electron) collisions produce effects are easily estimated. If two particles use the thermal energy $k_{_B}T$ of their random motion to fight the electrostatic repulsion between them, the closest distance r_o they can get to each other is

$$\frac{(Ze)^2}{4\pi\epsilon_o r_o} \;=\; k_{_B}T \qquad \Longrightarrow \qquad r_o \;=\; \frac{(Ze)^2}{4\pi\epsilon_o k_{_B}T} \qquad \text{Landau length} \tag{69}$$

The particles' scattering cross section would be $\sigma = \pi r_o^2$ if they bounced off each other like hard spheres of radius r_o. Cumulative small-angle scattering from long-range collisions affects the particle velocities about $\ln\Lambda$ faster than large-angle scattering from short-range collisions. Including this **Coulomb logarithm** factor (which will be calculated in a moment) yields

$$\sigma \;=\; \pi r_o^2 \ln\Lambda \;=\; \frac{\ln\Lambda (Ze)^4}{16\pi\epsilon_o^2 (k_{_B}T)^2}\,. \tag{70}$$

Using the thermal velocity $v_t = \sqrt{k_{_B}T/m}$, collisions act on a timescale

$$\tau_{\rm col} \;=\; \frac{1}{n\sigma v_t} \;=\; \frac{16\pi\sqrt{m}\epsilon_o^2 (k_{_B}T)^{3/2}}{\ln\Lambda n (Ze)^4}\,. \tag{71}$$

Thus the collision times due to ion-ion and electron-electron collisions are

$$\tau_{ii} \;=\; \frac{16\pi\sqrt{m_i}\epsilon_o^2 (k_{_B}T_i)^{3/2}}{\ln\Lambda n_i (Ze)^4} \;\approx\; 5.0\times10^{11}\frac{T_{i,\,keV}^{3/2}}{Z^4\ln\Lambda n_{i,\,cm^{-3}}}\sqrt{\frac{m_i}{m_p}}\ \text{sec} \tag{72}$$

$$\tau_{ee} \;=\; \frac{16\pi\sqrt{m_e}\epsilon_o^2 (k_{_B}T_e)^{3/2}}{\ln\Lambda n_e e^4} \;\approx\; 1.1\times10^{10}\frac{T_{e,\,keV}^{3/2}}{\ln\Lambda n_{e,\,cm^{-3}}}\ \text{sec} \tag{73}$$

If the velocity distribution of particles is initially non-Maxwellian (e.g., isotropic and monoenergetic, anisotropic Maxwellian with different temperatures in different directions, etc.), like-particle collisions will turn it into an isotropic Maxwellian within a time $\sim \tau_{\rm col}$. The collision time is calculated using the temperature of the final Maxwellian, $T = (3/2)\langle E\rangle$, where $\langle E\rangle$ is the (initial and final) average energy of the particles. Particles are usually assumed to have a Maxwellian velocity distribution, because τ_{ii} and τ_{ee} are almost always shorter than the fusion and confinement times. For example, combining Eqs. (62) and (72) produces

$$\frac{\tau_{ii}}{\tau_{\rm fus}} \;=\; \frac{16\pi\sqrt{m_i}\epsilon_o^2 (k_{_B}T_i)^{3/2}\,\langle\sigma v\rangle}{\ln\Lambda (Ze)^4} \;\approx\; 5.0\times10^{11}\frac{T_{i,\,keV}^{3/2}\,\langle\sigma v\rangle_{\rm cm^3/sec}}{Z^4\ln\Lambda}\sqrt{\frac{m_i}{m_p}} \tag{74}$$

Note that this ratio is independent of the density, since collisions and fusion are both two-body processes. Using Table 1 and Eq. (74), collisional scattering occurs 800x faster than fusion for D+T, 4000 faster for D+D, and 600x faster for D+^{3}He.

Coulomb Logarithm

Now the secret origins of the Coulomb logarithm will be revealed. As discussed in the classical mechanics summary, interactions of two moving particles with masses m_1 and m_2 may be simplified by using the reduced mass $m_r \equiv m_1 m_2/(m_1+m_2)$ and relative collision velocity v_r between the particles. This transforms the problem to that of an incident particle with mass m_r and velocity v_r interacting with a fixed target particle, as shown in Fig. 7(a). In the figure, the incident particle approaches the target particle with an impact parameter b, and it receives a net sideways momentum change Δp. Δp may be found from the peak Coulomb force between the particles $F \approx q_1 q_2/(4\pi\epsilon_o b^2)$ (for particle charges q_1 and q_2) and the duration of the encounter $\Delta t \approx 2b/v_r$:

$$\Delta p \;\approx\; F\,\Delta t \;\approx\; \frac{q_1 q_2}{2\pi\epsilon_o b v_r}\,. \tag{75}$$

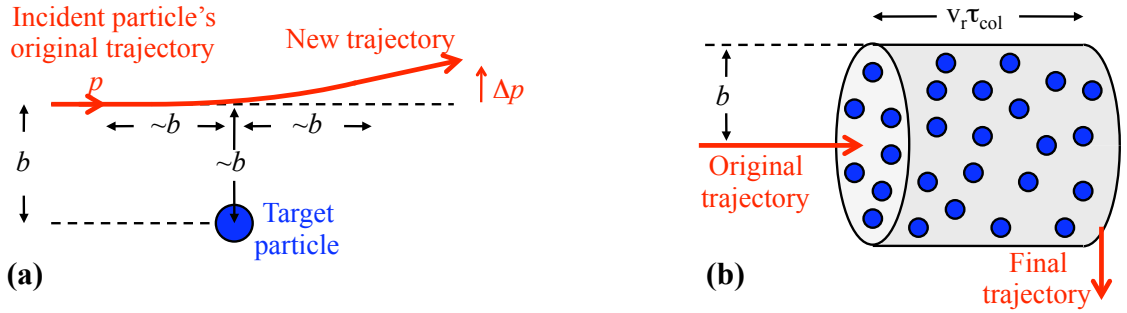

Figure 7. Scattering due to collisions between particles. **(a)** Due to the Coulomb force between an incident particle with momentum p and a stationary target particle, the incident particle experiences a sideways deflection in momentum Δp. If the impact parameter is b, the distance of closest approach is $\sim b$ and the path length over which the force is felt is $\sim 2b$. **(b)** An incident particle with velocity v_r passing through a population of target particles feels a deflecting force from each target particle. The impact parameter differs for each target particle. The smallest impact parameter allowed by quantum physics is the DeBroglie wavelength, and the largest impact parameter over which electrostatic force can be felt is the Debye shielding distance. After the incident particle travels for a time $\tau_{\rm col}$ or a distance $v_r\tau_{\rm col}$, the cumulative deflection of its trajectory will be 90^o.

Debye shielding limits the maximum impact parameter to $b_{\rm max} = \lambda_D$, while quantum effects provide a minimum value $b_{\rm min} = \lambda_{\rm DeBroglie}$ from Eq. (32). Equation (75) is the small-angle limit of the result derived more rigorously for Coulomb scattering in the classical mechanics summary. If the incident particle undergoes multiple collisions [Fig. 7(b)], it will execute a random walk in momentum-space, taking a step of size Δp each collision. From the mathematics summary, the cumulative mean square of the momentum deviation, $\langle(\Delta P)^2\rangle$, grows linearly with the number of steps, and it can be calculated using a method similar to that in Section 1.3:

$$\begin{aligned}\left\langle(\Delta P)^2\right\rangle \;&=\; \overbrace{\int_{b_{\rm min}=\lambda_{\rm DeBroglie}}^{b_{\rm max}=\lambda_D} (2\pi b\,db)\,(n v_r \Delta t)}^{\text{Number of collisions in time } \Delta t}\;\overbrace{(\Delta p)^2}^{\text{Scattering per collision}} \\ &=\; \Delta t\,\frac{q_1^2 q_2^2 n}{2\pi\epsilon_o^2 v_r}\int_{\lambda_{\rm DeBroglie}}^{\lambda_D}\frac{db}{b} \;=\; \Delta t\,\frac{q_1^2 q_2^2 n \ln\Lambda}{2\pi\epsilon_o^2 v_r}\,,\end{aligned} \tag{76}$$

where the Coulomb logarithm is defined as

$$\ln\Lambda \equiv \ln\left(\frac{\lambda_D}{\lambda_{\rm DeBroglie}}\right) = \ln\left(\frac{\sqrt{m_e\epsilon_o}\,k_B T}{e\hbar\sqrt{n}}\right) \approx 31 + \ln T_{\rm keV} - \frac{1}{2}\ln n_{\rm cm^{-3}} \,. \tag{77}$$

Although Eq. (77) uses the electron mass, the results are essentially the same for ions. The Coulomb logarithm varies so slowly it is usually treated as a constant. Typical values of $\ln\Lambda$ are 20 in a magnetic fusion plasma, 5 for inertial confinement fusion, and 2 in the core of a star.

The cumulative scattering of the particle reaches 90^o when the net deviation equals the particle's original momentum, or $\langle(\Delta P)^2\rangle = (m_r v_r)^2$. Using Fig. 7(b) and Eq. (76), this occurs after a time

$$\tau_{col} = \frac{2\pi\epsilon_o^2 m_r^2 v_r^3}{q_1^2 q_2^2 n \ln\Lambda} \,. \tag{78}$$

For collisions between like particles of charge Z, mass m, and thermal velocity v_t, the reduced mass $m_r = m/2$ and relative velocity $v_r \approx 2v_t = 2\sqrt{k_B T/m}$ may be substituted into Eq. (78):

$$\tau_{\rm col} = \frac{4\pi\sqrt{m}\epsilon_o^2 (k_B T)^{3/2}}{\ln\Lambda n (Ze)^4} \,. \tag{79}$$

(Eq. (71) agrees well with Spitzer and Braginskii, but Eq. (79) from this more detailed derivation is ∼4x too small. How can that be fixed?)

Runaway Electrons

For electron-electron collisions, the cross section from Eq. (70) may be rewritten in terms of the electron energy E_e, $k_B T \to m_r v_e^2/2 = E_e/2$:

$$\sigma = \frac{\ln\Lambda e^4}{4\pi\epsilon_o^2 E_e^2} \,. \tag{80}$$

Due to scattering, electrons will tend to lose their energy E_e over a mean free path length $l_{mfp} \equiv 1/(n_e\sigma)$. Note that the cross section decreases rapidly and hence the mean free path increases rapidly with increasing E_e; higher energy electrons scatter much less and can travel much further. If a sufficiently strong electric field E is applied, high-energy electrons will gain more energy per distance from the electric field (eE) than they lose on average due to collisions (E_e/l_{mfp}). Thus there will be **runaway electrons** that are accelerated by the field to higher and higher energies if

$$\begin{aligned} eE &> \frac{E_e}{l_{mfp}} = E_e n_e \sigma = \frac{\ln\Lambda n_e e^4}{4\pi\epsilon_o^2 E_e} \quad , \text{ or} \\ E_e &> \frac{\ln\Lambda n_e e^3}{4\pi\epsilon_o^2 E} \,. \end{aligned} \tag{81}$$

For a typical magnetic fusion plasma with $\ln\Lambda = 20$ and $n_e = 1\times10^{20}$ m^{-3}, even a relatively weak electric field $E = 10$ Volts/m would cause electrons with energies $E_e > 5$ keV to run away. The runaway electrons would gain a large amount of energy from the field, then waste it by bremsstrahlung or cyclotron radiation or by escaping the confinement system. This limits the utility of ohmic heating, in which an electric field drives a current through a plasma of nonzero resistivity to heat the plasma to fusion temperatures. If one attempts to heat a plasma above ~ 1 keV by this method, too much electron runaway will occur.

2.2 Velocity-Space Transport: Unlike-Particle Collisions

The most prevalent unlike-particle collisions are ion-electron collisions. These collisions are characterized by two different time constants, which are defined here as τ_{ei} and τ_{ie}.

The electron-ion collision time τ_{ei} is defined as the time required for electrons to change their direction of motion due to collisions with ions. This process is very similar to electrons being scattered by collisions with other electrons, so the collision time τ_{ee} from Eq. (73) may be modified for this purpose. In the present case, electrons collide with ions having charge Ze and density n_i instead of with electrons having charge $-e$ and density n_e. If Z is the average ion charge, the electron and ion densities are related by $n_e = Zn_i$. Therefore, one can make the substitution $n_e \to Z^2 n_i = Z n_e$ in Eq. (73) to obtain

$$\tau_{ei} \;=\; \frac{16\pi\sqrt{m_e}\epsilon_o^2 (k_{_B}T_e)^{3/2}}{\ln\Lambda n_e Z e^4} \;\approx\; 1.1\times 10^{10}\frac{T_{e,\,keV}^{3/2}}{Z\ln\Lambda n_{e,\,cm^{-3}}}\ \text{sec} \tag{82}$$

Similarly, the ion-electron collision time τ_{ie} is the time for angular scattering of ions by electrons. However, ions are more massive than electrons and hence are harder to scatter, so this time is longer than the corresponding τ_{ei}. τ_{ie} is also the timescale on which ion-electron collisions affect the relative energies of the ion and electron populations (not merely their directions of motion). It may be found by applying Eq. (76) to ion-electron collisions. The change in momentum corresponds to a change ΔE_i in an ion's energy:

$$2m_i\Delta E_i \;=\; \Big\langle (\Delta P)^2 \Big\rangle \;=\; \Delta t\,\frac{Z^2 e^4 n\ln\Lambda}{2\pi\epsilon_o^2 v_r}\,. \tag{83}$$

For comparable ion and electron temperatures, electrons move much faster than ions, so the relative collision velocity is $v_r \approx v_{te} = \sqrt{k_{_B}T_e/m_e}$. The energy change can be equal to the average electron energy, $\Delta E_i = 3k_{_B}T_e/2$, after a time

$$\tau_{ie} \;=\; \frac{6\pi\epsilon_o^2 m_i (k_{_B}T_e)^{3/2}}{\ln\Lambda n_e Z^2 e^4\sqrt{m_e}} \;\approx\; 8.0\times 10^{12}\frac{T_{i,\,keV}^{3/2}}{Z^2\ln\Lambda n_{e,\,cm^{-3}}}\,\frac{m_i}{m_p}\ \text{sec} \tag{84}$$

For $Z = 1$ and $T_i = T_e$, the ratios of the collision times are

$$\tau_{ee} : \tau_{ei} : \tau_{ii} : \tau_{ie} \;\sim\; 1 : 1 : \sqrt{\frac{m_i}{m_e}} : \frac{m_i}{m_e}\,. \tag{85}$$

Thus electrons quickly form a Maxwellian velocity distribution due to collisions with other electrons and nearly elastic angular scattering off ions. On a slower timescale, ions assume a Maxwellian distribution due to ion-ion collisions. On the slowest timescale, energy is transferred between the ion and electron populations if they are at different temperatures.

If $T_i \neq T_e$, the power per volume transferred from ions to electrons is

$$\frac{P_{ie}}{\text{volume}} \;\approx\; \frac{\frac{3}{2}n_i k_{_B}(T_i - T_e)}{\tau_{ie}}$$

$$=\; \frac{n_i n_e Z^2 e^4 \ln\Lambda\sqrt{m_i m_e}}{(2\pi)^{3/2}\epsilon_o^2 (m_i T_e + m_e T_i)^{3/2}}\,(T_i - T_e) \tag{86}$$

$$\approx\; 2.41\times 10^{-29} Z^2 n_{i\,cm^{-3}}\, n_{e\,cm^{-3}}\ln\Lambda\,\frac{m_p}{m_i}\,\frac{(T_{\mathrm{i,\,keV}} - T_{\mathrm{e,\,keV}})}{T_{\mathrm{e,\,keV}}^{3/2}}\,\frac{\text{Watts}}{\text{cm}^3}\,, \tag{87}$$

where Eqs. (86) and (87) are the results of Sivukhin and Landau's more accurate calculations [6, 7].

Energy loss by very high-energy ions is a special case of interest. As shown in Eqs. (56-60), fusion products are emitted with ∼MeV energies, and fuel ions can also be injected into a plasma as a high-energy beam. For ions with velocity $v_i \gg v_{te}$, the collision velocity is $v_r \approx v_i$. Using Eq. (83), high-energy ions lose all their energy $\Delta E_i = m_i v_i^2/2$ to electrons after a slowing-down time

$$\tau_{\text{slowing down}} \;=\; \frac{2\pi\epsilon_o^2 m_i^2 v_i^3}{Z^2 e^4 n_e \ln\Lambda} \; . \tag{88}$$

During this time, the ions move a distance

$$\begin{aligned} l_{\text{slowing down}} \;&\approx\; \frac{1}{2} v_i \tau_{\text{slowing down}} \;=\; \frac{\pi\epsilon_o^2 m_i^2 v_i^4}{Z^2 e^4 n_e \ln\Lambda} \\ &=\; \frac{4\pi\epsilon_o^2 E_i^2}{Z^2 e^4 n_e \ln\Lambda} \;\approx\; 4\times 10^{22} \frac{E_{i,\,MeV}^2}{Z^2 n_{e,\,cm^{-3}} \ln\Lambda} \;\; m \end{aligned} \tag{89}$$

2.3 Classical Spatial Diffusion

Spatial Diffusion without or Parallel to Magnetic Field

Particles diffuse in physical space as well as in velocity space. This process is very important, because particles escape from a plasma by diffusion, and also because particles diffusing within a plasma carry thermal energy (conducting heat) and charge (producing an electric current). It is straightforward to calculate spatial particle diffusion in a plasma without a magnetic field. The results are also applicable to particles diffusing parallel to a magnetic field in a magnetized plasma, since a magnetic field does not affect motion in the parallel direction (there is no $\mathbf{v}\times\mathbf{B}$ force). Particles diffusing perpendicular to a magnetic field will be treated subsequently.

As shown in the applied mathematics summary, gradients ∇n in a particle concentration induce particle fluxes $n\mathbf{v}$ which are related by a particle diffusion coefficient D:

$$n\mathbf{v} \;=\; -D\nabla n \qquad\qquad \textbf{Fick's law} \tag{90}$$

Inserting Eq. (90) into the continuity equation (7) produces the standard diffusion equation:

$$\frac{\partial n}{\partial t} \;=\; D\nabla^2 n \qquad\qquad \textbf{Diffusion equation} \tag{91}$$

Equation (91) implies that during a time τ, particles diffuse a typical distance $L \sim \sqrt{D\tau}$.

As shown in the math summary, the diffusion coefficient may be found from the average particle speed (in this case v_t) and average distance l_{mfp} or time between particle collisions. For diffusing electrons, electron-ion and electron-electron collisions are of comparable importance, $\tau_{ei} = \tau_{ee}/Z$. In contrast, ion-ion collisions cause ion diffusion much faster than ion-electron collisions, $\tau_{ii} \sim \sqrt{m_e/m_i}\;\tau_{ie}$. Using τ_{ei} to approximately account for electron collisions with both ions and electrons, the electron and ion diffusion constants parallel to (or without) a magnetic field are

$$D_e^{\parallel} \;=\; \frac{1}{3} v_{te} l_{mfp} \;=\; \frac{1}{3} v_{te}^2 \tau_{ei} \;=\; \frac{1}{3}\,\frac{k_B T_e}{m_e}\,\tau_{ei} \qquad\qquad D_i^{\parallel} \;=\; \frac{1}{3}\,\frac{k_B T_i}{m_i}\,\tau_{ii} \tag{92}$$

From the solid state physics summary, the thermal conductivity due to electrons is their specific heat capacity $3n_e k_B/2$ multiplied by their diffusion coefficient. As shown in Braginskii [7], the actual thermal conductivity is 6.4 times larger than this simple predicted value:

$$\kappa_e^{\parallel} \;\approx\; 6.4\left(\frac{3}{2} n_e k_B\right)\, D_e^{\parallel} \;=\; 3.2\frac{n_e k_B^2 T_e}{m_e}\tau_{ei} \; . \tag{93}$$

Ions carry the same energy as electrons ($\sim k_B T$) but move $\sim \sqrt{m_i/m_e}$ more slowly. Therefore the $\kappa^{\|}$ due to ions is $\sim \sqrt{m_i/m_e}$ times smaller than that of electrons and may be neglected.

The electrical resistivity η of electrons in a plasma is predicted by the Drude model from solid state physics. In brief, an applied electric field E gives an acceleration eE/m_e to electrons, and collisions cause a deceleration v/τ_{ei}, where v is the electron velocity. Balancing these two effects, the steady-state electron velocity is $v \approx eE\tau_{ei}/m_e$. The current density is $J = n_e e v \approx (n_e e^2 \tau_{ei}/m_e)E \equiv E/\eta$. Braginskii [7] has shown that runaway electrons, which are not particularly affected by collisions, lower the actual value of the resistivity by a factor of 2:

$$\eta_e^{\|} \;=\; \frac{1}{2}\,\frac{m_e}{n_e e^2 \tau_{ei}} \;=\; 1.6\times 10^{-9}\frac{\ln\Lambda}{T_{e\,keV}^{3/2}}\;\;\Omega\text{-m}\;. \tag{94}$$

Sometimes the electrical conductivity $\sigma \equiv 1/\eta$ is used. For a typical fusion plasma with $\ln\Lambda = 20$ and $T_e = 10$ keV, the resistivity is 1.0×10^{-9} $\Omega-$m, or approximately 18 times lower than the resistivity of room-temperature copper. Thus plasmas are extremely good conductors. Because ions are slower than electrons, their contribution to the parallel electrical resistivity can be ignored.

Spatial Diffusion Perpendicular to Magnetic Field

Parallel to a magnetic field, particles diffuse by traveling a distance l_{mfp} between collisions. Perpendicular to **B**, however, particles must remain in the same cyclotron orbit between collisions, so they can only diffuse a distance $\sim r_c$ each collision time. Collisions throw particles from one cyclotron orbit to an adjacent orbit (Fig. 8). Thus the electron and ion diffusion constants are

$$D_e^{\perp} \;\approx\; \left(\frac{r_{ce}}{l_{\rm mfp}}\right)^2 D_e^{\|} \;=\; \frac{2}{(\omega_{ce}\tau_{ei})^2}D_e^{\|} \;=\; \frac{1}{3}\,\frac{r_{ce}^2}{\tau_{ei}} \qquad\qquad D_i^{\perp} \;\approx\; \frac{2}{(\omega_{ci}\tau_{ii})^2}D_i^{\|} \;=\; \frac{1}{3}\,\frac{r_{ci}^2}{\tau_{ii}} \tag{95}$$

Note that ions diffuse $\sim \sqrt{m_i/m_e}$ faster than electrons perpendicular to a magnetic field, because ions have a larger cyclotron radius than electrons.

Equation (95) assumes that the particles have plenty of time for cyclotron motion in between collisions, or $\omega_c\tau_{\rm col} \gg 1$. To be more general, Eq. (95) may be modified so that it approaches $D^{\|}$ in the limit $\omega_c\tau_{\rm col} \ll 1$, or in other words for magnetic fields too weak to affect the particles:

$$D^{\perp} \;=\; \frac{D^{\|}}{1+(\omega_c\tau_{\rm col})^2/2}\;. \tag{96}$$

Thermal conductivity is mediated primarily by electrons parallel to a magnetic field but ions perpendicular to **B**, due to the different relative ion and electron diffusion constants. Including a factor of $\sqrt{2}$ from Braginskii's more detailed calculations [7], the perpendicular thermal conductivity is

$$\kappa_i^{\perp} \;\approx\; \sqrt{2}\,\left(\frac{3}{2}n_e k_B\right)\,D_i^{\perp} \;=\; \sqrt{2}\,\frac{n_i k_B^2 T_i}{m_i\omega_{ci}^2\tau_{ii}}\;. \tag{97}$$

Electrons moving perpendicular to **B** cannot run away, so the resistivity is simply the Drude value:

$$\eta_e^{\perp} \;=\; \frac{m_e}{n_e e^2\tau_{ei}} \;=\; 3.2\times 10^{-9}\frac{\ln\Lambda}{T_{e\,keV}^{3/2}}\;\;\Omega\text{-m}\;. \tag{98}$$

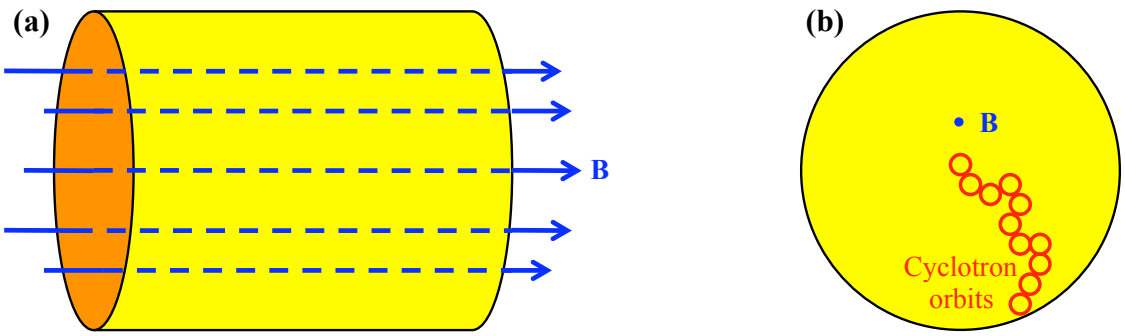

Figure 8. Classical diffusion perpendicular to a cylindrical magnetic field. **(a)** A confined plasma can assume a cylindrical shape, with magnetic field lines running longitudinally through the plasma. **(b)** In this cross section of the cylindrical plasma, the field lines are perpendicular to the page and plasma particles execute circular cyclotron orbits. Collisions bump particles from one orbit to another, letting the particles diffuse across the field lines via a random walk.

Bohm Diffusion

Early experiments with magnetic confinement found perpendicular diffusion rates much larger than predicted above. This enhanced diffusion is termed **Bohm diffusion** and is caused by fluctuating nonzero electric fields in the plasma. Random thermal motion of electrons relative to the ions in a plasma can create a maximum electric potential $\phi_{\max}$:

$$e\phi_{\max} \;=\; k_B T_e \;. \tag{99}$$

Assuming this potential difference exists between the center and edge of a cylindrical plasma of radius a, the corresponding maximum electric field is

$$E_{\max} \;\approx\; \frac{\phi_{\max}}{a} \;=\; \frac{k_B T_e}{ea} \;. \tag{100}$$

Using Eq. (47), the $\mathbf{E}\times\mathbf{B}$ drift associated with this electric field creates an outward particle flux

$$\begin{aligned} n v_\perp \;&=\; n\frac{|\mathbf{E}\times\mathbf{B}|}{B^2} \;<\; \frac{nE_{\max}}{B} \\ &<\; \frac{k_B T_e}{eB}\,\frac{n}{a} \;\approx\; -\frac{k_B T_e}{eB}\nabla n \;, \end{aligned} \tag{101}$$

where the rough approximation $\nabla n \approx -n/a$ was made. Equation (101) corresponds to a maximum diffusion coefficient $D \approx (k_B T_e)/(eB)$. The experimental data for Bohm diffusion is best matched by a diffusion coefficient D_B that is a fraction of this value:

$$D_B \;\approx\; \frac{1}{16}\,\frac{k_B T_e}{eB} \;=\; \frac{1}{16}\,\frac{v_{te}^2}{\omega_{ce}} \;. \tag{102}$$

The Bohm diffusion constant is generally larger than the classical $D^\perp$. Moreover, D_B varies like $1/B$, whereas the classical diffusion constant varies like $1/B^2$, so strong magnetic fields are less useful for plasma confinement than in the classical case. It is useful to note that $D_B/D^\perp_{\text{classical}} \approx \omega_c\tau_{\text{col}}/11$.

The Bohm diffusion time, or time for particles to diffuse across the radius a by this mechanism, is

$$\tau_B \;\equiv\; \frac{a^2}{D_B} \;=\; 1.6\times 10^{-2}\,\frac{a_m^2 B_T}{T_{e,\,keV}} \;. \tag{103}$$

For typical values $a = 0.1$ m, $B = 10$ T, and $T_e = 20$ keV, the Bohm time is 8×10^{-5} sec. To satisfy the Lawson criterion for D+T fusion in Eq. (68) would then require a density of 10^{18} ions/cm^3, much higher than is practical in magnetic fusion ($\sim 10^{14} - 10^{15}$ ions/cm^3). By carefully minimizing electric fields in the plasma, Bohm diffusion can be prevented. Confinement times at least 100 times longer than τ_B have been obtained in experiments.

2.4 Neoclassical Spatial Diffusion

General principles of toroidal magnetic confinement

In a cylindrical plasma, particles tend to escape at the ends, so magnetic fusion plasmas are usually bent into a doughnut or **torus** that does not have ends, as shown in Fig. 9. The central axis is defined as the line running through the center of the doughnut, and the major radius R is the distance from the central axis to the center of the tube of plasma. The minor radius a is the half-width of the tube of plasma. Sometimes we will mention the major circumference, $2\pi R$ (more or less), which travels 360^o around the central axis in the **toroidal** direction, or the minor circumference, $2\pi r$, which encloses the tube of plasma in the **poloidal** direction. Spatial diffusion is altered by the bent geometry of the torus and is called **neoclassical diffusion** [4, 8].

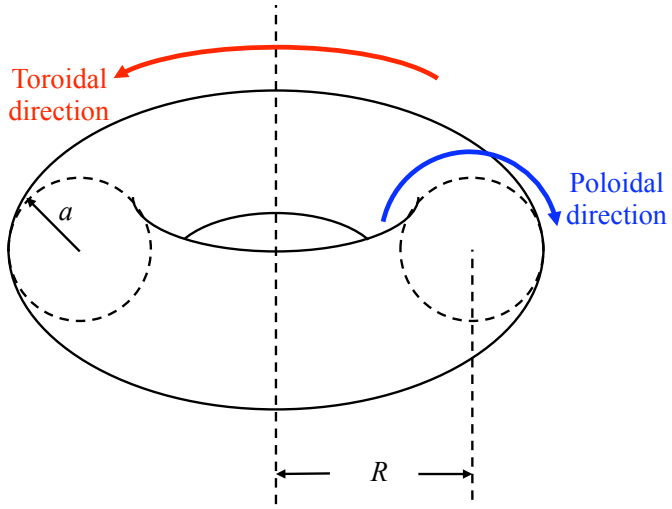

Figure 9. Confinement of a plasma in a toroidal magnetic geometry. To avoid having particles freely escape from the ends of a cylindrical plasma, the plasma can be bent into a toroidal shape without ends. The torus has a major radius R and minor radius a. The dotted line through the hole of the torus is called the central or major axis.

If magnetic field lines are bent into a circle, they form a toroidal field B_t, as shown in Fig. 10(a). Although particles can no longer escape along the field lines, there is a diabolical way in which they can escape across the field lines. Field lines with a greater circumference are more stretched out and hence weaker than those with a smaller circumference, so $\nabla \mathbf{B}$ points inward toward the central axis. Particles moving along the field lines experience the ∇B drift from Eq. (51). They also undergo the curvature drift from Eq. (49). Using the approximations $v_\parallel \sim v_\perp \sim v_t$ and $\nabla B \sim B/R$, the total drift velocity varies roughly like

$$(\mathbf{v}_{\text{drift}}) = (\mathbf{v}_{\text{drift}})_{\nabla B} + (\mathbf{v}_{\text{drift}})_{\text{curvature}} \sim \begin{cases} -\frac{r_{ce}}{R} v_{te} \hat{\mathbf{z}} & \text{for electrons} \\ +\frac{r_{ci}}{R} v_{ti} \hat{\mathbf{z}} & \text{for ions} \end{cases} \tag{104}$$

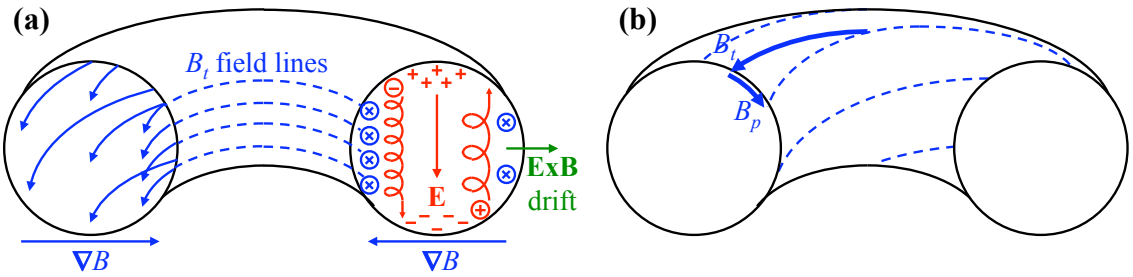

Figure 10. Particles freely escape from a plasma with only a toroidal magnetic field B_t. **(a)** A toroidal field is stronger toward the inner edge of the plasma, causing a ∇B drift of electrons downward and ions upward. This charge separation produces a downward electric field, which causes an outward $E \times B$ drift for both electrons and ions and allows them to escape. **(b)** Adding a poloidal component B_p to the magnetic field makes the field lines spiral around the torus, mixing different regions of the plasma and preventing the charge separation and hence the drift-associated particle losses.

Electrons drift downward while ions drift upward [Fig. 10(a)]. This separation of charges creates a vertical electric field, which then produces an outward $\mathbf{E} \times \mathbf{B}$ drift [Eq. (47)] for both ions and electrons. Thus ions and electrons drift outward across the magnetic field lines and escape.

This problem is solved by adding a poloidal component B_p so the magnetic field lines spiral around the torus [Fig. 10(b)]. Particles move along the field lines and are forced to continually travel around the minor circumference of the torus, preventing the separation of charges and the drift losses.

A useful definition is the **safety factor** q_s, the number of times a field line goes around the major circumference of the torus before it completes one spiral around the minor circumference:

$$q_s \equiv \frac{a}{R}\frac{B_t}{B_p} \qquad \textbf{Safety factor} \tag{105}$$

q_s is called the safety factor because it must be >1 to prevent instabilities, as Section 3.3 will show.

Adding B_p reduces but does not entirely prevent particle diffusion across the field lines. Particle diffusion depends on the relative rate of collisions, falling into the three categories discussed next.

Pfirsch-Schlüter regime

In the **Pfirsch-Schlüter regime** [Fig. 11(a)], many collisions occur before a particle travels once around the major (or minor) circumference of the torus. Thus particles diffuse along the field lines with diffusion constant $D_\parallel \sim v_t^2 \tau_{col}$ from Eq. (92).

As illustrated in Fig. 11(b), the upward drift from Eq. (104) moves ions in the upper half of the torus toward the edge of the plasma, while ions in the lower half move closer to the center of the plasma. (All of this is true for electrons too, but with the signs reversed.) Therefore, as ions follow the spiral field lines and circulate between the upper and lower halves of the torus, they alternatively drift away and toward the center of the plasma. This is a random walk process, where the duration of a step is the average time an ion spends in the upper or lower half.

From the definition of the safety factor q_s, a particle must travel a distance $q_s \pi R$ around the torus before it spirals from the top half to the bottom half [Fig. 11(b)]. Usually only the order of magnitude $q_s R$, called the **connection length**, is used. (What's a factor of π among friends?) The step duration $\tau_{\rm PS}$ is the time required for a particle to diffuse this far along the field lines:

$$\tau_{\rm PS} \sim \frac{(q_s R)^2}{D_\parallel} \sim \frac{(q_s R)^2}{v_t^2 \tau_{col}} \tag{106}$$

The corresponding length $L_{\rm PS}$ of a random walk step is the average distance a particle drifts at velocity v_d from Eq. (104) during the time $\tau_{\rm PS}$ it spends in the upper or lower half of the torus:

$$L_{\rm PS} = v_{\rm drift} \tau_{\rm PS} \sim \frac{r_c}{R} v_t \tau_{\rm PS} \tag{107}$$

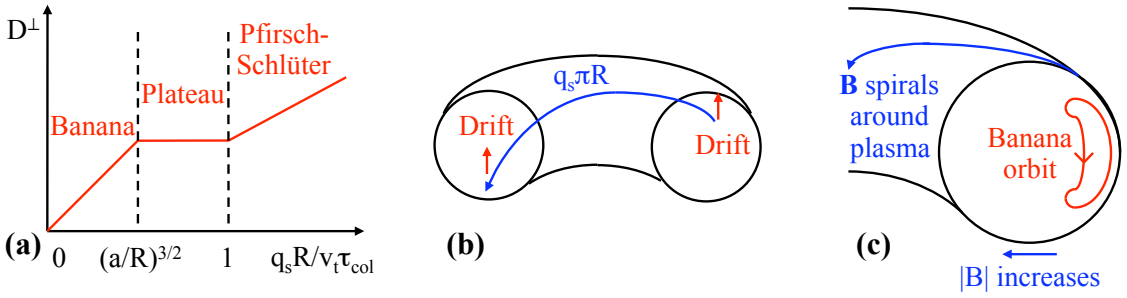

Figure 11. Neoclassical diffusion in a torus. **(a)** Diffusion in a toroidal plasma depends on the collision time $\tau_{\rm col}$. Long collision times cause banana diffusion, medium collision times cause plateau diffusion, and short collision times cause Pfirsch-Schlüter diffusion. **(b)** In the high-collisionality Pfirsch-Schlüter regime, collisions make particles diffuse along the spiral magnetic field lines such as the dashed line shown. The vertical drift draws particles in the upper half of the torus closer to the edge and those in the lower half of the torus closer to the center of the plasma. Particles alternate between these two situations after diffusing a distance $q_s \pi R \sim q_s R$ along the field lines. **(c)** In the low-collisionality banana regime, particles attempt to follow the field lines around the plasma as they travel around the torus. However, the magnetic field is stronger near the central axis of the torus, causing some particles to mirror-reflect and assume banana-shaped orbits of width $L_{\rm banana}$. Collisions are infrequent and tend to knock particles from one banana orbit to another. Note that particles actually travel around the torus while completing a banana orbit, instead of staying in one place as illustrated.

Combining Eqs. (106) and (107), the particle diffusion constant perpendicular to the magnetic field in the Pfirsch-Schlüter regime is

$$D_{PS} \sim \frac{L_{\rm PS}^2}{\tau_{PS}} \sim q_s^2 \frac{r_c^2}{\tau_{\rm col}} \qquad \textbf{Pfirsch-Schlüter diffusion} \tag{108}$$

This result is larger than the classical $D_\perp$ from Eq. (95) by a factor of $\sim q_s^2$. Since the above derivation assumed that particles must travel the distance $q_s R$ around the torus by collisional diffusion, the Pfirsch-Schlüter answer is valid when the mean free path is much shorter,

$$v_t \tau_{\rm col} < q_s R \qquad \textbf{Pfirsch-Schlüter regime} \tag{109}$$

This condition is typical of the low-temperature edge of a tokamak plasma.

Banana regime

When collisions are very infrequent, particles following the spiral field lines can make complete orbits around the minor circumference of the torus before colliding. Typically the magnetic field is inversely proportional with distance from the central axis, so orbiting particles encounter stronger fields as they approach the central axis. Particles with too much velocity $v_\perp$ and too little $v_\parallel$ relative to the field lines will mirror reflect in the stronger field rather than complete an orbit of the minor circumference. These particles are said to be trapped, and their mirror-reflected orbit assumes a banana shape [Fig. 11(c)]. Thus this low-collisionality regime is called the **banana regime**.

Using Eq. (55), particles will be trapped in mirror orbits if their velocity components are

$$\frac{v_\parallel}{v_\perp} < \sqrt{\frac{B_m}{B_o} - 1} \sim \sqrt{\frac{R+a}{R} - 1} = \sqrt{\frac{a}{R}} \,. \tag{110}$$

The fraction of particles in velocity space that are trapped is

$$f_{\rm trapped} \sim \sqrt{\frac{a}{R}} \,. \tag{111}$$

Collisions that scatter particles by an angle $\Delta\theta \sim \sqrt{a/R}$ in velocity space can cause a particle to escape from a trapped orbit to a fully circulating orbit and get trapped again in a different orbit. Recall that τ_{col} was defined as the time for a particle's velocity to change by $\pi/2 \sim 1$ radian. Because angular scattering by collisions is a diffusional process in velocity space, the time required is proportional to the square of the net amount of scattering. Therefore the effective collision time for particles to go from one trapped orbit to another is

$$\tau_{\rm eff} \sim \tau_{\rm col} (\frac{\Delta\theta}{1})^2 \sim \tau_{\rm col} \frac{a}{R} \,. \tag{112}$$

Trapped particles have most of their velocity in $v_\perp$, so $v_\perp \sim v_t$. From Eq. (110), the parallel velocity must then be

$$v_\parallel \sim \sqrt{\frac{a}{R}} v_\perp \sim \sqrt{\frac{a}{R}} v_t \,. \tag{113}$$

Particles must travel on the order of a connection length $q_s R$ along the magnetic field lines to trace out the arc of a banana orbit. The time required to do this is

$$\tau_{\rm banana} \sim \frac{q_s R}{v_\parallel} \sim \frac{q_s R}{v_t} \sqrt{\frac{R}{a}} \,. \tag{114}$$

One might think that trapped particles, on encountering the stronger magnetic field closer to the central axis, would return following the arc along which they came. In fact, the particles experience the vertical drift $v_{\rm drift} \sim v_t r_c/R$ from Eq. (104) during their transit, so the return arc is displaced by a vertical distance $L_{\rm banana}$ from the original arc. The net orbit assumes a banana shape with a width comparable to the vertical displacement,

$$L_{\rm banana} \;\sim\; v_{\rm drift}\tau_{\rm banana} \;\sim\; q_s r_c \sqrt{\frac{R}{a}}\,. \tag{115}$$

Particles diffuse out of the torus by being knocked by collisions from one trapped banana orbit to the next, taking a step of length $\sim L_{\rm banana}$ every $\sim \tau_{\rm eff}$. This is a random walk process governed by the spatial diffusion coefficient

$$D_{\rm banana} \;\sim\; f_{\rm trapped}\,\frac{L_{\rm banana}^2}{\tau_{\rm eff}} \;\sim\; \frac{q_s^2 r_c^2}{\tau_{\rm col}}\left(\frac{R}{a}\right)^{3/2} \qquad \textbf{Banana diffusion} \tag{116}$$

Note that Eq. (116) accounts for the fraction $f_{\rm trapped}$ of the particles that are trapped. Untrapped particles diffuse at a much slower rate determined by $D \sim D_{PS}$ and may be neglected here [8].

The banana regime requires that trapped particles have enough time to complete banana orbits before they collide, $\tau_{\rm eff} > \tau_{\rm banana}$. Using Eqs. (112) and (114), this means

$$\tau_{\rm eff} \;>\; \tau_{\rm banana} \qquad\Longrightarrow\qquad \tau_{\rm col} \;> \frac{q_s R}{v_t}\left(\frac{R}{a}\right)^{3/2} \qquad \textbf{Banana regime} \tag{117}$$

as shown in Fig. 11(a). The banana regime is typical of the hot center of a tokamak plasma.

A particularly useful result of neoclassical transport may be derived by noting the forces on particles in the toroidal direction. Particles are accelerated by a $\mathbf{v}\times\mathbf{B}$ force and decelerated by collisions. Balancing these forces yields

$$-nZeB_p v_r \;=\; \frac{nmv_\parallel}{\tau_{\rm col}}\,, \tag{118}$$

for particles of charge Z and radial velocity v_r. Assuming that v_r arises from diffusion and using the ideal gas law $dp = dn\,k_B T$, Eq. (90) may be written as

$$nv_r \;=\; -D_{\rm banana}\frac{dn}{dr} \;=\; -\,\frac{D_{\rm banana}}{k_B T}\,\frac{dp}{dr} \tag{119}$$

The toroidal flow of particles creates an electric current density J_b:

$$\begin{aligned} J_b \;&=\; Zenv_\parallel \;=\; -\,\frac{(Ze)^2 nB_p v_r \tau_{\rm col}}{m} && \text{[using Eq. (118)]} \\ &=\; \frac{(Ze)^2 B_p \tau_{\rm col}}{m}\,\frac{D_{\rm banana}}{k_B T}\,\frac{dp}{dr} && \text{[using Eq. (119)]} \\ &=\; \left|\frac{dp}{dr}\right|\sqrt{\frac{a}{R}}\,\frac{1}{B_p} && \textbf{Bootstrap current} \end{aligned} \tag{120}$$

Equation (120) made use of Eqs. (116) and (105) as well as $r_c \equiv \sqrt{mk_BT}/(ZeB) \approx \sqrt{mk_BT}/(ZeB_t)$ (since $B_t \gg B_p$ typically). The toroidal current in Eq. (120) creates a poloidal magnetic field that compresses the plasma, steepening the pressure gradient $|dp/dr|$ and further increasing the current. Because of this positive feedback, the current is called the **bootstrap current**. As will be shown in Section 7.2, tokamaks require a toroidal plasma current, and the bootstrap current might provide most (but not all) of that current.

Figure 12 shows another way to view the bootstrap current. Trapped particles make a banana-shaped orbit in the poloidal direction and have the corresponding motion following the spiral field lines in the toroidal direction. Typically the particle density increases toward the central axis, so a banana orbit closer to the central axis has more particles than one further out. Where the two orbits intersect, there are more particles from the inner orbit traveling in one direction than from the outer orbit traveling in the other direction. This net flow of charged particles, caused by the density (or equivalently pressure) gradient, creates the bootstrap current in the toroidal direction.

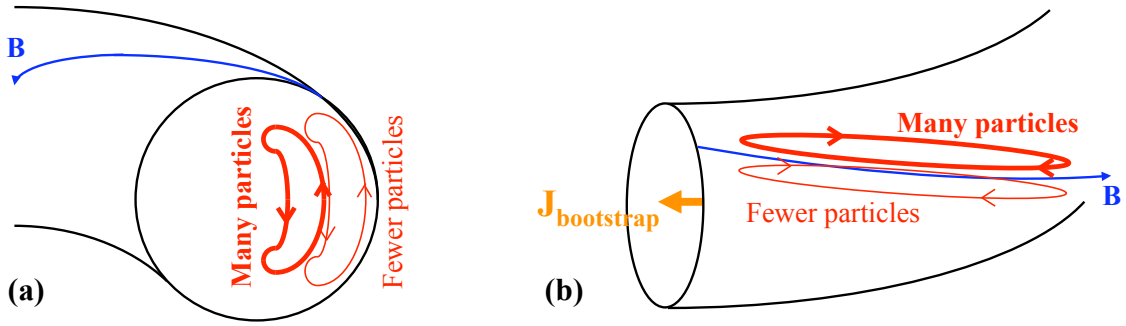

Figure 12. Bootstrap current. **(a)** Cross-sectional view and **(b)** side view. Typically the particle density increases with decreasing radial location, so inner banana orbits have more particles than outer banana orbits. Thus where inner and outer banana orbits overlap, there is a net flow of particles in one direction and hence an electric current, the toroidal bootstrap current $J_bootstrap$.

Plateau regime

Intermediate in collisionality between the banana and Pfirsch-Schlüter regimes,

$$\frac{q_s R}{v_t} < \tau_{\rm col} < \frac{q_s R}{v_t}\left(\frac{R}{a}\right)^{3/2} \qquad \textbf{Plateau regime} \tag{121}$$

trapped particles only have time to complete a fraction of a banana orbit on average before being scattered by a collision. The probability of completing a banana orbit is $\sim \tau_{\rm eff}/\tau_{\rm banana}$ and may be factored into the diffusion constant:

$$D_{\rm plateau} \sim \frac{\tau_{\rm eff}}{\tau_{\rm banana}} D_{\rm banana} \sim \frac{q_s r_c^2 v_t}{R} \qquad \textbf{Plateau diffusion} \tag{122}$$

Because this diffusion constant is independent of the collision time and thus forms a flat line in Fig. 11(a), this is called the plateau diffusion regime [8]. It is comforting to note that $D_{\rm plateau}$ in Eq. (122) matches both $D_{\rm PS}$ [Eq. (108)] evaluated at the boundary value $\tau_{\rm col} = q_s R/v_t$ and $D_{\rm banana}$ [Eq. (116)] at the boundary value $\tau_{\rm col} = (R/a)^{3/2} q_s R/v_t$.

3 Magnetohydrodynamics (MHD)

Magnetohydrodynamics (MHD) lumps ions and electrons together and treats a plasma like a single homogeneous fluid. While this simplification ignores much of the microscopic behavior of the plasma, it is very useful for analyzing macroscopic plasma phenomena. This section will present the basic principles of MHD and then use those to analyze macroscopic plasma behavior such as the forces on plasmas in magnetic confinement systems and instabilities of those plasmas.

3.1 MHD Equations

In MHD, the two-fluid equations for ions and electrons are combined together to treat the plasma as a single fluid with the following properties:

$$\rho \equiv n_i m_i + n_e m_e \approx n_i m_i \qquad \textbf{Mass density} \tag{123}$$

$$\rho_{\text{charge}} \equiv Z_i e n_i - e n_e \qquad \textbf{Charge density} \tag{124}$$

$$\mathbf{j} \equiv e(Z_i n_i \mathbf{v_i} - n_e \mathbf{v_e}) \qquad \textbf{Electric current} \tag{125}$$

$$\mathbf{v} \equiv \frac{n_i m_i \mathbf{v_i} + n_e m_e \mathbf{v_e}}{n_i m_i + n_e m_e} \approx \mathbf{v_i} \qquad \textbf{Fluid velocity} \tag{126}$$

$$p \equiv p_i + p_e = n_i k_B T_i + n_e k_B T_e \qquad \textbf{Pressure} \tag{127}$$

$$\eta \equiv \eta_e^{\parallel} \text{ [Eq. (94)] or } \eta_e^{\perp} \text{ [Eq. (98)]} \qquad \textbf{Electrical resistivity} \tag{128}$$

In this single-fluid model, the momentum equation becomes

$$\rho \left(\frac{\partial}{\partial t} + \mathbf{v} \cdot \nabla \right) \mathbf{v} = \mathbf{j} \times \mathbf{B} - \nabla p + \rho \mathbf{g} \qquad \textbf{Momentum equation} \tag{129}$$

Including the Lorentz force, Ohm's law may be written as

$$\mathbf{E} + \mathbf{v} \times \mathbf{B} = \eta \mathbf{j} \qquad \textbf{Ohm's law} \tag{130}$$

Conservation of mass takes the usual form for a fluid:

$$\frac{\partial \rho}{\partial t} + \nabla \cdot (\rho \mathbf{v}) = 0 \qquad \textbf{Conservation of mass} \tag{131}$$

Conservation of charge takes a similar form:

$$\frac{\partial \rho_{\text{charge}}}{\partial t} + \nabla \cdot \mathbf{j} = 0 \qquad \textbf{Conservation of charge} \tag{132}$$

For adiabatic compression, the MHD equivalent of Eq. (10) is

$$\frac{p}{\rho^\gamma} = \text{constant} \qquad \Longrightarrow \qquad dp = \gamma \frac{p}{\rho} d\rho \qquad \textbf{Adiabatic relation} \tag{133}$$

Using the ideal gas law for a plasma with volume V, Eq. (133) may be rewritten as

$$T V^{\gamma - 1} = \text{constant} \tag{134}$$

As shown by Eq. (134), a plasma may be heated by compressing it, for example by gravity (Section 5.3), implosion (Section 6.2), or magnetic fields (Section 7.3). The work pdV that is put into the plasma during compression raises the thermal energy.

If the plasma is incompressible, Eq. (131) becomes

$$\nabla \cdot \mathbf{v} = 0 \qquad \textbf{For incompressible fluid} \tag{135}$$

Strong time-varying electric fields are generally not important in MHD, so Ampère's law becomes

$$\nabla \times \mathbf{B} = \mu_o \mathbf{j} \qquad \textbf{Ampère's law for MHD} \tag{136}$$

For plasmas in equilibrium, terms involving $\partial/\partial t$, $\mathbf{v}$, and $\mathbf{E}$ may be neglected. Gravity is much weaker than the other forces of interest and may be ignored. Equation (129) may be simplified under these conditions to show that the particle pressure and magnetic forces must balance:

$$\nabla p = \mathbf{j}\times\mathbf{B} \qquad \textbf{Equilibrium pressure balance} \tag{137}$$

$$= \frac{1}{\mu_o}(\nabla\times\mathbf{B})\times\mathbf{B} \qquad \text{using Eq. (136)}$$

$$= -\nabla\frac{B^2}{2\mu_o} + \frac{(\mathbf{B}\cdot\nabla)\mathbf{B}}{\mu_o} \tag{138}$$

The first term in Eq. (138) describes the pressure $B^2/(2\mu_o)$ of a magnetic field. This is also the energy density of a magnetic field. (Energy per volume and force per area are equivalent units of measure.) In some respects, a magnetic field may be regarded as a massless gas with this pressure. The second term in Eq. (138) represents the tension force B^2/μ_o of magnetic field lines. If $\mathbf{B}$ does not vary along $\mathbf{B}$, this term is zero. In addition to the simple pressure they exert, magnetic field lines behave somewhat like rubber bands, trying to be as short and straight as possible.

A simple yet powerful implication of Eq. (137) is that in a plasma in equilibrium, the current and magnetic field are both perpendicular to the pressure gradient. In other words, they both lie on surfaces of constant pressure, no matter how complicated the geometry may be.

Neglecting the tension term, equilibrium at the boundary of a plasma with particle pressure p, internal magnetic pressure $B_{\text{int}}^2/(2\mu_o)$ and external magnetic pressure $B_{\text{ext}}^2/(2\mu_o)$ requires

$$p + \frac{B_{\text{int}}^2}{2\mu_o} = \frac{B_{\text{ext}}^2}{2\mu_o} \tag{139}$$

A useful quantity is β, defined as the ratio of particle pressure to external magnetic field pressure:

$$\beta \equiv \frac{\text{Particle pressure}}{\text{External magnetic pressure}} = \frac{n_i k_B T_i + n_e k_B T_e}{B_{\text{ext}}^2/2\mu_o}\,. \tag{140}$$

At typical fusion reactor temperatures, $\langle\sigma v\rangle$ increases like T_i^2, so the fusion power varies like

$$P_{\text{fus}} \propto n_i^2\langle\sigma v\rangle \propto n_i^2 T_i^2 \propto p^2 \propto \beta^2 B^4\,, \tag{141}$$

Increasing β allows a given magnetic field to confine more plasma and hence produce more fusion power. Because large electromagnets are expensive to build and/or operate, β should be as high as possible. Successful confinement requires $\beta \le 1$. For $T_i = T_e$ and $Z = 1$, this limits the density to

$$n_i = n_e \le 1.24\times10^{15}\,\frac{\beta B_T^2}{T_{\text{keV}}}\ \text{cm}^{-3} \tag{142}$$

For representative values $B = 20$ T and $T_i = T_e = 20$ keV, this density limit is $n_i = n_e < 2.5\times10^{16}$ cm^{-3}. As will be shown in Section 7.2, an internal magnetic field is necessary to prevent instabilities. This internal magnetic pressure takes away from potential internal plasma particle pressure and makes $\beta \ll 1$, significantly reducing the densities from the upper bounds calculated here.

A toroidal plasma tends to expand outward away from the central axis due to two forces. As shown in Fig. 13(a), poloidal magnetic field lines are bunched together along the inner edge of the torus and spaced out along the outer edge, creating a net outward difference in magnetic pressure called the **hoop force**. In addition, Fig. 13(b) shows that a torus has more surface area directed away from the central axis than toward it, so a uniform plasma pressure acting on these surfaces exerts a net outward force, named the **tire tube force** after its more commonplace manifestation. As illustrated in Fig. 13(c), a vertical magnetic field B_z must be applied to create an inward $\mathbf{J_t}\times\mathbf{B_z}$ force that counteracts these outward forces and holds the plasma in equilibrium [9].

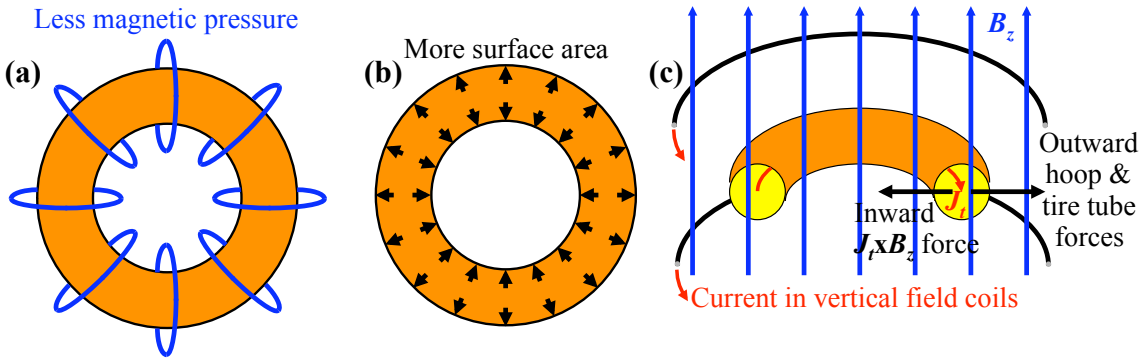

Figure 13. Magnetically confined toroidal plasmas require a vertical magnetic field for equilibrium. **(a)** Poloidal field lines are bunched together along the inner edge of the torus and spaced apart along the outer edge, creating a net outward difference in magnetic pressure, the hoop force. **(b)** A torus has more surface area directed away from the central axis than toward it, so the same plasma pressure acting on those surfaces produces a net outward force, the tire tube force. **(c)** Utilizing a vertical magnetic field B_z and a toroidal plasma current J_t creates an inward $J_t \times B_z$ force that balances the outward hoop and tire tube forces and holds the plasma in equilibrium.

The time variation of a magnetic field in a plasma may be found from Faraday's law. A simple form of Ohm's law, $\mathbf{E} = \eta \mathbf{j}$ (valid for $\mathbf{v} = 0$) may be used to rewrite Faraday's law:

$$\begin{aligned} \frac{\partial \mathbf{B}}{\partial t} &= -\nabla \times \mathbf{E} = -\nabla \times \eta \mathbf{j} \\ &= -\nabla \times \eta \left(\frac{\nabla \times \mathbf{B}}{\mu_o} \right) \qquad \text{using Eq. (136)} \\ &= \frac{\eta}{\mu_o} \nabla^2 \mathbf{B} = D_{\rm mag} \nabla^2 \mathbf{B} \qquad D_{\rm mag} \equiv \frac{\eta}{\mu_o} \end{aligned} \tag{143}$$

Equation (143) used Gauss's law, $\nabla \cdot \mathbf{B} = 0$, in evaluating $\nabla \times (\nabla \times \mathbf{B})$. Note that the final result takes the form of a diffusion equation. Magnetic field lines diffuse through a plasma with a diffusion constant $D_{\rm mag}$. Because plasmas have very low electrical resistivities, $D_{\rm mag}$ is very small, and magnetic field lines tend to be "frozen in place" within a plasma–they move with the plasma. For example, the resistivity from Eq. (98) for typical fusion plasma values of $T_e = 20$ keV and $\ln \Lambda = 20$ is $\eta = 7.2 \times 10^{-10}$ Ω-m. The time τ for a magnetic field line to diffuse a distance L is

$$\tau = \frac{L^2}{D_{\rm mag}} = \frac{\mu_o}{\eta} L^2 = 1700 \, L^2_{\rm meters} \ \text{sec} \, . \tag{144}$$

Diffusion across a typical plasma radius $L = 0.1$ m requires 17 seconds, much longer than the expected ~ 1 sec confinement time for a magnetic fusion plasma. To get the magnetic field lines inside the plasma in the first place, they must be present before the fuel becomes ionized.

Plasmas that are held in place by magnetic fields can find several ingenious ways of wiggling out of balance and dissipating their energy against the nearest material wall. In a cylindrical plasma as shown in Fig. 8(a), instabilities may take the general form

$$\text{Instability} \quad \propto \quad \exp[i(m\theta + kz)] \, . \tag{145}$$

One may also apply Eq. (145) to a toroidal plasma (Fig. 9) by letting z become the distance around the major circumference of the torus. A convenient way to classify MHD instabilities is by their mode number m. The following sections present simple analyses of the $m = 0$, $m = 1$, and $m \geq 2$ instabilities. For more detailed analysis of MHD equilibrium and instabilities, see [4, 9].

3.2 Sausage Instability

The $m = 0$ instability is a cylindrically symmetric mode called the **sausage instability**, since it causes a cylindrical plasma to pinch off in places and look like a string of sausages, as shown in Fig. 14(a) and (b). To understand the physical mechanism of the sausage instability, one can consider a cylindrical plasma with a sharp boundary at radius a and an axial current I_z flowing through it as illustrated in Fig. 14(a). The axial current creates a magnetic field B_θ around the plasma as shown in the figure. Using Ampère's law, the magnetic field strength just outside the plasma is

$$B_\theta \;=\; \frac{\mu_o I_z}{2\pi a}\,. \tag{146}$$

The outside pressure exerted on the plasma by this magnetic field is

$$P_{\text{outside}} \;=\; \frac{B_\theta^2}{2\mu_o} \;=\; \frac{\mu_o I_z^2}{8\pi^2 a^2}\,. \tag{147}$$

As shown by Eq. (147), if the radius a begins to constrict at some point along the plasma, the outside magnetic pressure will increase at that point. The increased pressure will cause the plasma to constrict even more, as plasma particles simply move to nearby unconstricted regions without offering much resistance. Thus the system is unstable to this sort of collapse.

This instability can be prevented by having a magnetic field B_z inside the plasma as shown in Fig. 15(a). Because magnetic field lines are trapped within the plasma, the axial magnetic flux $\pi a^2 B_z$ through the plasma remains constant regardless of changes in the plasma radius a. Therefore if the field strength is B_{zo} when $a = a_o$, the axial field strength B_z when a is allowed to vary is

$$B_z \;=\; \left(\frac{a_o}{a}\right)^2 B_{zo}\,. \tag{148}$$

Constricting the plasma will also constrict the B_z field lines, creating an internal magnetic pressure that opposes the constriction:

$$P_{\text{inside}} \;=\; \frac{B_z^2}{2\mu_o} \;=\; \frac{1}{2\mu_o}\left(\frac{a_o}{a}\right)^4 B_{zo}^2\,. \tag{149}$$

Using Eqs. (147) and (149), the net pressure $P_{\text{inside}} - P_{\text{outside}}$ changes with variations da in the plasma radius in the following way:

$$\frac{d(P_{\text{inside}} - P_{\text{outside}})}{da} \;=\; -\,\frac{2B_z^2 - B_\theta^2}{\mu_o a}\,. \tag{150}$$

For stability, a decrease in a should increase the pressure difference $P_{\text{inside}} - P_{\text{outside}}$, thereby opposing a further decrease in the radius. Thus stability requires

$$\frac{d(P_{\text{inside}} - P_{\text{outside}})}{da} \;<\; 0 \qquad \Longrightarrow \qquad \frac{B_\theta}{B_z} \;<\; \sqrt{2} \qquad \textbf{Requirement for preventing sausage instability} \tag{151}$$

This result is also valid for a toroidal plasma with the substitution $B_\theta \to B_p$ and $B_z \to B_t$.

During the sausage instability, the constricted radius moves inward very quickly (at roughly the ion thermal velocity) with the strong B_θ field following along right behind it. This large time-varying magnetic field at the constriction point can induce large electric fields there via Faraday's law. The large electric fields can accelerate ions to fusion energies; this was the cause of anomolous fusion reactions in some early plasma confinement systems. (This mechanism is not of interest for producing fusion energy, because much more energy is required to create the plasma, and then that energy is lost when the plasma is disrupted by the sausage instability.)

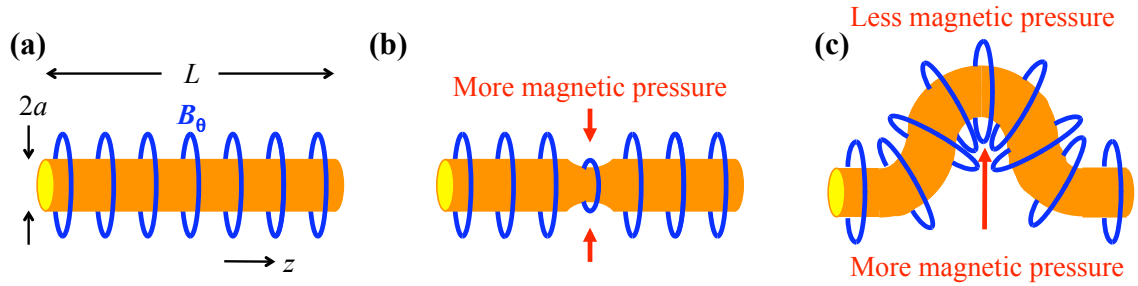

Figure 14. Sausage and kink instabilities. **(a)** A cylindrical column of plasma confined by a purely angular magnetic field B_θ (created by an axial current I_z in the plasma) is prone to instabilities. **(b)** In the sausage ($m = 0$) instability, a constriction in the plasma column increases the external magnetic pressure, causing even further constriction until the plasma pinches in two. **(c)** In the kink ($m = 1$) instability, a kink in the plasma column compresses B_θ on one side of the kink and relaxes it on the other side, causing a lateral pressure difference that pushes the plasma kink even further off axis until it hits the wall.

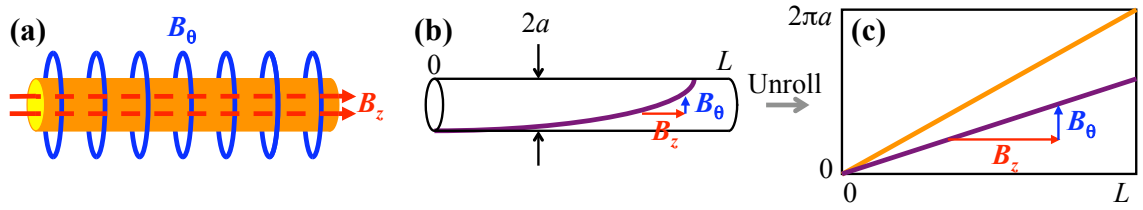

Figure 15. Adding an axial magnetic field B_z inside the plasma prevents the sausage and kink instabilities. **(a)** The pressure of B_z resists the pinching of the sausage instability, and the tension of the B_z field lines resists the bending of the kink instability. **(b)** At the plasma surface, the internal B_z and external B_θ add together to form a spiral magnetic field. **(c)** The cylindrical plasma surface may be "unrolled" to better visualize the spiral field. If the slope B_θ/B_z of the spiral magnetic field equals or exceeds the slope $2\pi a/L$ of the diagonal of the unrolled surface, the magnetic field will make at least one complete spiral over the length of the plasma and the kink instability can develop.

The phenomenon of a plasma current creating a magnetic field that helps confine or compress the plasma is called the **pinch effect** [9]. Z pinches like the above example use an axial plasma current I_z to create an angular field B_θ around the plasma, while theta pinches use an angular plasma current I_θ to produce an axial magnetic field. Screw or zeta pinches have plasma currents and magnetic fields with both axial and angular components. Magnetic fusion approaches such as tokamaks, reversed field pinches, and field reversed configurations use pinch-created magnetic fields in conjunction with magnetic fields created by external coils, as will be shown in Section 7.2.

3.3 Kink Instability

By definition, the $m = 1$ instability is an asymmetric mode that makes one complete cycle each time it spirals around a cylindrical plasma, as shown in Fig. 14(c). Because the cylindrical plasma is kinked to one side, this is called the **kink instability**. The physical mechanism of the instability is that if a kink in the plasma begins to form, the external B_θ lines will be compressed on one side of the kink and expanded on the other. This causes a difference in magnetic pressure across the kink (similar to the hoop force) which makes the instability grow worse. As with the sausage instability, adding internal axial field lines B_z will prevent the kink instability [Fig. 15(a)]. A kink would stretch the B_z lines; their tension strongly resists such stretching and thus stabilizes the plasma if B_z is strong enough.

The required strength of B_z may be found by considering a cylindrical plasma of length L and radius a with a sharp boundary. At the surface of the plasma, the internal B_z field and external B_θ field add together to create spiral magnetic field lines, as shown in Figure 15(b). If these lines complete at least one circle of the plasma over the entire length L, the kink instability can make one complete cycle and hence is permitted to develop.

The situation may be visualized more easily by "unrolling" the external surface of the cylindrical plasma as in Fig. 15(c) to form a rectangle of height $2\pi a$ and length L. The angular and axial magnetic fields add together to form field lines with slope B_θ/B_z. One complete spiral over the length of the cylinder corresponds to the diagonal of the rectangle, which has slope $2\pi a/L$. Therefore the stability requirement that the magnetic field lines not make a complete spiral means that the slope of the field lines should be less than the slope of the diagonal of the cylinder:

$$\frac{B_\theta}{B_z} < \frac{2\pi a}{L} \qquad \textbf{Kruskal-Shafranov condition to prevent kink instability in cylindrical plasma} \tag{152}$$

Using Eq. (146) to express B_θ in terms of the axial plasma current I_z that creates it, stability against the kink mode in a cylindrical plasma requires that the current be limited to

$$I_z < \frac{B_z}{\mu_o}\frac{(2\pi a)^2}{L} \qquad \textbf{Current limit to prevent kink instability in cylindrical plasma} \tag{153}$$

These results can be adapted to a toroidal plasma with major radius R and minor radius a using the substitutions $B_\theta \to B_p$, $B_z \to B_t$, $L \to 2\pi R$, and $I_z \to I_t$:

$$\frac{B_\theta}{B_z} < \frac{a}{R} \quad \text{or} \quad I_t < \frac{B_t}{\mu_o}\frac{2\pi a^2}{R} \qquad \textbf{Kruskal-Shafranov condition to prevent kink instability in toroidal plasma} \tag{154}$$

Equation (154) means that for stability, the safety factor from Eq. (105) (this is why it is called the safety factor) must be

$$q_s \equiv \frac{a}{R}\frac{B_t}{B_p} > 1 \qquad \textbf{Safety factor to prevent kink instability} \tag{155}$$

The diameter of cylindrical plasmas is typically much less than their length, $2a/L \le 1/3$, and a similar relationship is generally true for toroidal plasmas, $a/R \le 1/3$. Thus the stability conditions in Eqs. (152) and (154) are almost always more stringent than the condition (151) to prevent the sausage instability. A plasma that satisfies the Kruskal-Shafranov condition is generally stable against both $m = 0$ and $m = 1$ instabilities. One should also avoid rational values of the safety factor, $q_s = M/N$ where M and N are integers. For rational values, the field lines close on themselves after a certain number of trips around the torus, allowing instabilities to complete a cycle and grow.

If the plasma is very narrow and long, the axial B_z may not provide sufficient stability against kink modes. A kink with a wavelength much longer than the plasma radius r could deviate from the axis by an amount comparable to r without stretching the B_z lines enough to provide an adequate restoring force. Surrounding the plasma with an electrically conducting wall can stabilize such long-wavelength kink modes. A kink would compress the external magnetic field between the plasma kink and the wall, leading to an increased magnetic pressure that counteracts the kink.

Another stabilizing influence is magnetic shear, or a magnetic field whose direction varies with the radial position inside the plasma. The local magnetic field may provide a perfect environment for an instability to develop, but as the instability grows and reaches a larger radius, it will find a different magnetic field that inhibits its further growth.

3.4 Rayleigh-Taylor and Flute Instabilities

The **Rayleigh-Taylor instability** occurs when a heavy (high density) fluid is above a light (low density) fluid and both fluids are subject to a downward gravitational force or similar force due to acceleration, as shown in Fig. 16(a). A ripple at the boundary will grow larger and larger [Fig. 16(b)], letting some of the light fluid rise and some of the heavy fluid sink. Eventually, all of the heavy fluid will be below the light fluid.

As will be shown in Section 6, the Rayleigh-Taylor instability occurs in inertial confinement fusion. However, there is a similar instability in magnetically confined plasmas. MHD instability modes with $m \geq 2$ are called **flute instabilities**, because they make a cylindrical plasma look like a fluted column [Fig. 16(c)]. As will be explained shortly, the plasma acts like the heavy fluid and the external magnetic field acts like the light fluid, leading to instabilities at the plasma surface.

First the Rayleigh-Taylor instability will be analyzed. The instability grows exponentially with a growth rate γ that can be calculated using a simplified version of an original derivation by Chandrasekhar. Consider the situation in Fig. 16(a) where a heavy fluid of density ρ_1 occupies the space $z > 0$ and a light fluid of density ρ_2 fills the space $z < 0$. A downward gravitational acceleration g acts on both fluids, and the fluids are initially motionless.

A wavelike perturbation at the boundary between the fluids will perturb the local density and pressure by the amounts $\delta\rho$ and δp respectively. The perturbation will also introduce a nonzero velocity $\mathbf{v}$. The perturbation and its associated quantities will vary like

$$\delta\rho\ ,\ \ \delta p\ ,\ \text{ and }\ \mathbf{v}\ \ \propto\ \ \exp(ikx + \gamma t) \tag{156}$$

The MHD equations may be applied to this perturbation and simplified to first order in the perturbation. The x and z components of Eq. (129) become

$$\rho\gamma v_x \ = \ -ik\delta p \tag{157}$$

$$\rho\gamma v_z \ = \ -\frac{d}{dz}(\delta p) - \delta\rho g \tag{158}$$

Likewise, Eq. (136) reduces to

$$ikv_x + \frac{dv_z}{dz} \ = \ 0 \tag{159}$$

Using Eq. (136) for an incompressible plasma, Eq. (131) becomes

$$\gamma\,\delta\rho + v_z\frac{d\rho}{dz} \ = \ 0 \tag{160}$$

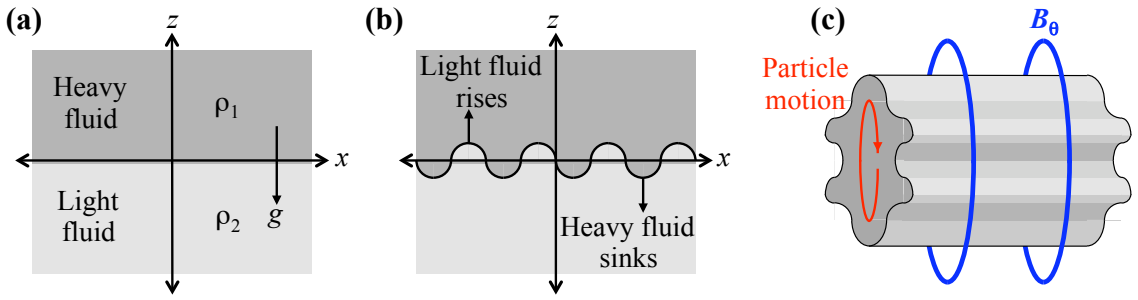

Figure 16. The Rayleigh-Taylor and flute instabilities. **(a)** A light fluid supporting a heavy fluid under gravitational or other acceleration is prone to the Rayleigh-Taylor instability. **(b)** A ripple at the boundary between the fluids grows larger and larger, allowing some of the heavy fluid to sink and some of the light fluid to rise, until all the heavy fluid is below the light fluid. **(c)** The flute ($m \geq 2$) instability in a plasma column is very similar, with the plasma as the heavy fluid and the external magnetic field as the light fluid. The centrifugal force of particles circling around the column plays the role of gravity. The resulting ripples at the surface make the plasma look like a fluted column.

Multiplying Eq. (157) by ik and using Eq. (159), one obtains

$$k^2 \delta p \;=\; \rho\gamma\, ikv_x \;=\; -\rho\gamma \frac{dv_z}{dz} \tag{161}$$

Combining Eqs. (158) and (160), one finds

$$\frac{d}{dz}\delta\rho \;=\; -\rho\gamma v_z + \frac{g}{\gamma}\frac{d\rho}{dz}v_z \tag{162}$$

Choosing either side of the boundary ($d\rho/dz = 0$) and eliminating δp between Eqs. (161-162) yields

$$\left(\frac{d^2}{dz^2} - k^2\right) v_z \;=\; 0 \qquad \Longrightarrow \qquad v_z \;=\; v_{zo} e^{-|k|z} \qquad \text{on both sides of boundary} \tag{163}$$

Thus v_z is maximum (v_{zo}) at the boundary and decreases exponentially with distance from the boundary, with a decay length comparable to the perturbation wavelength at the boundary ($\sim 1/k$).

It is convenient to define the difference in a quantity across the boundary:

$$\Delta_o(f) \;\equiv\; f(z = 0^+) - f(z = 0^-) \tag{164}$$

Applying Δ_o to both sides of Eq. (161) produces

$$k^2 \Delta_o(\delta p) \;=\; -\gamma \Delta_o\left(\rho \frac{dv_z}{dz}\right) \tag{165}$$

Similarly, applying Δ_o to Eq. (162) gives

$$\Delta_o(\delta p) \;=\; \frac{g}{\gamma} v_{zo} \Delta_o(\rho) \tag{166}$$

The instability growth rate γ may be found by combining Eqs. (165) and (166) to eliminate $\Delta_o(\delta p)$:

$$\begin{aligned} \Delta_o\left(\rho\frac{dv_z}{dz}\right) &= \frac{k^2}{\gamma^2} g v_{zo} \Delta_o(\rho) \\ \Longrightarrow \quad \gamma &= \sqrt{gk\left(\frac{\rho_1-\rho_2}{\rho_1+\rho_2}\right)} \qquad (167) \\ &= \sqrt{gk} \qquad \text{for } \rho_1 \gg \rho_2 \qquad (168) \end{aligned}$$

Although this derivation used the assumption of incompressible fluids for simplicity, Eqs. (167) and (168) also apply to compressible fluids.

The flute instability in a cylindrical plasma column is very similar to the Rayleigh-Taylor instability. In this case, the plasma and the magnetic field play the roles of the heavy and light fluids, respectively. The centrifugal force of plasma particles circling around the plasma column takes the place of gravity. Ripples develop at the plasma surface (just as they develop at the fluid boundary in the Rayleigh-Taylor instability), making the plasma look like a fluted column. The mode number m determines the number of bulges around the plasma column.

Because the flute instability is driven by the centrifugal force of plasma particles following curved magnetic field lines, it can be prevented with the proper curvature of the field lines. Lines that curve outward, like the B_θ lines surrounding the column in Fig. 16(c), generate centrifugal force that pulls the plasma outward into the "light fluid" of the magnetic field and leads to instability. In contrast, magnetic field lines that curve inward generate centrifugal force that pulls particles into the plasma, ensuring stability. Therefore, the magnetic confinement geometry should preferably have lines that curve inward (at least most of the time as seen by typical plasma particles). If lines must curve outward, the plasma can be at least partially stabilized by any factors that tend to blur the sharp boundary between the heavy plasma and light magnetic field fluids, such as a large cyclotron radius of the particle orbits about the magnetic field lines.

4 Waves in Plasmas

Although there is a whole zoo of waves that can occur in plasmas [1, 4], they may be separated into different cages based on whether they are electrostatic or electromagnetic, primarily involve electrons or ions, and propagate parallel, perpendicular to, or in the absence of a background magnetic field $\mathbf{B_0}$. In each case, it is important to find the **dispersion relation** between the wave's angular frequency ω and its wavevector $\mathbf{k}$.

4.1 Electrostatic Electron Waves

Electrostatic waves have an oscillating electric field but no oscillating magnetic field. Electrostatic electron waves, shown in Fig. 17(a), involve alternating compression and rarifaction of the electron density as the electrons oscillate longitudinally along $\mathbf{k}$, the direction the wave travels. At the high frequencies typical of these waves, inertia prevents the ions from moving much. Thus ions may be regarded as a fixed background of constant-density positive charge. There is excess negative charge in regions of electron compression and excess positive charge in regions of electron rarifaction.

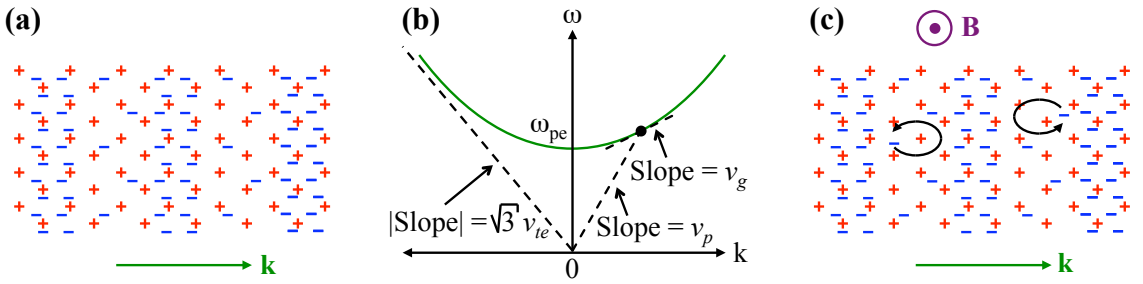

Figure 17. Electrostatic electron waves. (a) The electron density is alternately compressed and rarified, while the ion density remains approximately constant. **(b)** The dispersion relation for waves without (or parallel to) an applied magnetic field has a minimum frequency ω_{pe} and asymptotically approaches a slope $\sqrt{3}\,v_{te}$ at high frequencies. In any dispersion relation, for a wave of a given k (such as the point shown), the phase velocity v_p of the wave is the slope ω/k from the origin to that point and the group velocity v_g is the instantaneous slope $d\omega/dk$ at that point. **(c)** For waves perpendicular to an applied magnetic field, cyclotron motion acts as an additional restoring force for displaced electrons.

$\mathbf{B_0 = 0}$

The simplest case to analyze is one in which there is no externally applied magnetic field $\mathbf{B_0}$. Equations involving the electron density n, velocity v, pressure p, and electric field E may be linearized by treating the waves as small perturbations of a homogeneous background. A subscript 0 denotes a homogeneous equilibrium value, and subscript 1 denotes a small added perturbation:

$$n = n_0 + n_1 \qquad p = p_0 + p_1 \qquad v = v_1 \;\; (v_0 = 0) \qquad \mathbf{E} = \mathbf{E_1} \;\; (\mathbf{E_0} = 0) \tag{169}$$

The perturbations are assumed to vary in a typical wave fashion:

$$n_1,\ v_1,\ p_1,\ \text{and}\ \mathbf{E_1} \ \propto\ \exp[i(\mathbf{k}\cdot\mathbf{x} - \omega t)]\ . \tag{170}$$

Linearizing the continuity eq. (7) by substituting the expressions from Eq. (169) and keeping only terms that are first-order in the perturbed quantities, one finds

$$\frac{\partial n_1}{\partial t} + n_0 \nabla\cdot\mathbf{v_1} = 0 \qquad \Longrightarrow \qquad \frac{\partial^2 n_1}{\partial t^2} = -\,n_0 \nabla\cdot\frac{\partial \mathbf{v_1}}{dt}\ . \tag{171}$$

Similarly, the linearized Poisson equation is

$$\nabla\cdot\mathbf{E_1} = \frac{-e n_1}{\epsilon_o}\ . \tag{172}$$

The linearized adiabatic condition from Eq. (10) is

$$\nabla p_1 \;=\; \gamma \frac{p_0}{n_0} \nabla n_1 \;. \tag{173}$$

Now we have enough tools to linearize the momentum eq. (8) and show that it becomes a wave equation for the perturbation:

$$\begin{aligned}
m n_0 \frac{\partial \mathbf{v_1}}{\partial t} &= -e n_0 \mathbf{E_1} \;-\; \nabla p_1 \\
&= -e n_0 \mathbf{E_1} \;-\; \gamma \frac{p_0}{n_0} \nabla n_1 && \text{[using Eq. (173)]} \\
m n_0 \nabla \cdot \frac{\partial \mathbf{v_1}}{\partial t} &= -e n_0 \nabla \cdot \mathbf{E_1} \;-\; \gamma \frac{p_0}{n_0} \nabla^2 n_1 && \text{[taking } \nabla \cdot \text{ both sides]} \\
-m \frac{\partial^2 n_1}{\partial t^2} &= \frac{e^2 n_0}{\epsilon_o}\, n_1 \;-\; \gamma \frac{p_0}{n_0} \nabla^2 n_1 && \text{[using Eqs. (171) and (172)]} \qquad (174) \\
\omega^2 &= \omega_{pe}^2 \;+\; 3 v_{te}^2 k^2 && \text{[using Eq. (170) and } p_0 = n_0 k_B T_e] \qquad (175)
\end{aligned}$$

Because the waves adiabatically compress the electrons in one dimension, $\gamma = 3$ has been used. The first term on the right side of Eq. (175) derives from the electric field $\mathbf{E_1}$ and is simply the plasma oscillation restoring force discussed in Section 1.2. The second term represents the restoring force due to the pressure difference between compressed and rarified regions of the wave.

The dispersion relation from Eq. (175) is plotted in Fig. 17(b). For a wave with a particular wavevector k and frequency ω, such as the point indicated in Fig. 17(b), the phase velocity $v_p \equiv \omega/k$ of the wave is simply the slope of the line between the origin and that point. The group velocity $v_g \equiv d\omega/dk$ of the wave is the instantaneous slope of the dispersion curve at that point. One may regard the group velocity as how fast a wave actually moves through a plasma; the phase velocity is simply how fast phase ripples appear to be moving within the wave.

Figure 17(b) shows that waves with $\omega < \omega_{pe}$ do not propagate (electron Debye shielding screens them out), while electrostatic waves at high frequency asymptotically approach a velocity $\sqrt{3} v_{te}$.

$\mathbf{B_0} \neq \mathbf{0}$ and $\mathbf{k} \parallel \mathbf{B_0}$

For electrostatic waves moving along a magnetic field $\mathbf{B_0}$, $\mathbf{v_1} \parallel \mathbf{k} \parallel \mathbf{B_0}$, the magnetic field exerts no force, $\mathbf{v_1} \times \mathbf{B_0} = 0$. Thus the equations derived for $\mathbf{B_0} = 0$ still apply.

$\mathbf{B_0} \neq \mathbf{0}$ and $\mathbf{k} \perp \mathbf{B_0}$

Electrostatic electron waves moving perpendicular to $\mathbf{B_0} \equiv B_0 \hat{\mathbf{z}}$ are similar to the plasma oscillations discussed in Section 1.2, but with an added $\mathbf{v} \times \mathbf{B_0}$ restoring force. The magnetic field turns the simple oscillatory electron motion in the x direction into a cyclotron orbit in the $x - y$ plane [Fig. 17(c)]. Identifying the oscillation amplitude x with the cyclotron radius r_{ce}, the electron's velocity in the y direction is $v_y = \omega_{ce} x$. This creates a magnetic restoring force in the x direction:

$$F_x \;=\; -e v_y B_0 \;=\; -e B_0 \omega_{ce} x \tag{176}$$

Adding this restoring force in Eqs. (20) and (21) yields the electron equation of motion

$$\begin{aligned}
\frac{d^2 x}{dt^2} \;+\; (\omega_{pe}^2 + \omega_{ce}^2) x &= 0 \,, \quad \text{or} \\
\omega^2 \;=\; \omega_{pe}^2 + \omega_{ce}^2 &\equiv \omega_{uh}^2 \,,
\end{aligned} \tag{177}$$

in which ω_{uh} is called the **upper hybrid frequency**.

Waves at an arbitrary angle are generally a scary combination of the $\mathbf{k} \parallel \mathbf{B_0}$ and $\mathbf{k} \perp \mathbf{B_0}$ modes.

4.2 Electrostatic Ion Waves

Electrostatic ion waves occur at low enough frequencies that the ions can oscillate. Their charge drags the nimble electrons along with them, so that these waves involve alternating compression and rarifaction of both the ion and electron densities [Fig. 18(a)].

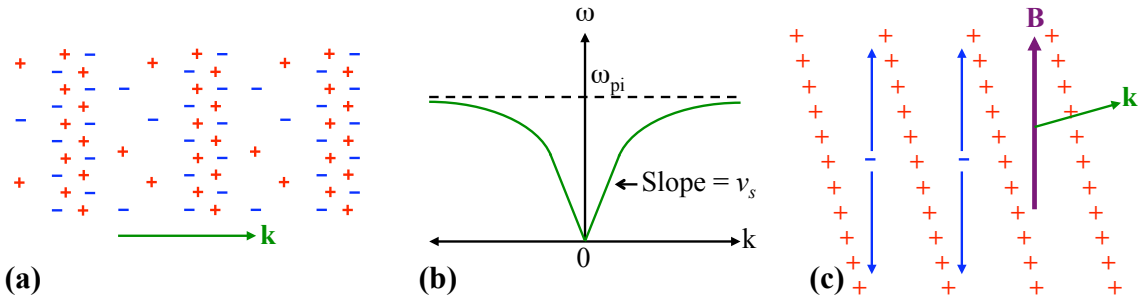

Figure 18. Electrostatic ion waves. **(a)** Ions and electrons move together as they are alternately compressed and rarified. **(b)** The dispersion relation has a velocity v_s at low frequencies and asymptotically approaches the ion plasma frequency ω_{pi}. **(c)** Electrons make tighter spirals than ions around magnetic field lines. When $\mathbf{k}$ is almost perpendicular to $\mathbf{B}$, the ions are free to oscillate parallel to $\mathbf{k}$, while the electrons must oscillate parallel to $\mathbf{B}$ as shown to follow the ions. When $\mathbf{k}$ is exactly parallel to $\mathbf{B}$, the electrons can no longer move between ion wavefronts in this fashion. Charge neutralization then constrains the ions to oscillate only the short distance that the electrons can perpendicular to $\mathbf{B}$.

$\mathbf{B_0 = 0}$

For electrostatic ion waves, Eq. (174) may be applied to ions by setting $m = m_i$ and $n_0 = n_i$. The term arising from E_1 may be neglected, since the electrons move to cancel out the ions' electric field. Pressure terms from both ions and electrons should be included, because both particle species are compressed. The result of these modifications is

$$\frac{\partial^2 n_1}{\partial t^2} = \frac{\gamma_i p_i + \gamma_e p_e}{n_i m_i}\nabla^2 n_1 = \frac{\gamma_i k_B T_i + Z\gamma_e k_B T_e}{m_i}\nabla^2 n_1 \qquad (n_e = Z n_i) \qquad \text{or}$$

$$\omega^2 = \frac{\gamma_i k_B T_i + Z\gamma_e k_B T_e}{m_i} k^2 \equiv v_s^2 k^2 \,, \quad \text{where} \tag{178}$$

$$v_s = \sqrt{\frac{\gamma_i k_B T_i + Z\gamma_e k_B T_e}{m_i}} \qquad \textbf{Speed of sound in plasma} \tag{179}$$

$$= 6.18 \times 10^5 \sqrt{\frac{m_p}{m_i}}\sqrt{T_{\rm keV}}\ \frac{\rm m}{\rm sec} \qquad \text{for } T \equiv T_i = T_e \text{ and } Z = 1 \tag{180}$$

v_s is called the speed of sound by analogy with sound waves in conventional fluids. The ions are adiabatically compressed in one dimension, so $\gamma_i = 3$ is used in Eq. (180). The isothermal value $\gamma_e = 1$ is used for electrons since they are much faster and have time to equalize their temperature. For typical fusion values of $m_i \sim 2m_p$ and $T = 20$ keV, the sound speed is $v_s \sim 2 \times 10^6$ m/sec.

The dispersion relation is linear at small k (long wavelengths) but asymptotically approaches the ion plasma frequency ω_{pi} at large k (short wavelengths), because the ions do not like to oscillate faster than ω_{pi}. This is illustrated in Fig. 18(b).

$\mathbf{B_0 \neq 0}$ and $\mathbf{k} \parallel \mathbf{B_0}$

As with electrostatic electron waves, a magnetic field exerts no force on electrostatic ion waves propagating parallel to the field, so the equations for the $\mathbf{B_0} = 0$ case may still be used.

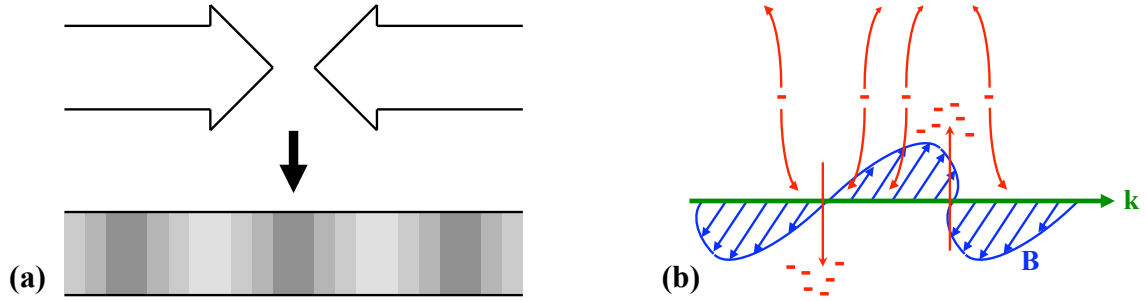

Figure 19. Anisotropic particle velocity distributions tend to cause instabilities that generate waves. (a) Two opposing streams of particles are prone to the counterstreaming instability, compressing the particles in regions and generating electrostatic waves. **(b)** Electrons (or ions) moving primarily in one dimension (say vertically) can trigger the Weibel instability. If a small perturbing wavelike magnetic field arises, it will bend the electrons trajectories so that downward- and upward-moving electrons separate into different "traffic lanes." These electric currents make the perturbing magnetic field grow. The currents dance around, so the magnetic field is actually part of a full-fledged electromagnetic wave. Such instabilities can be prevented by minimizing anisotropy in particle velocity distributions.

$\mathbf{B_0 \neq 0}$ and k almost $\perp \mathbf{B_0}$

The $\mathbf{v} \times \mathbf{B_o}$ magnetic restoring force added a term ω_{ce}^2 to the dispersion relation for electrostatic electron waves propagating perpendicular to $\mathbf{B_0}$. For the same reasons, an electrostatic ion wave traveling almost perpendicular to $\mathbf{B_0}$ should have a term ω_{ci}^2 added to Eq. (178):

$$\omega^2 \;=\; \omega_{ci}^2 \;+\; v_s^2 k^2 \;. \tag{181}$$

The qualification that $\mathbf{k}$ is *almost* perpendicular to $\mathbf{B_0}$ requires explanation. Because electrons have a much smaller cyclotron radius than ions, it is much more difficult for them to oscillate perpendicular to magnetic field lines. In this case, the ions oscillate along $\mathbf{k}$ as they are alternately compressed and rarified as usual. However, the magnetic field prevents the electrons from oscillating much in that direction, so they must travel back and forth along the field lines to neutralize the ion charge in each wavefront [Fig. 18(c)]. Electrons are much faster than ions, $v_{te} \gg v_{ti}$, and thus are fast enough to travel the longer distances required to do this.

$\mathbf{B_0 \neq 0}$ and k exactly $\perp \mathbf{B_0}$

When $\mathbf{k}$ is exactly perpendicular to $\mathbf{B_0}$, electrons can no longer travel between ion wavefronts by moving along the field lines. Buildup of unneutralized space charge prevents the ions from oscillating perpendicular to $\mathbf{B_0}$ more than the electrons can, and the electrons can only move as much as cyclotron motion allows. Expressing this constraint as $v_{i1} = v_{e1} = \omega_{ce} x$, one finds

$$\begin{aligned} m_i \frac{d^2x}{dt^2} \;&=\; Zev_{iy}B_o \;=\; \omega_{ce} ZeB_o x \;, \quad \text{or} \\ \omega^2 \;&=\; \omega_{ce}\omega_{ci} \;\equiv\; \omega_{lh}^2 \qquad\qquad \omega_{lh} = \textbf{lower hybrid frequency} \end{aligned} \tag{182}$$

Counterstreaming instability

When two opposing particle beams intersect (or equivalently, when a beam passes through a stationary plasma), regions of the beams can be momentarily compressed, triggering ion or electron electrostatic waves [Fig. 19(a)]. The beams give energy to the waves, which grow exponentially from this counterstreaming instability until they disrupt the beams. Since strongly anisotropic particle velocity distributions are the root of this problem, the best solution is to have approximately isotropic distributions whenever possible, especially when the particle density is high. Anisotropic velocity distributions can also produce electromagnetic waves [Fig. 19(b) and Section 4.3].

4.3 Electromagnetic Electron Waves

Electromagnetic waves have an oscillating magnetic field $\mathbf{B_1}$ as well as an oscillating electric field $\mathbf{E_1}$. When they travel through a plasma, their electric field drags particles back and forth [Fig. 20(a)]. Usually the affected particles are electrons, since most electromagnetic waves have frequencies too high for much ion motion. The electric current of these moving particles in turn modifies the waves.

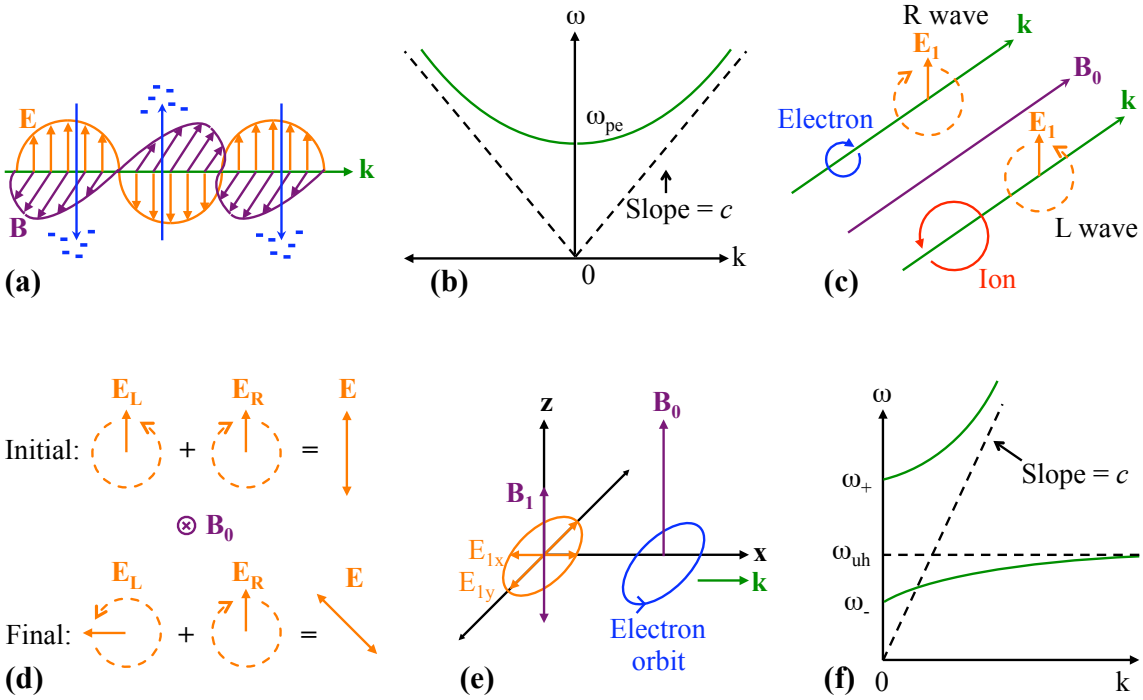

Figure 20. Electromagnetic electron waves. **(a)** When an electromagnetic wave travels through a plasma, its oscillating electric field drags electrons back and forth. **(b)** The interaction with electrons alters the usual dispersion relation of electromagnetic waves so that waves with $\omega < \omega_{pe}$ cannot propagate. At high frequencies the electrons cannot move much and the wave velocity approaches the usual c. **(c)** Electromagnetic waves with right- (R) or left-handed (L) circular polarization can propagate along an applied magnetic field $\mathbf{B}_0$. Electrons spiral around $\mathbf{B}_0$ in the same direction as R waves, and ions spiral in the same direction as L waves. **(d)** Plane-polarized waves may be regarded as the sum of L and R waves. After traveling through a plasma at their different velocities, the L and R waves have different relative phases, causing Faraday rotation of their composite plane wave. **(e)** An electromagnetic X wave travels perpendicular to $\mathbf{B}_0$ with its oscillating magnetic field parallel to $\mathbf{B}_0$. The waves oscillating electric field has both transverse (E_{1y}) and longitudinal (E_{1x}) components, making an ellipse during each wave cycle. **(f)** X waves with $\mathbf{E}_1$ rotating in the opposite direction as the electrons can propagate with frequencies $\omega > \omega_+$. Waves with $\mathbf{E}_1$ rotating in the same direction as the electrons must have frequencies $\omega_{uh} > \omega > \omega_-$.

$\mathbf{B_0 = 0}$

In the simplest case there is no externally applied magnetic field $\mathbf{B_0}$. Newton's second law for an electron with velocity $\mathbf{v_1}$ oscillating in the electric field of an electromagnetic wave is

$$m_e \frac{\partial \mathbf{v_1}}{\partial t} = -e\mathbf{E_1} \tag{183}$$

The electric current density due to moving electrons is $\mathbf{j_1} = -en_e\mathbf{v_1}$. Differentiating this with respect to time and using Eqs. (183) and (22) yields

$$\frac{\partial \mathbf{j_1}}{\partial t} \;=\; -en_e\frac{\partial \mathbf{v_1}}{\partial t} \;=\; \frac{e^2 n_e}{m_e}\mathbf{E_1} \;=\; \epsilon_o\omega_{pe}^2\mathbf{E_1} \tag{184}$$

Ampère's law for the electromagnetic wave may be written as

$$\frac{1}{\mu_o}\nabla\times\mathbf{B_1} \;=\; \epsilon_o\frac{\partial \mathbf{E_1}}{\partial t} \;+\; \mathbf{j_1} \tag{185}$$

Differentiating Eq. (185) with respect to time, one finds

$$\frac{1}{\mu_o}\nabla\times\frac{\partial \mathbf{B_1}}{\partial t} \;=\; \epsilon_o\frac{\partial^2 \mathbf{E_1}}{\partial t^2} \;+\; \frac{\partial \mathbf{j_1}}{\partial t} \;=\; \epsilon_o\left(\frac{\partial^2}{\partial t^2} \;+\; \omega_{pe}^2\right)\mathbf{E_1} \qquad \text{[using Eq. (184)]} \tag{186}$$

$$\;=\; \epsilon\frac{\partial^2 \mathbf{E_1}}{\partial t^2} \qquad\qquad \epsilon \;\equiv\; \epsilon_o\left(1-\frac{\omega_{pe}^2}{\omega^2}\right) \tag{187}$$

where Eq. (187) used the wave substitution $\partial/\partial t \to -i\omega$.

Faraday's law for the electromagnetic wave is

$$\frac{\partial \mathbf{B_1}}{\partial t} \;=\; -\nabla\times\mathbf{E_1} \tag{188}$$

Taking $\nabla\times$ both sides of Eq. (188) and using $\nabla\cdot\mathbf{E_1}=0$ for transverse waves produces

$$\nabla\times\frac{\partial \mathbf{B_1}}{\partial t} \;=\; -\nabla\times(\nabla\times\mathbf{E_1}) \;=\; \nabla^2\mathbf{E_1}-\nabla(\nabla\cdot\mathbf{E_1}) \;=\; \nabla^2\mathbf{E_1} \tag{189}$$

Finally, combining Eqs. (186) and (189) and using $\mu_o\epsilon_o = 1/c^2$, $\partial/\partial t \to -i\omega$, and $\nabla \to i\mathbf{k}$ gives

$$\left(\frac{\partial^2}{\partial t^2} \;+\; \omega_{pe}^2\right)\mathbf{E_1} \;=\; c^2\nabla^2\mathbf{E_1} \qquad\Longrightarrow\qquad \omega^2 \;=\; \omega_{pe}^2 \;+\; c^2k^2 \tag{190}$$

This dispersion relation is plotted in Fig. 20(b). Like electrostatic electron waves, electromagnetic waves with frequencies less than the cutoff frequency ω_{pe} cannot propagate. At high frequencies the electrons' inertia prevents them from moving much, so the wave more closely resembles an electromagnetic wave in the vacuum and its velocity approaches c. Note from Eq. (187) that the permittivity of a plasma is less than that of the vacuum and is actually negative for $\omega < \omega_{pe}$.

Electromagnetic waves with $\omega < \omega_{pe}$ simply reflect off a plasma, and this has many physical implications. Radio waves with frequencies less than the ω_{pe} of the ionosphere surrounding the earth can be transmitted from the ground and bounced off the ionosphere to distant locations on the earth. A spacecraft re-entering the earth's atmosphere heats the air before it into a plasma shockwave that blocks radio communication between the spacecraft and the ground. Ordinary metals are reflective at optical frequencies because their free electrons act like a dense plasma. Plasma density can be measured by determining the cutoff frequency or dispersion relation of electromagnetic waves launched into the plasma.

$\mathbf{B_0} \neq \mathbf{0}$ and $\mathbf{k} \parallel \mathbf{B_0}$

Electromagnetic waves traveling parallel to an applied magnetic field $\mathbf{B_0}$ are affected by electrons spiraling around $\mathbf{B_0}$, so the natural modes to consider are right- (R) and left-handed (L) circularly polarized waves. The electron positions r_1 and wave fields E_1 and B_1 may be written using complex notation, with an exponential sign that is positive for R waves and negative for L waves:

$$r_1 \;\equiv\; x_1 \;+\; iy_1 \;=\; r_{1o}\,\exp[\pm i(kz-\omega t)] \tag{191}$$

$$E_1 \;\equiv\; E_{1x}+iE_{1y} \;=\; E_{1o}\,\exp[\pm i(kz-\omega t)] \tag{192}$$

$$B_1 \;\equiv\; B_{1x}+iB_{1y} \;=\; B_{1o}\,\exp[\pm i(kz-\omega t)] \tag{193}$$

In this notation, Newton's second law for the Lorentz force on electrons becomes

$$m_e \frac{\partial^2 r_1}{\partial t^2} \;=\; ieB_0 \frac{\partial r_1}{\partial t} \;-\; eE_1 \qquad\qquad \Longrightarrow \qquad\qquad \frac{m_e}{e}\, r_{1o} \;=\; \frac{E_{1o}}{\omega^2 \pm \omega\omega_{ce}} \tag{194}$$

Likewise, Faraday's law from Eq. (188) becomes

$$i\frac{\partial B_1}{\partial t} \;=\; \frac{\partial E_1}{\partial z} \qquad\qquad \Longrightarrow \qquad\qquad B_{1o} \;=\; \frac{ik}{\omega} E_{1o} \tag{195}$$

With the same notation, Ampère's law from Eq. (185) is

$$c^2 \frac{\partial B_1}{\partial z} \;=\; -\frac{\partial E_1}{\partial t} \;+\; i\,\frac{en_e}{\epsilon_o}\,\frac{\partial r_1}{\partial t} \qquad\qquad \Longrightarrow \qquad\qquad c^2 k B_{1o} \;=\; i\omega E_{1o} - i\omega\omega_{pe}^2 \frac{m_e}{e} r_{1o} \tag{196}$$

Substituting Eqs. (194) and (195) into Eq. (196) to express everything in terms of E_{1o}, one finds

$$\omega^2 \;=\; \frac{\omega_{pe}^2}{1 \pm \omega_{ce}/\omega} \;+\; c^2k^2 \qquad \begin{matrix} + \text{ sign for L waves} \\ - \text{ sign for R waves} \end{matrix} \tag{197}$$

For $\mathbf{B_0} \to 0$ ($\omega_{ce} \to 0$), Eq. (197) just reduces to Eq. (190). With or without $\mathbf{B_0}$, the ω_{pe}^2 term arises from the oscillating electrons that interact with the wave. For waves traveling along a nonzero $\mathbf{B_0}$, this term is modified because the electrons also orbit around $\mathbf{B_0}$ at the cyclotron frequency ω_{ce}. R waves rotate the same way as the electrons, and L waves rotate the other way, as shown in Fig. 20(c). Note that Eq. (197) blows up for R waves with $\omega = \omega_{ce}$ since the wave's electric field rotates in the same direction and at the same frequency as the electrons, continually transferring energy from the wave to the electrons. If ions had been included in the analysis, one would similarly have found that L waves with $\omega = \omega_{ci}$ resonate with ions (which orbit in the opposite direction from electrons), continually giving wave energy to the ions. This phenomenon is called **electron or ion cyclotron resonance heating** and is used to selectively heat electrons or ions in plasmas.

A plane-polarized electromagnetic wave may be regarded as a superposition of L and R waves, as depicted in Fig. 20(d). Due to their different dispersion relations, L and R waves of a given frequency have different velocities. Therefore L and R waves will have different relative phases after propagating through a plasma, and hence their sum will be a wave whose plane of polarization has rotated. This is called **Faraday rotation**; see the optics summary for more information.

$\mathbf{B_0} \neq \mathbf{0}$, $\mathbf{k} \perp \mathbf{B_0}$, and $\mathbf{E_1} \parallel \mathbf{B_0}$

By adding a vertical applied field $\mathbf{B_0}$ to Fig. 20(a), one can picture electromagnetic waves traveling perpendicular to $\mathbf{B_0}$ with $\mathbf{E_1}$ parallel to $\mathbf{B_0}$. Because electrons sloshing up and down in the vertical $\mathbf{E_1}$ electric field experience no $\mathbf{v} \times \mathbf{B_0}$ force from the vertical $\mathbf{B_0}$ magnetic field, $\mathbf{B_0}$ does not affect the waves. The waves in this situation are called **ordinary or O waves**, since their dispersion relation is the same as Eq. (190) for electromagnetic waves with no $\mathbf{B_0}$.

$\mathbf{B_0} \neq \mathbf{0}$, $\mathbf{k} \perp \mathbf{B_0}$, and $\mathbf{E_1} \perp \mathbf{B_0}$

In contrast to O waves, electromagnetic waves traveling perpendicular to $\mathbf{B_0}$ but with $\mathbf{E_1}$ perpendicular to $\mathbf{B_0}$ are modified by the applied magnetic field; they are called **extraordinary or X waves**. As illustrated in Fig. 20(e), $\mathbf{B_0}$ may be defined as pointing in the z direction and $\mathbf{k}$ in the x direction. The transverse electric field of the wave will then point in the y direction, E_{1y}. As usual, this electric field makes electrons move back and forth. However, the perpendicular magnetic field converts this oscillatory electron motion in the y direction into cyclotron orbits in the $x-y$ plane. The electron motion in the x direction creates a second electric field component E_{1x} associated with the wave. Thus X waves have both a tranverse electric field E_{1y} (like other electromagnetic waves) and a longitudinal electric field E_{1x} (more like electrostatic waves). Because X waves also have an oscillating magnetic field B_1, they are still classified among the electromagnetic waves.

With the usual wave substitution $\partial/\partial t \rightarrow -i\omega$, Newton's second law from Eq. (1) may be rewritten:

$$-im_e\omega v_{1x} \;=\; -e(E_{1x} + v_{1y}B_0) \qquad\qquad -im_e\omega v_{1y} \;=\; -e(E_{1y} - v_{1x}B_0) \tag{198}$$

Solving Eqs. (198) for v_{1x} and v_{1y}, one finds

$$v_{1x} = \frac{e}{m_e\omega}\left(-iE_{1x} - \frac{\omega_{ce}}{\omega}E_{1y}\right)\left(1 - \frac{\omega_{ce}^2}{\omega^2}\right)^{-1} \qquad v_{1y} = \frac{e}{m_e\omega}\left(-iE_{1y} + \frac{\omega_{ce}}{\omega}E_{1x}\right)\left(1 - \frac{\omega_{ce}^2}{\omega^2}\right)^{-1} \tag{199}$$

Using $\mathbf{j_1} = -en_e\mathbf{v_1}$ and wave substitutions $\partial/\partial t \rightarrow -i\omega$ and $\nabla \rightarrow i\mathbf{k}$, Eq. (186) may be written as

$$\frac{\omega}{\mu_o}\mathbf{k}\times\mathbf{B_1} \;=\; -\epsilon_o\omega^2\mathbf{E_1} - i\omega\mathbf{j_1} \;=\; -\epsilon_o\omega^2\mathbf{E_1} + ien_e\omega\mathbf{v_1} \tag{200}$$

Keeping the longitudinal term $\nabla\cdot\mathbf{E_1} = ikE_{1x}$, Eq. (189) may be expressed as

$$\omega\mathbf{k}\times\mathbf{B_1} \;=\; -k^2\mathbf{E_1} + \mathbf{k}kE_{1x} \tag{201}$$

Combining Eqs. (200) and (201) produces

$$c^2(-k^2\mathbf{E_1} + \mathbf{k}kE_{1x}) \;=\; \omega^2\mathbf{E_1} + i\frac{en_e}{\epsilon_o}\omega\mathbf{v_1} \tag{202}$$

Using Eq. (199), $\omega_{pe} \equiv n_e e^2/m_e\epsilon_o$, and $\omega_{ce} \equiv eB_0/m_e$, the x and y components of Eq. (202) are

$$i\frac{\omega_{pe}^2\omega_{ce}}{\omega}E_{1x} \;=\; \left[(\omega^2 - c^2k^2)\left(1 - \frac{\omega_{ce}^2}{\omega^2}\right) - \omega_{pe}^2\right]E_{1y} \tag{203}$$

$$-i\frac{\omega_{pe}^2\omega_{ce}}{\omega}E_{1y} \;=\; \left[\omega^2\left(1 - \frac{\omega_{ce}^2}{\omega^2}\right) - \omega_{pe}^2\right]E_{1x} \tag{204}$$

After combining Eqs. (203) and (204) to write everything in terms of E_{1x}, some algebra yields

$$\omega^2 \;=\; c^2k^2 \;+\; \omega_{pe}^2\,\frac{\omega^2 - \omega_{pe}^2}{\omega^2 - \omega_{uh}^2} \tag{205}$$

Because the oscillating E_{1x} and E_{1y} fields are 90^o out of phase with each other, their sum $\mathbf{E_1}$ is field that moves in an ellipse in the $x-y$ plane [Fig. 20(e)]. It can move either in the same direction or the opposite direction as the orbiting electrons, so the cutoff frequency at which X waves cease to propagate [$k = 0$ in Eq. (205)] assumes different values for the two cases:

$$\omega_\pm \;\equiv\; \frac{1}{2}\left(\pm\omega_{ce} + \sqrt{\omega_{ce}^2 + 4\omega_{pe}^2}\,\right) \tag{206}$$

Equation (205) blows up for $\omega = \omega_{uh}$; at this frequency, $\mathbf{E_1}$ rotates in the same direction at the same frequency as electrons in electrostatic upper hybrid oscillations (177), so the X wave's energy is efficiently absorbed and converted to such oscillations. X waves can only propagate for $\omega_{>}\omega_{+}$ and $\omega_{uh} > \omega > \omega_{-}$, as shown in Fig. 20(f).

Weibel instability

Just as anisotropic particle velocity distributions can lead to electrostatic wave instabilities like the counterstreaming instability, they can also cause electromagnetic wave instabilities. The **Weibel instability** is a good example and is illustrated in Fig. 19(b). This phenomenon is triggered by particles moving primarily in one dimension, such as the electrons moving vertically in the figure. If a wavelike perturbing magnetic field arises, it will produce $\mathbf{v}\times\mathbf{B}$ forces that bend the particle trajectories, separating them into separate "traffic lanes" of particles moving up versus down. These traffic lanes are net electric currents that reinforce the perturbing magnetic field. The currents tend to dance around, so the magnetic field is actually part of an electromagnetic wave. As with the counterstreaming instability, the wave feeds off the anisotropy and grows exponentially until it disrupts the velocity distributions. The simplest way to avoid such instabilities is to avoid highly anisotropic velocity distributions, especially when the plasma is very dense.

4.4 Electromagnetic Ion Waves

$\mathbf{B_0 = 0}$

The very nature of electromagnetic ion waves involves an applied magnetic field $\mathbf{B_0}$ [Fig. 21], as will be shown by the following cases; they cannot propagate without such a field.

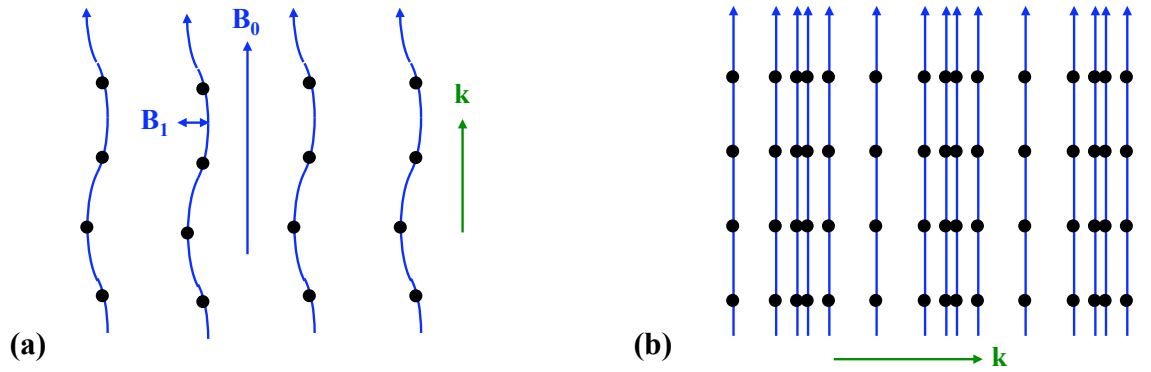

Figure 21. Electromagnetic ion waves. **(a)** Alvén waves, which propagate parallel to an applied magnetic field $\mathbf{B}_0$, create transverse oscillations of the field lines. Particles (dots) stay with the field lines, so the lines oscillate like strings having the magnetic field tension and the particle mass density. **(b)** Magnetosonic waves, which propagate perpendicular to an applied field $\mathbf{B}_0$, alternately compress and rarify both the particles (like electrostatic ion waves) and the field lines.

$\mathbf{B_0 \neq 0}$ and $\mathbf{k \parallel B_0}$

Electromagnetic ion waves propagating along $\mathbf{B_0}$ are called **Alvén waves**. They have an oscillating magnetic field $\mathbf{B_1}$ in the transverse direction, so the net field $\mathbf{B_0 + B_1}$ looks like the $\mathbf{B_0}$ field lines vibrating from side to side with the small perturbation $\mathbf{B_1}$ [Fig. 21(a)]. As explained in Section 3.1, the tension of magnetic field lines is B_0^2/μ_o. Because the ions tend to follow the vibrating field lines, they effectively impart their mass density $m_i n_i$ to the lines. (The electron mass density is negligible in comparison.) Therefore, the magnetic field lines may be treated as vibrating strings with these values of tension and mass density. Borrowing the results for transverse waves on strings from classical mechanics, the electromagnetic ion waves obey

$$\omega^2 \;=\; \frac{\text{Tension/cross sectional area}}{\text{Mass/volume}}\,k^2 \;=\; \frac{B_0^2}{\mu_o m_i n_i}\,k^2 \;\equiv\; v_A^2\,k^2 \tag{207}$$

$$v_A \;\equiv\; \frac{B_0}{\sqrt{\mu_o m_i n_i}} \;=\; 2.18\times 10^{13}\,\frac{1}{\sqrt{n_{\text{i, cm}^{-3}}}}\sqrt{\frac{m_p}{m_i}}\,B_T\;\;\frac{\text{m}}{\text{sec}} \qquad \textbf{Alfvén wave velocity} \tag{208}$$

For typical magnetic fusion plasmas with $n_i \sim 10^{14}$ cm^{-3} and $B \sim 10$ T, $v_A \sim 10^7$ m/sec.

$\mathbf{B_o \neq 0}$ and $\mathbf{k \perp B_o}$

Whereas Alvén waves cause transverse vibrations of the $\mathbf{B_0}$ field lines, electromagnetic ion waves propagating perpendicular to $\mathbf{B_0}$ cause compression and rarifaction of the field lines, as shown in Fig. 21(b). The compression is opposed not only by the ion and electron pressures (as in electrostatic ion waves) but also by the magnetic pressure $p_m = B_0^2/2\mu_o$. Because of the similarity to sound waves, these are called **magnetosonic waves**. Including the magnetic pressure in Eq. (178) and assuming that the magnetic field is compressed in two dimensions ($\gamma_m = 2$), one finds

$$\omega^2 \;=\; \frac{\gamma_i p_i + \gamma_e p_e + \gamma_m p_m}{n_i m_i}k^2 \;=\; \left(\frac{\gamma_i k_B T_i + Z\gamma_e k_B T_e}{m_i} + \frac{B_0^2}{\mu_o n_i m_i}\right)k^2 \;=\; (v_s^2 + v_A^2)k^2\;,\;\text{or}$$

$$v \;=\; \sqrt{v_s^2 + v_A^2} \qquad \textbf{Magnetosonic wave velocity} \tag{209}$$

5 Stellar Fusion

Stars are natural fusion reactors and exhibit a wide range of plasma physics phenomena, so they are worth analyzing in some detail. By considering the basic physics of hydrostatic equilibrium and energy transport, we will calculate the temperature, pressure, luminosity, and other properties of stars. The fusion reactions that can occur in stars will then be considered in light of these physical conditions. Moreover, processes attending the births and deaths of stars will be discussed. Finally, all of these calculations will be compared with observed data for stars.

5.1 Hydrostatic Equilibrium

The temperatures, pressures, and other properties of stars may be calculated simply by considering hydrostatic equilibrium, the balance of inward and outward forces within stars. A good place to begin is to find the mean mass density $\overline{\rho}$; for a spherical star of mass M and radius R, this is just

$$\overline{\rho} \;=\; \frac{3M}{4\pi R^3}\,. \tag{210}$$

Using observed values for the sun's mass $M_\odot = 1.989\times10^{30}$ kg and radius $R_\odot = 6.96\times10^8$ m, one finds a mean solar density of $\overline{\rho_\odot} = 1.41$ g/cm^3. This is 1.41 times the density of water and 20 times the density of cryogenic uncompressed liquid hydrogen. The peak density in the center of the sun is approximately 70 times higher than this mean density, as will be calculated shortly.

If almost all of the matter in the star is protons and electrons, the proton density n_p may be found from the stellar mass density and the atomic mass $m_{_H}$ of hydrogen. (Stars usually contain quite a bit of helium, but the pure-hydrogen assumption is fine for now.)

$$n_p \;\approx\; \rho/m_{_H}\,. \tag{211}$$

Using $\overline{\rho_\odot}$ for the sun, the mean proton density is $\overline{n_p} \approx 8.5\times10^{23}$ cm^{-3}. The electron density is

$$n_e \approx n_p \qquad\qquad \text{(neglecting ions other than protons)} \tag{212}$$

If a star is neither collapsing nor expanding, the inward and outward forces within it must balance. Consider a thin shell of radius r and thickness dr within the star, as shown in Fig. 22(a). Gravitational attraction between the matter in the shell and all the matter deeper inside the star creates an inward force per area on the shell of $G\rho(r)m(r)dr/r^2$, where $G \approx 6.67\times10^{-11}$ m^{3}kg^{-1}sec^{-2} is Newton's gravitational constant, $\rho(r)$ is the density of the shell, and $m(r)$ is the stellar mass inside the radius r. This causes the pressure to increase as one goes further into the star, and this pressure difference between the inside and outside of the shell creates a net outward force per area of $-(dp/dr)dr$. Balancing these outward and inward forces yields the equation,

$$-\frac{dp}{dr} \;=\; \frac{G\,\rho(r)\,m(r)}{r^2} \qquad\qquad \textbf{Hydrostatic equilibrium} \tag{213}$$

$$\text{where}\;\; m(r) \;=\; \int_0^r \rho(r')\,4\pi r'^2 dr' \tag{214}$$

Equations (213) and (214) are coupled together, and the situation is further complicated by the dependence of $\rho(r)$ on the pressure and temperature, both of which are functions of the radius. One can only solve these coupled equations numerically, yet it is possible to make rough estimates using the simple stellar model in Fig. 22(b). The left side of Eq. (213) may be used to estimate the drop between the central pressure p_c and surface pressure p_s occuring over the full radius R, using quantities on the right side of Eq. (213) that are roughly intermediate between the surface and center values, $\rho(r) \approx \overline{\rho}$, $m(r) \approx M/2$, and $r \approx R/2$:

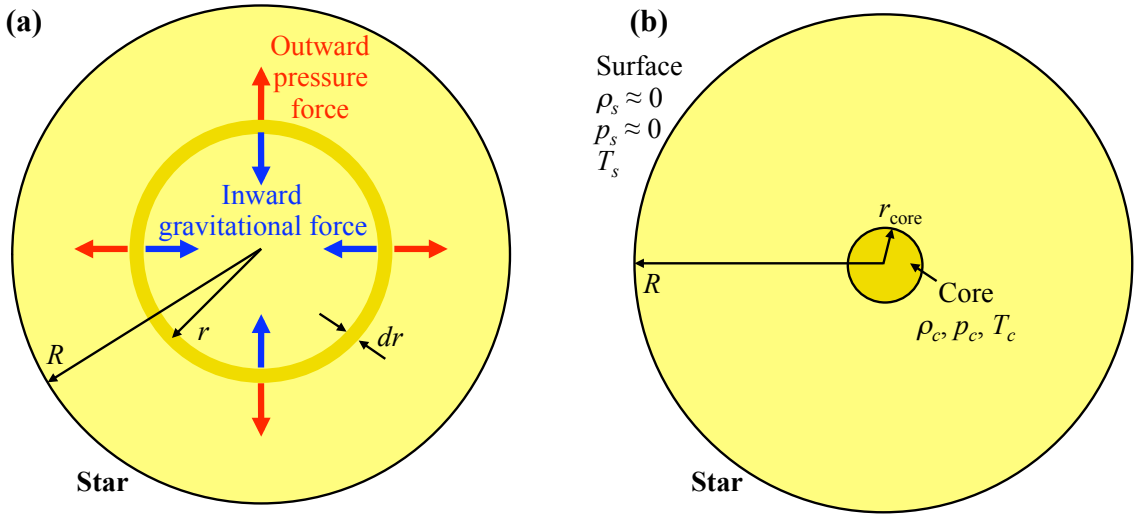

Figure 22. Hydrostatic equilibrium and stellar structure. **(a)** Consider a thin shell of radius r and thickness dr within a star. For the star to be in equilibrium, the inward gravitational and outward pressure forces on the shell must balance each other. **(b)** Most of the fusion reactions occur in a small core region with very high central values of the density ρ_c, pressure p_c, and temperature T_c. The surface has essentially zero density and pressure and a relatively low temperature T_s.

$$\frac{p_c - p_s}{R} \approx \frac{G\,\overline{\rho}\,(M/2)}{(R/2)^2} \quad \Longrightarrow \quad p_c \approx \frac{2\,G\,\overline{\rho}\,M}{R} \quad \text{since } p_s \approx 0 \tag{215}$$

$$\approx \frac{3}{2\pi}\frac{G\,M^2}{R^4} \quad \text{using Eq. (210)} \tag{216}$$

With the values $M_\odot$ and $R_\odot$ for the sun, Eq. (216) gives $p_c \approx 5\times10^{14}$ Pa. More precise calculations [10, 11] give central pressures of $p_c \approx 2.7\times10^{16}$ Pa $= 2.7\times10^{11}$ bar, where 1 bar is approximately the atmospheric pressure at sea level on earth (1 atmosphere $= 1.013$ bar $= 1.013\times10^5$ Pa).

Using the ideal gas law and Eqs. (211)-(212), the pressure due to both protons and electrons is

$$p \;=\; (n_p + n_e)\,k_{_B}\,T \;\approx\; 2\,\Re\,\rho\,T\;, \tag{217}$$

where the molar gas constant is $\Re \equiv k_{_B}/m_{_H} \approx 8.315$ J/(^{o}K·mol). In modeling stars, an equation of state is needed to relate the local pressure, density, and temperature to each other. While the ideal gas law was used here for this purpose, other equations of state are sometimes more appropriate–for example, the Fermi equation for degenerate electrons in very dense stars.

The stellar temperature may be estimated by applying Eq. (217) to a point intermediate between the star's center and surface and using typical intermediate values for the quantities, $p \approx p_c/2$, $\rho \approx \overline{\rho}$, and $T \approx (T_c - T_s)/2$, where T_c and T_s are the temperatures at the center and surface:

$$\frac{p_c}{2} \approx 2\,\overline{\rho}\,\Re\,\frac{T_c - T_s}{2} \quad \Longrightarrow \quad T_c \approx \frac{p_c}{2\,\Re\,\overline{\rho}} \quad \text{since } T_c \gg T_s$$

$$\approx \frac{G\,M}{\Re\,R} \quad \text{using Eq. (215)} \tag{218}$$

Using $M_\odot$ and $R_\odot$, Eq. (218) gives $T_c \approx 2.3 \times 10^7$ ^{o}K for the sun. This is quite close to the result of numerical calculations, $T_c \approx 1.6 \times 10^7$ ^{o}K $= 1.4$ keV. Note that this temperature is surprisingly low compared to the optimum temperatures for fusion reactions that were discussed in Section 1.5. Therefore, fusion reactions in stars proceed at a comparatively slow rate, as will be discussed.

Equation (217) may be employed to find the central density. Using $p_c \approx 2.7 \times 10^{16}$ Pa and $T_c \approx 1.6 \times 10^7$ ^{o}K for the sun, one finds a central mass density of $\rho_c \approx 100$ g/cm^3, or central proton and electron densities of $n_{p,\,c} \approx n_{e,\,c} \approx 6 \times 10^{25}$ cm^{-3}.

The preceding calculations included the pressure from ions and electrons but not the pressure from photons. A star is filled with thermal radiation that is in equilibrium with the local temperature of matter in each region of the star. From statistical physics, the pressure of this radiation is

$$p_{rad} \;=\; \frac{4}{3}\,\frac{\sigma_{_{SB}}}{c}\,T^4\;, \tag{219}$$

where $\sigma_{_{SB}} \approx 5.67 \times 10^{-8}$ W/(m^2 ^{o}K^4) is the Stefan-Boltzmann constant. Using $T_c \approx 1.6 \times 10^7$ ^{o}K for the sun, this radiation pressure is $p_{rad} \approx 1.7 \times 10^{13}$ Pa $= 1.7 \times 10^8$ bar, so it was okay to neglect the radiation pressure compared to the particle pressure. Nonetheless, the radiation pressure can become significant for stars with higher temperatures and/or lower densities than the sun.

As shown in the general relativity summary, the mass of a star is sufficient to warp space and time to a measurable degree. These general relativistic effects are smaller than the classical effects considered above by a factor of $\sim (GM)/(c^2R)$. For the sun, this factor is $\sim 2 \times 10^{-6}$, so general relativity may be ignored in simple models of the sun and other similar stars. However, general relativity can become quite important in the final collapse of large stars that have $M/R \gg M_\odot/R_\odot$.

5.2 Energy Transport

Energy generated by fusion reactions in the center of a star can be transported to the star's surface by radiation, conduction, or convection. As will be shown, radiative energy transport is generally most important.

Radiative Energy Transport

Photons carry energy from the center of a star to its surface, as illustrated in Fig. 23(a). Scattering of the photons off electrons and ions during the journey from the center to the surface determines the rate of energy transport. Photon-electron scattering is called Thomson scattering, and its cross section depends on the "classical electron radius" $r_e \equiv e^2/(4\pi\epsilon_o m_e c^2) \approx 2.828 \times 10^{-15}$ m. Since the electron is a point particle, this quantity is not actually the electron's radius, but rather a measure of the "effective reach" of its electric field in events like Thomson scattering. As derived in the relativistic quantum field theory summary, the Thomson cross section is

$$\sigma_{_{\rm Thomson}} \;=\; \frac{8\pi}{3}\,r_e^2 \;=\; 6.653 \times 10^{-29}\ {\rm m}^2\;. \tag{220}$$

The mean free path of a photon before it is scattered by Thomson scattering is

$$(l_{mfp})_{_{\rm Thomson}} \;=\; \frac{1}{n_e\,\sigma_{_{\rm Thomson}}} \tag{221}$$

Using the mean density calculated earlier, $\overline{n_e} \approx 8.5 \times 10^{29}$ m^{-3}, one finds $(l_{mfp})_{_{\rm Thomson}} \approx 1.8 \times 10^{-2}$ m. More detailed calculations [10, 11] show that scattering from ions tends to shorten the mean free path to $l_{mfp} \approx 2 \times 10^{-3}$ m. Of course, these results are highly dependent on the local density, and the ion scattering effect is also strongly dependent on the temperature. Thus this mean free path length for photons should only be regarded as a crude estimate.

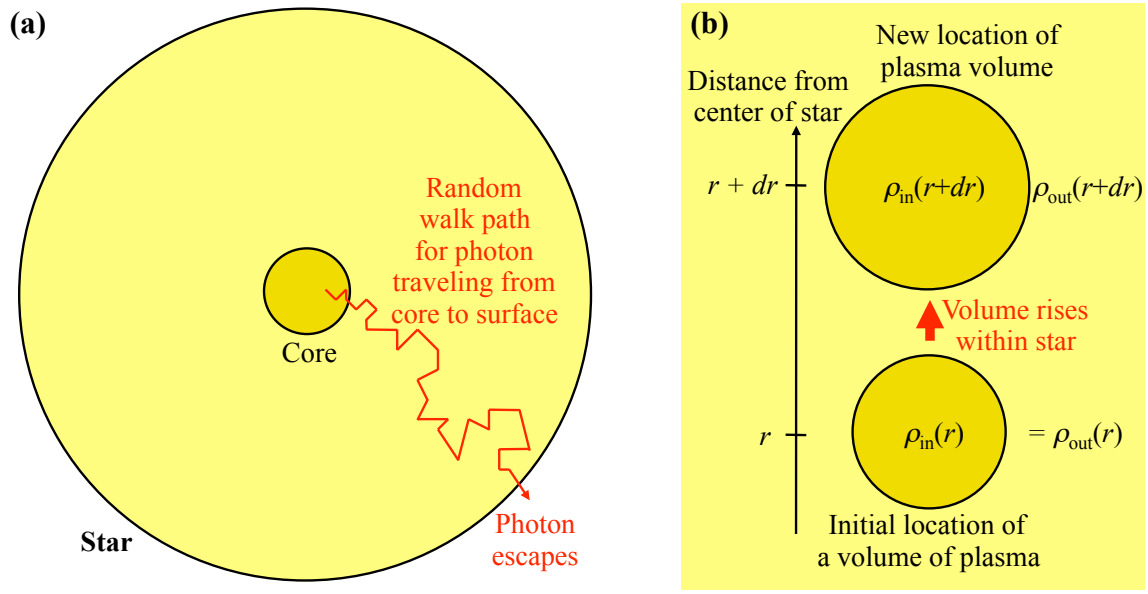

Figure 23. Energy transport in a star. **(a)** Radiative energy transport. Fusion energy produced in a stars core is transported to the surface in the form of photons. During transit, the photons repeatedly scatter off electrons and ions. An example random walk for a stellar photon is shown above. Because the mean free path between a photons scatterings is much shorter than the stars radius, photon transport may be modeled as a diffusional process. **(b)** Convective energy transport. A certain volume of plasma may rise to a higher altitude within a star, taking its thermal energy with it. Since pressure decreases with altitude, the volume will expand and its density will decrease. If the new density inside the volume is greater than the local outside density, the volume will sink to its original location and such convective energy transport will not occur.

Because the mean free path before a photon is scattered is many orders of magnitude smaller than a star's radius, transport of photons from a star's center to its surface may be treated as a diffusion process. As discussed in Section 2.3, the diffusion constant for particles of velocity v and mean free path l_{mfp} is $D = v\, l_{mfp}/3$. Therefore, the diffusion constant for photons in a star is

$$D_{\rm rad} \;=\; \frac{1}{3}\, c\, l_{mfp}\;. \tag{222}$$

In diffusion problems, the time τ for particles to diffuse a distance L from their sources is $\tau = L^2/D$. Thus the typical time $\tau_{\rm photon\ escape}$ for a photon to travel from a star's center to its surface is

$$\tau_{\rm photon\ escape} \;=\; \frac{3\, R^2}{c\, l_{mfp}}\;. \tag{223}$$

For $l_{mfp} \approx 2 \times 10^{-3}$ m, this time is $\tau_{\rm photon\ escape} \approx 2.4 \times 10^{12}$ sec $= 72,000$ years. The photons emanating from the sun's surface today were originally created tens of thousands of years ago!

The energy transported by the diffusion of the photons may also be calculated. From *Statistical Physics* ?.?, the radiation energy density of thermal photons is

$$U_{\rm rad} \;=\; 4\,\frac{\sigma_{SB}}{c}\,T^4\;. \tag{224}$$

The local radiation energy density depends on the radial location within the star,

$$\frac{dU_{\rm rad}}{dr} \;=\; \frac{dU_{\rm rad}}{dT}\,\frac{dT}{dr} \;=\; 16\,\frac{\sigma_{SB}}{c}\,T^3\,\frac{dT}{dr}\;. \tag{225}$$

Radiative energy diffuses down the gradient found in Eq. (225) with the diffusion constant D_{rad}, so the outward flux of radiative energy in the radial direction is

$$J_{\rm rad} \;=\; -D_{\rm rad}\frac{dU_{\rm rad}}{dr} \;=\; -\frac{16}{3}\,l_{mfp}\,\sigma_{SB}\,T^3\,\frac{dT}{dr}\;. \tag{226}$$

The effective thermal conductivity $\kappa_{\rm rad}$ of the photons may be obtained by rewriting Eq. (226):

$$J_{\rm rad} \;=\; -\kappa_{\rm rad}\,\frac{dT}{dr}\;, \qquad\qquad \text{with}\quad \kappa_{\rm rad} \;\equiv\; \frac{16}{3}\,l_{mfp}\,\sigma_{SB}\,T^3\;. \tag{227}$$

The luminosity or total power radiated from inside the radius r within the star is simply

$$L(r) \;=\; 4\pi r^2\,J_{\rm rad} \;=\; -\frac{64}{3}\pi\,r^2\,l_{mfp}\,\sigma_{SB}\,T^3\,\frac{dT}{dr}\;. \tag{228}$$

Equation (228) may be used to make a rough estimate of the sun's luminosity. Most of the fusion energy is generated in the center of the sun (say $r < R/2$), so the luminosity at $r = R/2$ should be the same as the observed luminosity at the surface. Estimating that $T \approx T_c/2$ and $-dT/dr \approx (T_c - T_s)/R \approx T_c/R$ at the midpoint, one finds

$$L \;\approx\; \frac{2}{3}\pi\,R\,l_{mfp}\,\sigma_{SB}\,T_c^4\;. \tag{229}$$

Using solar values of $R_\odot$, $l_{mfp} \approx 2\times10^{-3}$ m, and $T_c \approx 1.6\times10^7$ ^{o}K, one finds $L \approx 1\times10^{28}$ W. Actually the luminosity of the sun is $L_\odot \approx 3.78\times10^{26}$ W. The estimate was too high because it is highly dependent on the temperature, and the actual temperature at the mid-point in the sun is lower than $T_c/2$. Nonetheless, the estimate was in the right ballpark and illustrates the basic physics of radiative energy transport in stars.

Note that the sun's luminosity was calculated without even discussing its fusion rate. Regardless of whether it is producing fusion energy, a star of a given size will compress and heat its center as in Eq. (218) and transport that energy to its surface as in Eq. (228). If fusion energy is produced in the core, it will replace the energy lost by transport to the surface, and the star will be stable. If fusion energy is not produced, loss of energy from the core will cause the star to contract and feed off its gravitational energy, as will be shown in Section 5.3.

Conductive Energy Transport

Electrons can also transport energy in stars. Using typical solar values of $T = T_c/2 = 8\times10^6$ ^{o}K, $\ln\Lambda \approx 3$, and $l_{mfp} \approx 2\times10^{-3}$ m for photons, the electron thermal conductivity from Eq. (93) is 25,000x smaller than $\kappa_{\rm rad}$ from Eq. (227). Therefore, conductive energy transport by electrons (and ions) may be neglected in comparison with radiative energy transport by photons.

One exception to this rule is that electron heat conduction can become very significant if the electrons behave as a gas of degenerate Fermi particles instead of as an ideal gas as they have been treated here. From statistical physics, the Fermi energy E_F for free electrons is

$$E_F \;=\; \frac{\hbar^2}{2m_e}\,\left(3\pi^2 n_e\right)^{2/3} \;=\; 3.65\times10^{-15}\,n_{\rm e,\,cm^{-3}}^{2/3}\;\;\text{eV}\;. \tag{230}$$

As long as $k_B T \gg E_F$, the electrons will behave as a classical ideal gas. However, if $k_B T \ll E_F$, the electrons will be degenerate and will conduct heat very well, just as they do in metals. This is because degenerate electrons carry larger energies $\sim E_F$ instead of $\sim k_B T$, move at higher speeds $\sim v_F \equiv \sqrt{2E_F/m_e}$ instead of $\sim v_{te}$, and travel further before colliding, since the particle phase space is too full to permit many collisions. Electrons will then become the dominant energy transport mechanism and cool the core of the star. In calculations of the electron pressure, it would also be necessary to use the pressure-density relationship for a Fermi gas instead of that for an ideal gas. If $k_B T \sim E_F$, the electrons will be partially degenerate.

For the sun's central electron density $n_{e,c} \approx 6 \times 10^{25}$ cm^{-3}, the Fermi energy is $E_F \approx 560$ eV. Since this is significantly smaller than the central temperature $T_c \approx 1400$ eV, we have been justified in treating the electrons classically. Note from Eq. (230) that the Fermi energy for ions is m_e/m_i smaller than that for electrons, so degeneracy of the ions is not a concern.

Convective Energy Transport

Energy may also be transported by convection, in which regions of plasma rise within a star, carrying their thermal energy with them. Suppose some volume of plasma rises by an amount dr, as shown in Fig. 23(b). As pressure decreases with altitude, the volume's pressure will drop and the volume will expand. The densities outside and inside the risen volume are

$$\rho_{\rm out}(r+dr) \;=\; \rho(r) - \left|\frac{d\rho}{dr}\right| dr \tag{231}$$

$$\rho_{\rm in}(r+dr) \;=\; \rho(r) - \frac{d\rho}{dp}\left|\frac{dp}{dr}\right| dr \;=\; \rho(r) - \frac{1}{\gamma}\,\frac{\rho}{p}\left|\frac{dp}{dr}\right| dr\;, \tag{232}$$

in which Eq. (232) used Eq. (133). The gradients $d\rho/dr$ and dp/dr are both negative, so they have been written as the negative of their absolute values to make the minus signs explicitly clear.

Stability against convection requires that $\rho_{\rm in} > \rho_{\rm out}$, causing the risen volume of plasma to sink back to its original level. Using Eqs. (231) and (232), this condition implies that

$$\left|\frac{d\rho}{dr}\right| \;>\; \frac{1}{\gamma}\,\frac{\rho}{p}\left|\frac{dp}{dr}\right| \qquad \begin{array}{c}\textbf{for stability}\\ \textbf{against convection}\end{array} \tag{233}$$

For an ideal gas, ρ may be rewritten in terms of the temperature and pressure:

$$\frac{p}{\rho T} \;=\; \text{constant} \qquad \Longrightarrow \qquad \frac{d\rho}{dr} \;=\; \frac{\rho}{p}\,\frac{dp}{dr} \;-\; \frac{\rho}{T}\,\frac{dT}{dr}\;. \tag{234}$$

Substituting Eq. (234) into Eq. (233), one obtains

$$\left|\frac{dT}{dr}\right| \;\le\; \left(1 - \frac{1}{\gamma}\right)\frac{T}{p}\left|\frac{dp}{dr}\right| \qquad \begin{array}{c}\textbf{Thermal gradient}\\ \textbf{limited by convection}\end{array} \tag{235}$$

If $|dT/dr|$ calculated from radiative energy transport in Eq. (228) is less than the right side of Eq. (235), convection will not occur and photons will be the dominant method of energy transport. However, if $|dT/dr|$ calculated from Eq. (228) exceeds the right side of Eq. (235), convection will occur, and convective energy transport will limit the actual temperature gradient to be equal to the right side of Eq. (235).

5.3 Fusion Reactions and Power

Having calculated the temperature, density, luminosity, and other conditions in stars, we can now examine the energy production under those conditions. While fusion is the most important energy source in stars, thermal energy and gravitational potential energy should also be considered. Multiplying the left and right sides of Eq. (213) by $-\int dr\, 4\pi r^3$ and integrating yields the thermal and gravitational energies and gives a useful relation between them:

$$\text{Left side:}\quad \int_0^R \frac{dp}{dr} 4\pi r^3 dr = \int_0^R 3p 4\pi r^2 dr = 2\int_0^R \frac{3}{2}(n_p + n_e) k_B T 4\pi r^2 dr = 2\,E_T = \begin{matrix}2\times \text{ total thermal} \\ \text{energy of star}\end{matrix} \tag{236}$$

$$\text{Right side:}\quad \int_0^R \frac{-G\,\rho(r)\,m(r)}{r}\, 4\pi r^2 dr \;=\; E_G \;=\; \begin{matrix}\text{Total gravitational} \\ \text{potential energy of star}\end{matrix} \tag{237}$$

$$\text{Left side} = \text{right side} \implies 2\,E_T \;=\; -E_G \qquad \textbf{Virial theorem} \tag{238}$$

Equation (236) used integration by parts. The resulting Eq. (238) is a form of the virial theorem from classical mechanics. To understand the physical meaning of Eq. (238), one can consider a star that contracts in size. Because the star's mass becomes more closely packed, the gravitational potential energy will decrease by an amount $|\Delta E_G|$ and become more negative. Since energy is conserved, this released gravitational energy must go somewhere. According to Eq. (238), half of it will become additional thermal energy in the star, $\Delta E_T = |\Delta E_G|/2$; gravity basically performs work on the star by compressing it, thereby heating it in accordance with Eq. (134). The other half of the released potential energy cannot be retained within the star and thus is radiated away from the star's surface.

Therefore, a star can contract and radiate a total energy of up to $|E_G|/2$ without even tapping into its nuclear energy sources. The length of time that the sun could maintain its present luminosity in this way is called the Kelvin time,

$$\tau_{\text{Kelvin}} \;=\; \frac{|E_{G\,\odot}|}{2L_\odot} \;\approx\; \frac{8}{15}\pi^2 \frac{G\,\overline{\rho_\odot}^2\, R_\odot^5}{L_\odot}\,, \tag{239}$$

in which the crude approximations $\rho(r) = \overline{\rho_\odot}$ and $m(r) = (4/3)\pi r^3\,\overline{\rho_\odot}$ were used with Eq. (237) to obtain the estimated answer in Eq. (239). Using the solar values, the Kelvin time is $\tau_{\text{Kelvin}} \approx 3\times 10^{14}$ sec ≈ 10 million years. Hence gravitational energy could sustain the sun for a long time by human standards, though not for the estimated 4.5 billion years that the sun has existed. For that, a nuclear energy source is required.

Stars produce most of their energy by fusing ^{1}H into ^{4}He. The mass of one ^{1}H nucleus is $m_p = 1.6726 \times 10^{-27}$ kg and that of one ^{4}He nucleus is $m_\alpha = 6.6432 \times 10^{-27}$ kg. The total mass of four protons is larger than the mass of the helium nucleus they produce by fusion, so the excess mass is converted into energy,

$$E_{fus} \;=\; \Delta m c^2 \;=\; (4m_p - m_\alpha)c^2 \;=\; 26.5 \text{ MeV} \tag{240}$$

The fraction of the initial hydrogen mass that is converted to energy is

$$\frac{\Delta m}{m} \;=\; \frac{4m_p - m_\alpha}{4m_p} \;=\; 0.007 \tag{241}$$

Assuming that the sun was initially composed entirely of hydrogen, complete fusion of that hydrogen into helium would maintain the sun's present luminosity for a time

$$\tau_{\text{solar fusion}} \;=\; \frac{0.007 M_\odot c^2}{L_\odot} \;=\; 3.3 \times 10^{18} \text{ sec} \;=\; 100 \text{ billion years.} \tag{242}$$

The actual life span of the sun is predicted to be only 10 billion years. The sun originally contained some helium, it will consume its hydrogen faster than the present rate as it nears the end of its life, and it will still contain some hydrogen even when it is no longer able to sustain fusion reactions. Currently the sun is about halfway through its life span.

There are several pathways by which ^{1}H can be fused into ^{4}He. The simplest is the proton-proton chain, which is named after its first step:

$$\left.\begin{array}{lrcl} (1) & {}^1\mathrm{H} + {}^1\mathrm{H} & \rightarrow & {}^2\mathrm{H} + \mathrm{e}^+ + \nu_e \\ (2) & {}^2\mathrm{H} + {}^1\mathrm{H} & \rightarrow & {}^3\mathrm{He} + \gamma \\ (3) & {}^3\mathrm{He} + {}^3\mathrm{He} & \rightarrow & {}^4\mathrm{He} + 2\,{}^1\mathrm{H} \end{array}\right\} \quad \textbf{Proton-proton chain 1 (\textit{pp1})} \tag{243}$$

There are two alternative proton-proton chains, *pp*2 and *pp*3. In these versions, steps (1) and (2) proceed as above, but the third step is $^3\mathrm{He} + {}^4\mathrm{He} \rightarrow {}^7\mathrm{Be} + \gamma$. Then the ^{7}Be acquires another proton, either after (*pp*2) or before (*pp*3) undergoing a beta decay, ultimately producing two ^{4}He.

Step (1) is the rate-limiting step in the proton-proton chains, since the reaction requires both a fusion event and a weak nuclear decay. Thus the rate of step (1) may be used with Eq. (61) to calculate the total rate of fusion energy production per volume by all the proton-proton chains:

$$\frac{P_{fus}}{\text{vol.}} = \frac{1}{2} n_p^2 \langle \sigma v \rangle_{pp} \frac{E_{fus}}{2} . \tag{244}$$

The fusion of a pair of protons represents only half of a final ^{4}He, so the energy E_{fus} produced per ^{4}He has been divided by 2. Using the central density previously calculated and assuming that half of the hydrogen has already been burned, one finds $n_p \approx 3 \times 10^{31}$ m^{-3}. At $T_c = 1.5 \times 10^7$ ^{o}K =1.4 keV, the Maxwellian-averaged reactivity is $\langle \sigma v \rangle_{pp} = 1 \times 10^{-49}$ m^3/sec. Neutrinos carry away some energy from the proton-proton cycles, so the average fusion energy from Eq. (240) is lowered to $E_{fus} \approx 23$ MeV. Using these values in Eq. (244), the fusion power density is $P_{fus}/\text{vol.} \approx 83$ W/m^3.

Fusion in a layer at radius r within a star contributes to the luminosity passing through that radius:

$$\frac{dL(r)}{dr} = 4\pi r^2 \frac{P_{fus}}{\text{vol.}} . \tag{245}$$

Because both the temperature and the density decrease with radius, almost all of the fusion occurs in the core of the star (provided that unburned fuel remains there), as pictured in Fig. 23. As a simple model, consider a core of radius r_{core} with uniform $P_{fus}/\text{vol.} \approx 83$ W/m^3 as calculated above. For this core to account for the entire luminosity of the sun, its radius must be

$$\frac{r_{\text{core}}}{R_\odot} = \left(\frac{L_\odot}{(83 \text{ W/m}^3)(4/3)\pi R_\odot^3} \right)^{1/3} \approx 0.15 . \tag{246}$$

Therefore, the sun's fusion power is produced within a small, dense, hot core.

Another fusion pathway within stars employs ^{12}C as a catalyst; the carbon accumulates four protons in a series of reactions, then releases them as a ^{4}He nucleus. This carbon cycle proceeds as follows:

$$\left.\begin{array}{lrcl} (1) & {}^{12}\mathrm{C} + {}^1\mathrm{H} & \rightarrow & {}^{13}\mathrm{N} + \gamma \\ (2) & {}^{13}\mathrm{N} & \rightarrow & {}^{13}\mathrm{C} + \mathrm{e}^+ + \nu_e \\ (3) & {}^{13}\mathrm{C} + {}^1\mathrm{H} & \rightarrow & {}^{14}\mathrm{N} + \gamma \\ (4) & {}^{14}\mathrm{N} + {}^1\mathrm{H} & \rightarrow & {}^{15}\mathrm{O} + \gamma \\ (5) & {}^{15}\mathrm{O} & \rightarrow & {}^{15}\mathrm{N} + \mathrm{e}^+ + \nu_e \\ (6) & {}^{15}\mathrm{N} + {}^1\mathrm{H} & \rightarrow & {}^{12}\mathrm{C} + {}^4\mathrm{He} \end{array}\right\} \quad \textbf{Carbon cycle} \tag{247}$$

Due to the large charges of the nuclei in the carbon cycle, the Coulomb barriers are higher and the reactions require higher temperatures than the proton-proton chains. However, if the temperature is high enough and enough carbon is present, the carbon cycle can outpace the *pp* chains, because none of the steps in the carbon cycle requires simultaneous fusion and weak decay events. The carbon cycle begins to dominate at $T_c > 1.8 \times 10^7$ ^{o}K, somewhat hotter than the sun's temperature.

After a star has fused its central hydrogen into helium, the drop in fusion power will cause the star to contract. As has been discussed with regard to Eq. (238), the contraction will cause the star to heat up. Once its center reaches $T_c \approx 1 \times 10^8$ ^{o} K, helium burning becomes possible:

$$\left.\begin{array}{ll} (1) & {}^4\mathrm{He} + {}^4\mathrm{He} \rightarrow {}^8\mathrm{Be} \\ (2) & {}^8\mathrm{Be} + {}^4\mathrm{He} \rightarrow {}^{12}\mathrm{C} + \gamma \end{array}\right\} \quad \textbf{Helium burning} \tag{248}$$

Although ^{8}Be decays after $\sim 3 \times 10^{-16}$ sec, it exists long enough for step (2) above to have a non-negligible chance of occurring. Helium burning releases 7.3 MeV per final ^{12}C, or 2.4 MeV per initial ^{4}He. This may be compared with 26.5 MeV per ^{4}He for hydrogen fusion. Thus for a given mass, helium fusion can produce $\sim 1/10$ as much energy as hydrogen fusion, or in other words helium fusion can sustain a star at a given luminosity for only $\sim 1/10$ as long as hydrogen fusion.

In the temperature range $T_c = 10^8 - 10^9$ ^{o}K that can occur in the final phases of stellar evolution, heavier elements may be formed by a bewildering array of reactions, such as $^{12}\mathrm{C}+{}^4\mathrm{He} \rightarrow {}^{16}\mathrm{O}+\gamma$ and $^{12}\mathrm{C}+{}^{12}\mathrm{C} \rightarrow {}^{23}\mathrm{Na}+{}^1\mathrm{H}$. Most of these reactions do not produce much energy, and they cannot sustain a star for a relatively long period of time. However, they do explain how many of the heavier elements in the universe have been produced.

It is worth comparing stellar fusion with the man-made approaches that will be discussed in Sections 6 and 7, inertial confinement fusion, thermonuclear explosive devices, and magnetic fusion:

- **Fusion power density.** The sun's fusion power density is $P_{fus}/\mathrm{vol.} \approx 83$ W/m^3 in the core, or 0.27 W/m^3 averaged over the sun's entire volume. In contrast, man-made fusion approaches must produce all their power, typically > 1 GW, within at most a few m^3 of plasma, since the hardware to maintain a much larger volume of plasma would be prohibitively expensive.

- **Fusion time.** Fusion time is another way to state the same problem. The sun takes ~ 10 billion years to consume its fusion fuel, but in order to be efficient, a bomb or ICF capsule must consume its fuel within a fraction of a second. While magnetic fusion approaches have the luxury of somewhat more time, they must still must operate very rapidly by stellar standards.

- **Ion temperature.** To increase the fusion power density and decrease the fusion time, man-made approaches must have $T_i \sim 10 - 100$ keV instead of $T_i \approx 1.4$ keV as in the sun.

- **Confinement.** Whereas a star's gravity keeps ions from escaping before they fuse, man-made approaches must use magnetic fields or the particles' own inertia to keep them from escaping.

- **Radiation losses.** If photons are in thermal equilibrium with the plasma, $T_{\mathrm{rad}} \approx T_i$, radiation losses will be $\propto T^4$. This loss is large for stars but downright obscene for the higher T_i of man-made fusion. The loss can be minimized by surrounding the plasma with enough material to impede the radiation's escape, like the mantles of stars or the uranium tamper in a thermonuclear explosive device. That is not practical for inertial confinement and magnetic fusion, so an alternate solution is to let the radiation escape to keep $T_{\mathrm{rad}} \ll T_i$. Then the radiation loss is the bremsstrahlung $\propto \sqrt{T_e}$ value. As shown in Section 1.5, only a few fusion fuels can produce enough energy to overcome this bremsstrahlung loss.

5.4 Stellar Evolution

Having examined the behavior of stars during the main phase of their life cycle, we will now discuss how stars initially form and how they expire when they have exhausted their fusion fuel.

A **protostar** is a cloud of mostly hydrogen that is contracting and heating up [in accordance with Eqs. (238) and (239)] to form a star. One can calculate the minimum mass $M_{\min}$ a protostar must have in order to initiate fusion reactions and become a star. Using Eq. (218) and $T_c \approx 1.6 \times 10^7$ ^{o}K for the sun, the central temperature of a protostar is

$$T_c = 1.6 \times 10^7 \ ^o\text{K} \left(\frac{M}{M_\odot}\right) \left(\frac{R_\odot}{R}\right) \tag{249}$$

Similarly, using Eq. (230) and the central Fermi temperature $T_F \approx 6.5 \times 10^6$ ^{o}K for the sun, the central Fermi temperature of a protostar may be written as

$$T_F = 6.5 \times 10^6 \ ^o\text{K} \left(\frac{n_{ec}}{n_{ec\odot}}\right)^{2/3} \tag{250}$$

$$\approx 6.5 \times 10^6 \ ^o\text{K} \left(\frac{\overline{n_e}}{\overline{n_{e\odot}}}\right)^{2/3} = 6.5 \times 10^6 \ ^o\text{K} \left(\frac{M}{M_\odot}\right)^{2/3} \left(\frac{R_\odot}{R}\right)^2 \tag{251}$$

Proton-proton reactions become significant once the central temperature rises to $T_c \approx 8 \times 10^6$ ^{o}K. If the protostar has a mass $M > M_{\min}$, it will collapse until the central temperature from Eq. (249) is hot enough to produce fusion reactions, and a star will be born. If $M < M_{\min}$, the Fermi temperature will exceed T_c and the protostar's core will become electron-degenerate before it reaches fusion temperatures. The degenerate electrons' thermal conductivity will cool the core and their Fermi pressure will prevent further collapse. The result is a stable, unignited gas giant like Jupiter. Using Eqs. (249) and (251) and setting $T_c = T_F = 8 \times 10^6$ ^{o}K yields $M_{\min} \approx 0.3 M_\odot$. The approximation in Eq. (251) was rather crude, and one can debate the exact point at which T_F becomes too high to permit fusion reactions; more detailed calculations give:

$$M_{\min} \approx 0.08 M_\odot \qquad \textbf{Minimum mass for star formation} \tag{252}$$

Toward the end of its life, after a star has consumed most of the hydrogen in its core, it collapses and heats up until it is hot enough to fuse the hydrogen that remains in its mantle; this is called **shell burning**. The fusion reactions in the mantle cause the surface layers of the star to expand drastically and cool, resulting in an enormous **red giant** star. Further contraction and heating of the core can lead to the fusion of helium and progressively higher elements. In these final stages, a star often blows off its outer layers.

The remaining stellar core collapses to form one of three objects, depending on its mass M:

1. White dwarf. If $M < M_{\text{white dwarf max}}$, the star contracts until its degenerate electrons' Fermi pressure supports it, forming a white dwarf that slowly radiates away its residual energy.

2. Neutron star. If $M_{\text{white dwarf max}} < M < M_{\text{neutron star max}}$, gravity overcomes the Fermi pressure at the white dwarf stage. The star continues to contract until it squeezes its protons and electrons together to form neutrons by inverse beta decay. Such a neutron star acts like a giant nucleus of neutrons and is supported against further collapse by the neutrons' Fermi pressure.

3. Black hole. If $M > M_{\text{neutron star max}}$, gravity overcomes even the Fermi pressure of the degenerate neutrons and the star continues to collapse. From general relativity, the star becomes a black hole once its radius becomes less than the **Schwarzschild radius** $R_S \equiv 2GM/c^2$. Nothing–not even light–that ventures within the Schwarzschild radius can resist being sucked in by the extreme gravitational field. See the general relativity summary for more information.

The limiting masses $M_{\text{white dwarf max}}$ and $M_{\text{neutron star max}}$ may be estimated in a simple fashion. Consider a collapsed star with a density n of degenerate fermions. The degenerate fermions are electrons in a white dwarf and neutrons in a neutron star. For a very dense star that approaches the appropriate limiting mass, the degenerate particles will have such a large Fermi energy that they will be relativistic. From the statistical physics summary, the Fermi energy per degenerate relativistic fermion is

$$E_F \sim \hbar c n^{1/3} \sim \frac{\hbar c N^{1/3}}{R} , \tag{253}$$

where n has been estimated from the total number N of the fermions and the radius R of the star.

The gravitational potential energy per degenerate fermion is roughly

$$E_G \sim -\frac{GMm_{\text{per fermion}}}{R} = -\frac{Gm_{\text{per fermion}}^2 N}{R} , \tag{254}$$

in which the total mass of the collapsed star has been written as $M = Nm_{\text{per fermion}}$, where $m_{\text{per fermion}}$ is the amount of stellar mass per degenerate fermion. In a white dwarf composed of typical fusion products, on average one proton and one neutron accompany each electron, so $m_{\text{per fermion}} = m_e + m_p + m_n \approx 2m_n$. In a neutron star, most of the mass is in the form of the degenerate neutrons, so $m_{\text{per fermion}} = m_n$.

Thus the total energy per degenerate fermion consists of two terms, both of which vary like $1/R$:

$$E \sim E_F + E_G \sim \frac{\hbar c N^{1/3}}{R} - \frac{Gm_{\text{per fermion}}^2 N}{R} , \tag{255}$$

The collapsed star will seek a stable equilibrium that minimizes E. If $E > 0$ in Eq. (255), the energy will be decreased by increasing R. Part of the fermions will then become nonrelativistic, causing the radial dependence of E_F to change to $\sim 1/R^2$ as in Eq. (251). Eventually E_G will begin to dominate over E_F and the system will reach equilibrium at some finite radius R.

On the other hand, if $E < 0$ in Eq. (255), the energy can be decreased without bound by decreasing R, and the star will be unstable to further gravitational collapse. Setting $E = 0$ in Eq. (255), the threshold for stability occurs at a maximum number of degenerate fermions,

$$N_{\max} = 3\left(\frac{\hbar c}{G}\right)^{3/2} \frac{1}{m_{\text{per fermion}}^3} , \tag{256}$$

where the coefficient 3 comes from calculating the Fermi and gravitational energies more precisely by numerically integrating to determine the density profile [12].

The maximum fermion number is equivalent to a maximum stellar mass of

$$M_{\max} \equiv N_{\max} m_{\text{per fermion}} \approx 3\left(\frac{\hbar c}{G}\right)^{3/2} \frac{1}{m_{\text{per fermion}}^2} . \tag{257}$$

The radius of a stable collapsed star near the limiting mass may be found by inserting Eq. (256) into Eq. (253) and assuming that the fermions are somewhat relativistic, $E_F \sim m_{\text{of fermion}} c^2$ (here $m_{\text{of fermion}}$ is the actual mass of each degenerate fermion):

$$R \approx 3\sqrt{\frac{\hbar^3}{Gc}} \frac{1}{m_{\text{of fermion}}\, m_{\text{per fermion}}} . \tag{258}$$

The factor of 3 in Eq. (258) again comes from more detailed calculations [12].

Applying Eqs. (257) and (258) to a white dwarf ($m_{\text{of fermion}} = m_e$, $m_{\text{per fermion}} \approx 2m_n$) produces

$$M_{\text{white dwarf max}} \approx 1.5M_\odot \qquad R \approx 10^7 \text{ m} \qquad \overline{\rho} \sim 10^6 \text{ g/cm}^3 \qquad \textbf{White dwarf} \tag{259}$$

Equations (257) and (258) may also be applied to a neutron star ($m_{\text{of fermion}} = m_{\text{per fermion}} = m_n$), although general relativity and other effects lower the maximum mass by about a factor of 2 [12]:

$$M_{\text{neutron star max}} \approx 3M_\odot \qquad R \approx 10^4 \text{ m} \qquad \overline{\rho} \sim 10^{15} \text{ g/cm}^3 \qquad \textbf{Neutron star} \tag{260}$$

Thus white dwarfs have masses up to $1.5M_\odot$, neutron stars are in the range $1.5 - 3M_\odot$, and black holes formed from stars have masses greater than $3M_\odot$.

Pulsars are particularly interesting types of neutron stars that emit periodic bursts of radiation. When a star collapses, its magnetic field is compressed and greatly strengthened. Trapped electrons above the magnetic poles emit narrow beams of cyclotron radiation. A pulsar rotates about an axis that is different from its magnetic axis, causing beams of cyclotron radiation to sweep the sky during each rotation. Depending on the pulsar, the cyclotron radiation may be anywhere from radio to gamma wavelengths, and the rotation period may range from milliseconds to seconds [12].

5.5 Observational Data on Stars

A detailed discussion of stellar observational techniques and data is beyond the scope of this summary. Nonetheless, one should have a rudimentary understanding of how certain measurements are made and how they confirm the preceding theoretical analysis of stars.

To a good approximation, stars act as black-body emitters of radiation. Using the Wien displacement law from statistical physics, the surface temperature T_s of a star may be found from the peak wavelength λ_{peak} of the radiation emitted by the star:

$$4.965 k_B T_s \approx \frac{hc}{\lambda_{\text{peak}}} \qquad \textbf{Wien displacement law} \tag{261}$$

For example, the peak emission wavelength of the sun is near the middle of the visible spectrum, $\lambda_{\text{peak}} \approx 5 \times 10^{-7}$ m, so its surface temperature is $T_{s\,\odot} \approx 5800\ ^o\text{K}$.

Typical surface temperatures $T_s \sim 6000\ ^o\text{K} \sim 0.5$ eV are low enough that electrons will be bound to ions but high enough that some of the electrons will be in excited states. Spectroscopic observations of transitions between these electronic states indicate the elemental composition of the stellar surface. While the relative composition of a star's interior will differ from its surface, these surface measurements provide evidence of the specific nuclear reactions discussed earlier.

Further evidence for the nuclear reactions is provided by measuring the flux of solar neutrinos arriving at the earth. Electron neutrinos are emitted by key steps in the proton-proton chains and the carbon cycle, Eqs. (243) and (247). Because the neutrinos have such a small interaction cross section, most of them escape from the sun and radiate through space. Along the way, they change into a mixture of roughly equal parts electron neutrinos, muon neutrinos, and tau neutrinos. Sensitive detectors on earth have been able to measure enough of the neutrinos to confirm the expected solar output.

Finding the luminosity of a star requires measuring its distance and its apparent visual magnitude as observed from the earth. Distances to nearby stars may be measured by trigonometric parallax as the earth orbits the sun. For more distant stars, one basically assumes that their luminosities are the same as the measured luminosities of closer stars with the same spectral properties.

The luminosity, radius, and surface temperature of a star are related by the Stefan-Boltzmann law for black-body radiators from the statistical physics summary:

$$L = 4\pi R^2 \sigma_{SB} T_s^4 \qquad \textbf{Stefan-Boltzmann law} \tag{262}$$

Using $L_\odot$ and $R_\odot$ for the sun in Eq. (262) yields a surface temperature of 5750 ^{o}K, in good agreement with the value calculated from the Wien displacement law. If a star's luminosity and surface temperature are determined, Eq. (262) can be used to calculate the star's radius.

If a star is in orbit with a companion star or very massive planet (and the orbit is seen approximately edge-on from earth), the orbit may be deduced from cyclical red- and blue-shifts in the star's spectrum, and then the star's mass may be found from the orbit. Observations show that stars' luminosities are strongly dependent on their masses, and this relationship may be understood theoretically. From Eqs. (221) and (210), the photon mean free path varies like $l_{mfp} \propto 1/\rho \propto R^3/M$. Likewise, from Eq. (218), the central temperature varies like $T_c \propto M/R$. Plugging these relations into $L \propto R\, l_{mfp}\, T_c^4$ from Eq. (229), one obtains $L \propto M^3$. Actually, the scattering cross section of photons by ions depends on temperature and thus indirectly on mass, and this additional mass dependence in l_{mfp} alters the power dependence to be more like

$$L \propto M^{3.5} \qquad \textbf{Mass-luminosity relation} \tag{263}$$

Note that since the luminosity is $\propto M^{3.5}$ but the fusion fuel supply is only $\propto M$, the life span of a star is $\propto 1/M^{2.5}$; larger stars burn out much more quickly than smaller ones.

Assuming that the central temperature is roughly the same in all hydrogen-burning stars, from Eq. (218) one would expect $R \propto M$. Based on empirical data, the real relationship is approximately

$$R \propto M^{0.7} \qquad \textbf{Mass-radius relation} \tag{264}$$

$$\propto L^{0.2} \qquad \text{using Eq. (263)} \tag{265}$$

There are two main reasons why the mass-radius relationship is not quite linear. The assumption that the central temperatures in stars are the same is not strictly valid–larger stars have hotter cores. Moreover, a star's radius is determined by a complex combination of radiative and convective energy transport in different regions from the center to the surface.

Hertzsprung-Russell diagrams plot the luminosity versus surface temperature for a whole range of stars. From Eq. (262), one would expect $L \propto T_s^4$ for stars that have the same radius, as shown in Fig. 24(a). Yet because stars' radii vary with their luminosities as in Eq. (265) the net result is

$$L \propto T_s^{6.7} \qquad \textbf{Luminosity-temperature relation for main sequence stars} \tag{266}$$

The exponent in Eq. (266) is approximate and empirical, just like the earlier exponents on which it is based. A range of typical stars is plotted in Fig. 24(b). Most stars fall on the curve given by Eq. (266), which is called the **main sequence**. However, some stars are far off the main sequence. Comparing with Fig. 24(a), one can see that stars in the upper right corner of Fig. 24(b) must have radii far larger than we have predicted. These are either protostars or red giants. Similarly, stars in the lower left corner of Fig. 24(b) must have anomolously small radii; they are white dwarfs.

Observed stars are of many different ages, and approximately 90% of them are on the main sequence. Thus a typical star spends about 90% of its life on the main sequence. As has been mentioned, more massive stars use up their fuel more rapidly, so stars at the more massive/luminous end of the main sequence are the first to finish their main sequence phase. Therefore, for a cluster of stars of the same age, one can determine the cluster's age by plotting a Hertzsprung-Russell diagram of the stars and noting the luminosity/mass at which the main sequence terminates. The less massive/luminous end of the main sequence is bounded by the minimum stellar mass of Eq. (252).

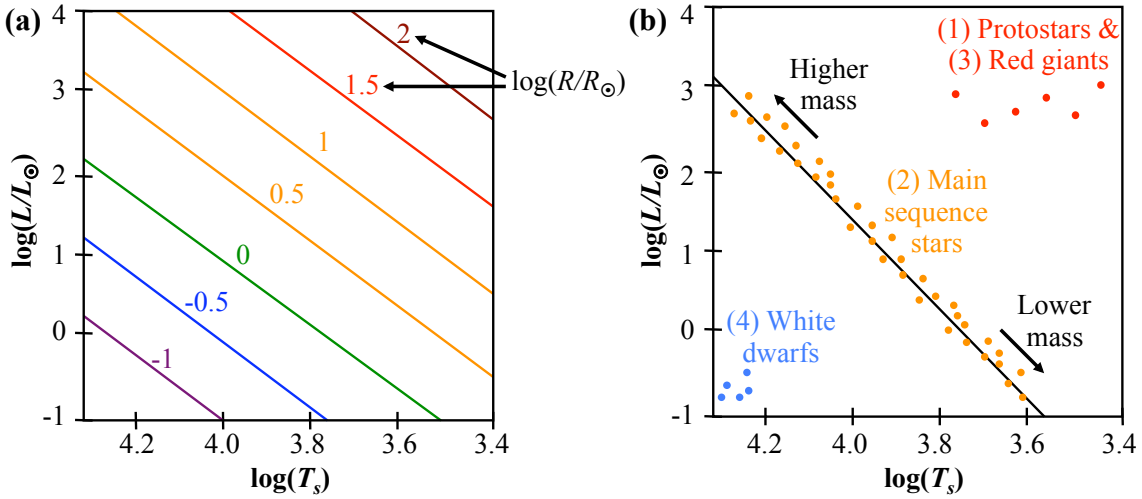

Figure 24. Hertzsprung-Russell diagrams plotting stellar luminosity versus surface temperature. **(a)** The luminosity-temperature relation is $L \propto T_s^4$ for stars of a specified radius [given as $\log(R/R_\odot)$ on each line]. **(b)** Typical observed values for a range of stars are plotted. Stars initially form as large, cold protostars (1) collapse and heat up. Stars spend most of their lifespan on the main sequence (2), more massive stars toward one end of the main sequence and less massive stars toward the other end. After consuming most of their fusion fuel, stars move off the main sequence and become red giants (3). Eventually all of the fuel is exhausted and stars become white dwarfs (4) that slowly radiate away their residual thermal energy.

Because of distance, the only star whose surface can be studied in detail is the sun. The sun's surface rotates with a period of approximately 25 days at the equator and over 31 days near the poles, so the sun definitely doesn't act like a rigid body. Local magnetic fields on the surface can be determined from the Zeeman splitting in spectral lines. Magnetic flux tubes with fields of up to 0.4 T are generated by mechanisms that aren't well understood, and they leave and re-enter the sun's surface at various points. Where the flux tubes intersect the surface, the gas temperature is approximately 3700 ^{o}K, somewhat cooler than the average surface temperature of 5800 ^{o}K. (A magnetic flux tube inhibits convective heat transport to the local surface. Also, its magnetic pressure partially supports the pressure of the surrounding surface material, so the gas within the tube does not need as much pressure/temperature.) Using Eq. (262), these cooler areas emit $(3700^o\text{K}/5800^o\text{K})^4 \approx 0.17$ as much light as the surrounding surface, causing them to appear dark in comparison; they are called **sunspots**. Because they are associated with leaving and re-entering flux tubes, sunspots tend to occur in pairs. For unknown reasons, the sun's overall magnetic field reverses directions every 11 years, and this cycle governs the activity of the flux tubes and sunspots.

A thin atmosphere of gas extends above the visible surface of the sun. The inner part of the atmosphere is called the chromosphere, and the outer part is termed the corona. The corona is quite diffuse and actually extends outward by several solar radii. Shock waves generated within the sun dissipate their energy within the corona, heating it to $1 - 2 \times 10^6$ ^{o}K, far hotter than the surface. Because of its high temperature, the corona emits radiation in the X-ray region.

Electrons, protons, and a few heavier ions escape from the sun and radiate outward through the solar system at $\sim$ 300 km/sec. The earth's magnetic field generally deflects this **solar wind**. However, peaks in the solar wind during flares in solar activity can create auroras in the upper atmosphere at the earth's poles and generate disturbances in the earth's ionosphere that interfere with radio communications.

6 Inertial Confinement Fusion

One approach to man-made fusion is to raise fusion fuel to densities and temperatures comparable to or exceeding those at the sun's core. Only the sun's vast amount of surrounding matter confined by its gravitational field can oppose the extreme pressure of fusion fuel under those conditions. Therefore, man-made systems that achieve the same conditions must operate transiently, rapidly compressing and heating the fuel to obtain enough fusion reactions before the fuel blows apart from its extreme pressure. Only the fuel's inertia slows its outward expansion, so this approach is called inertial confinement fusion (ICF). This section will describe ICF reactors that use small fusion explosions; fusion explosive devices (hydrogen or H bombs) apply similar principles on a much larger scale. Basic designs for these systems will be presented, and then the physics of implosion, ignition, and energy gain will be discussed.

6.1 Basic Designs

The key requirement for ICF reactors and fusion explosives is that most of the fuel must fuse before it blows apart. For the fusion reactions to occur rapidly enough, the fuel must initially be compressed to a certain density, which can be calculated. For a DT mixture with density $n_D = n_T$, the mass density is $\rho = (m_D + m_T)n_D \approx 5m_p n_D$; from Eq. (62), fusion occurs on a timescale

$$\tau_{\rm fus} \;=\; \frac{1}{n_D \left\langle \sigma v \right\rangle_{DT}} \;\approx\; \frac{5m_p}{\rho \left\langle \sigma v \right\rangle_{DT}} \,. \tag{267}$$

The compressed plasma expands at the speed of sound $v_s \equiv \sqrt{k_{_B}T/m_i}$ (where $m_i \approx 2.5m_p$ is the average ion mass), causing the density and temperature and thus the fusion reactions to drop off quickly (i.e., fusion rate $\propto n^2 \propto R^{-6}$). If fusion stops once the plasma radius expands by 1/3 of its compressed value $R_{\rm compr}$, the confinement time during which fusion occurs is

$$\tau_{\rm conf} \;=\; \frac{1}{3}\frac{R_{\rm compr}}{v_s} \;\approx\; \frac{R_{\rm compr}}{3}\sqrt{\frac{2.5m_p}{k_{_B}T}} \tag{268}$$

For a significant amount of fusion to occur, the confinement time must be longer than the fusion time, $\tau_{\rm conf} > \tau_{\rm fus}$. Using Eqs. (267) and (268), this condition is equivalent to

$$(\rho R)_{\rm compr} \;>\; \frac{6}{\left\langle \sigma v \right\rangle_{DT}}\sqrt{2.5m_p k_{_B}T} \;\approx\; 6 \text{ g/cm}^2 \quad \text{for DT with } T = 20 \text{ keV} \tag{269}$$

ICF fuel capsules have a compressed radius much less than 1 mm, so the required density is much higher than that of solid DT. Other fusion fuels are more difficult to fuse than DT and will require even higher values of ρR and temperature.

An external energy source called a **driver** must be used to very rapidly raise the fusion fuel to the required density and temperature. In ICF reactors, laser or particle beams serve as the driver. In fusion explosives, the driver is a fission bomb.

As shown in Fig. 25, laser or particle beams may be used either directly or indirectly to drive ICF [13, 14]. In direct drive, the beams are focused directly on a DT fuel capsule, compressing and heating it to fusion conditions. In indirect drive, the beams are focused into a hollow **hohlraum** of high-Z material (e.g., gold or lead) that surrounds the DT fuel capsule. The hohlraum walls are heated to a temperature of 200-300 eV and emit black-body radiation in the X-ray range. These X rays then compress and heat the DT to fusion conditions. Using the black-body X rays instead of focusing the laser/particle beams directly on the capsule greatly improves the uniformity with which the capsule surface is irradiated, thereby reducing surface perturbations which could grow into large instabilities during capsule implosion. Hohlraums for particle beams also contain internal shields (not shown) to prevent the beams from directly striking the DT capsule, prematurely heating the fuel, and making it harder to compress. Note that the hohlraum is destroyed in each blast.

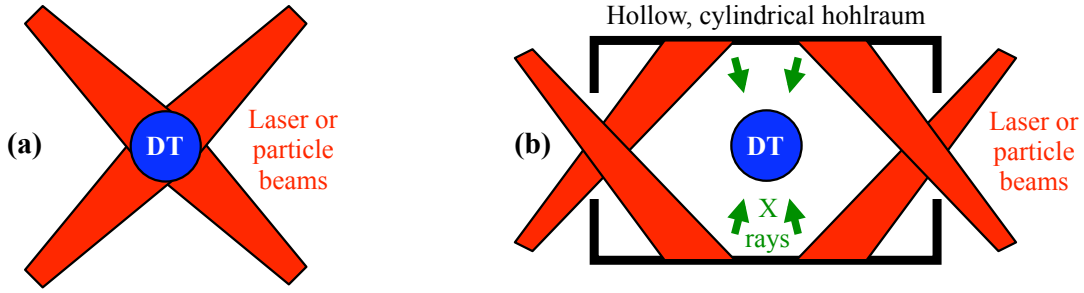

Figure 25. Inertial confinement fusion (ICF) using laser or particle beams. **(a)** In direct drive, the beams are focused directly on a DT fuel capsule, compressing and heating it to fusion conditions. **(b)** In indirect drive, a hollow hohlraum of high-Z material is used to convert the beam energy into X rays, which then irradiate the DT fuel capsule.

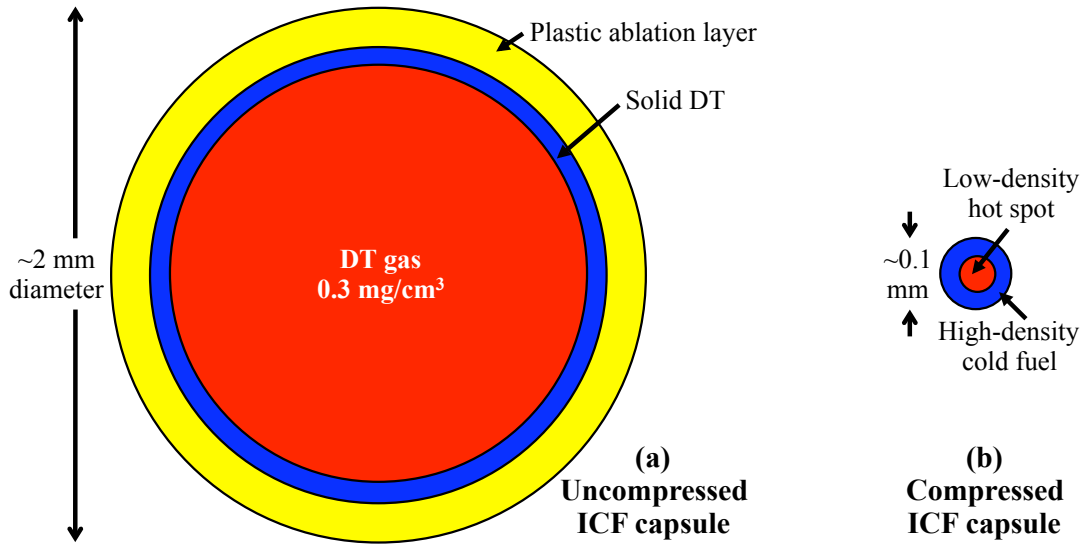

Figure 26. Typical DT fuel capsule for ICF before and after compression. **(a)** Before compression, the capsule has an outer ablative layer of plastic, a layer of solid cryogenic DT fuel, and an inner DT gas core. **(b)** The plastic is ablated away by the time of maximum compression, leaving a ~ 10 keV low-density hot spot of DT fuel surrounded by a much denser but colder layer of DT. Fusion begins in the hot spot and propagates outward into the rest of the DT.

Figure 26 shows a typical ICF fuel capsule before and after compression [13]. The driver gives a work $p\,dV$ to the capsule, where p is the driver pressure and dV the change in capsule volume during compression; thus spherical shells can absorb more energy than solid pellets of the same mass. Before compression, the capsule has an outer layer of plastic that can be ablated by the external irradiation, acting as rocket exhaust to compress the rest of the capsule. Inside the ablation layer is a shell of cryogenic solid DT. The hollow center of the capsule is filled with DT gas. The outer plastic layer is ablated away by time t of maximum compression. A central hot spot of radius $r_{\rm hs}$ is heated to fusion temperatures (~ 10 keV) by the converging shock waves, but it has a relatively low density and only contains $\sim 2\%$ of the total DT fuel. The remainder of the fuel forms a colder but denser shell surrounding the hot spot with an outer radius $\sim 2r_{\rm hs}$. Fusion reactions initiate in the hot spot and spread outward into the rest of the DT, heating the fuel as they go.

Liquid lithium-6 might be flowed over the inner walls of an ICF reactor to protect them from the repeated miniature nuclear explosions and breed tritium for new fusion capsules.

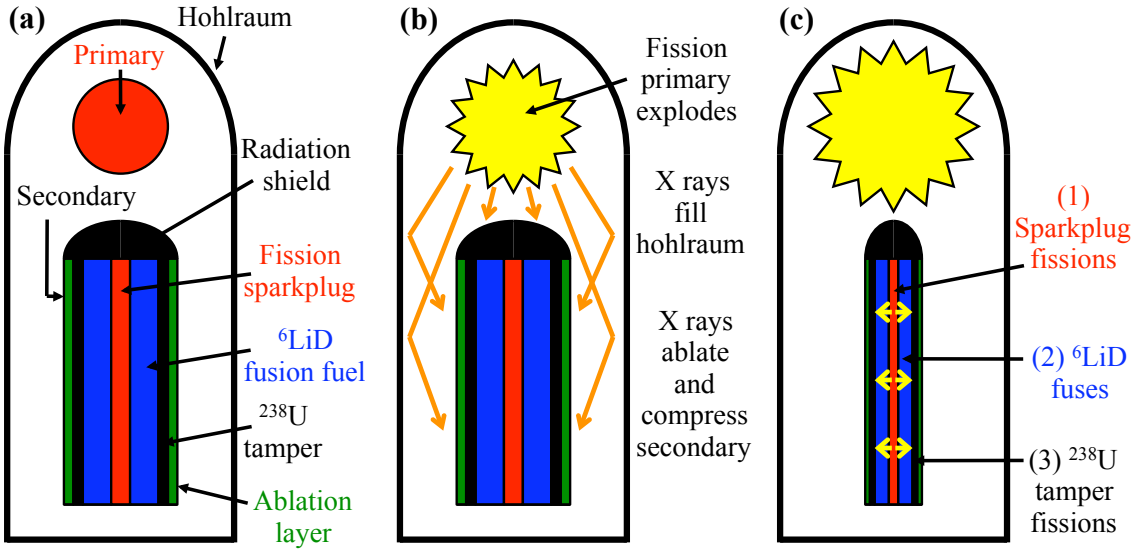

Figure 27. Fusion explosive device [15-18]. **(a)** In the Teller-Ulam design, a hohlraum encloses a fission bomb primary and a secondary that contains both fission and fusion fuel. **(b)** Detonation of the fission primary creates X rays that ablate and compress the secondary. **(c)** Compression of the secondary triggers reactions in its fission and fusion fuel.

To be storable, fusion explosive devices use solid room-temperature lithium deuteride instead of cryogenic DT or DD fuel. LiD permits coupled tritium-breeding and fusion reactions [15]:

$$\begin{array}{lccccccccc} \text{(A)} & \text{n} & + & {}^{6}\text{Li} & \longrightarrow & 4.8\text{ MeV} & + & {}^{4}\text{He} & + & \text{T} \\ & \uparrow & & & & & & & & \downarrow \\ \text{(B)} & \text{n} & + & {}^{4}\text{He} & + & 17.6\text{ MeV} & \longrightarrow & \text{D} & + & \text{T} \end{array} \qquad \textbf{^{6}LiD Jetter cycle} \ (270)$$

92.5% of natural lithium is ^{7}Li, which can replace step A above with the endothermic reaction n $+{}^{7}\text{Li} \rightarrow -2.5$ MeV $+{}^{4}\text{He} + \text{T} + \text{n}$. D + D fusion can also play a critical role in producing neutrons.

Figure 27 presents the ca. 1951 Teller-Ulam design for a fusion explosive device. This design and the accompanying information are drawn solely from unclassified sources [15-18] and from obvious extensions of indirect-drive ICF, which appears to copy much from its older and larger relative. **No classified sources were used.** As a result, the design details may be somewhat off.

As shown in Fig. 27, a hohlraum casing of high-Z material (e.g., lead) encloses a fission bomb **primary** and a cylindrical **secondary** that contains both fission and fusion fuel. A shield prevents the primary from directly bombarding the secondary with radiation. At the center of the secondary is a subcritical fission **sparkplug** of uranium-235 or plutonium-239. Surrounding the sparkplug is solid lithium deuteride. Around the ^{6}LiD is a uranium tamper and then an outer layer of ablative material (e.g., plastic or just extra uranium). Note that the secondary could also be spherical and/or hollow. Typically the primary and secondary are supported within the hohlraum by a lightweight low-Z foam that will not interfere with the detonation process. The fission primary explodes first, emitting radiation that heats the hohlraum, filling it with black-body thermal X rays. The X rays ablate the outer layer of the secondary, and the exhaust compresses the rest of the secondary. The radiation shield prevents direct X rays, neutrons, and electrons from prematurely heating the fuel in the secondary. Compression of the secondary causes the sparkplug to become supercritical and fission rapidly. Heat and neutrons generated by the sparkplug initiate fusion in the ^{6}LiD, and energetic neutrons from the fusion reactions cause the uranium tamper to fission.

6.2 ICF Conditions

Drivers

Although indirect drive loses much of the driver energy while converting it to X rays, there are several reasons for choosing it over direct drive: (1) The black-body radiation within the hohlraum is much more uniform than the driver beams, minimizing perturbations that could lead to asymmetry or instability during the implosion. (2) X rays more efficiently penetrate the dense ablated plasma surrounding the fuel capsule, partially compensating for the loss in converting driver energy to X rays. (3) Energetic electrons produced during laser beam absorption are much further from the fuel capsule with indirect drive, thereby reducing premature heating of the fuel. (4) Indirect-drive ICF better models the operation of fusion bombs, which is the most feasible application of ICF.

The maximum efficiency with which a hohlraum can convert laser energy to energy striking the fuel capsule is $10 - 20\%$. This efficiency is the product of two factors. The first is the $\sim 70\%$ maximum efficiency for converting laser beam energy to X rays in a hohlraum; this conversion efficiency is roughly the same for ion beams as well. The second factor is the fraction of the X-ray energy that strikes the fuel capsule. This fraction depends on the geometry and the ratio of the capsule surface area to the hohlraum's inner surface area, but it is typically $\sim 15 - 30\%$ at best. This maximum value arises because the hohlraum must be significantly larger than the capsule to accomodate the laser beams and to make the black-body X-ray radiation uniform to the required tolerance.

A hohlraum cannot operate effectively above a certain temperature. If this temperature is exceeded, material ablated from the inner surface of the hohlraum will form a plasma so dense that it prevents the driver beams from entering the hohlraum; the plasma frequency approaches or exceeds the driver beam's frequency. Furthermore, parametric instabilities of the laser beams interacting with such a dense plasma would accelerate electrons, which could preheat the fuel capsule. For a 0.35 μm laser driver, the maximum permissable hohlraum temperature is approximately 300 eV.

To date, most of the high-energy ICF drivers have been lasers. Shorter laser wavelengths are greatly preferred in order to better penetrate through the plasma that is created inside the hohlraum. The National Ignition Facility and its forerunner Nova at the Lawrence Livermore National Laboratory use neodymium glass lasers with a wavelength of 1.06 μm frequency-tripled to a final wavelength of 0.35 μm. These lasers have a maximum overall efficiency of 1-2%, which is much too low for an actual reactor. Krypton fluoride excimer lasers with a wavelength of 0.26 μm and a maximum efficiency of $6 - 8\%$ have been proposed by Los Alamos. It is hoped that novel solid state lasers such an ytterbium-doped fluorapatite crystal pumped by an InGaAs laser diode array could produce similar wavelengths with efficiencies as high as 10%, though much research remains to be done.

Although particle beams are more difficult to focus than lasers, they could make attractive drivers because of the higher efficiency of particle accelerators. Heavy ion accelerators have a predicted $20 - 35\%$ efficiency but still need a great deal of development. Sandia National Laboratory has developed a series of light ion drivers with pulse energies up to 100 kJ. Electron beam drivers are not desirable since electrons scatter and penetrate more easily than ions and could preheat the fuel.

ICF drivers must concentrate their energy into pulses that are shorter than the capsule implosion time. For a capsule with a radius of ~ 1 mm and an average implosion velocity $\sim 2 \times 10^7$ cm/sec, this implosion time is ~ 5 nsec. It is also important for the driver power to start low and steadily increase during the pulse time. Such adiabatic compression reduces the shock waves and the shock-induced premature heating that could occur in the fuel if full power were applied immediately.

Implosion

In a hohlraum filled with radiation at temperature $T_{\rm rad}$, the surface of the fusion capsule quickly comes to the same temperature, vaporizes, and explodes outward at an exhaust velocity of

$$v_{\rm exh} \approx \sqrt{\frac{k_B T_{\rm rad}}{m_{\rm exh}}}\,, \tag{271}$$

where $m_{\rm exh}$ is the mass of particles in the vaporized exhaust. Clearly minimizing the exhaust particle mass will maximize the exhaust velocity. Thus the best ablation material would be frozen ^{1}H, which is feasible for ICF capsules, although a hydrogen-rich plastic is the most practical choice. For $m_{\rm exh} = m_p$ and $T_{\rm rad} = 200 - 300$ eV, Eq. (271) yields $v_{\rm exh} \approx 1.4 - 1.7 \times 10^7$ cm/sec.

The outward motion of material ablated from the capsule's surface forces the rest of the capsule to implode inward. If the capsule is ablated from an initial mass $M_{\rm initial}$ to a final mass $M_{\rm final}$, the peak implosion velocity $v_{\rm impl}$ may be found from the equation for conventional rockets:

$$v_{\rm impl} = v_{\rm exh} \ln\left(\frac{M_{\rm initial}}{M_{\rm final}}\right) \qquad \textbf{Rocket equation for implosion velocity} \tag{272}$$

Thus for ICF with $v_{\rm exh} \approx 1.4 - 1.7 \times 10^7$ cm/sec and $M_{\rm initial}/M_{\rm final} = 4 - 8$, the implosion velocity is in the range $v_{\rm impl} \approx 2 - 4 \times 10^7$ cm/sec.

One can calculate the pressure of the exhaust on the capsule. The radiation flux incident on the capsule is $I_{\rm rad} = \sigma_{SB} T_{\rm rad}^4$. Experimentally, about 30% of this incident energy is converted to exhaust energy (the remainder going into capsule energy or being lost), so the exhaust pressure is

$$P_{\rm exh} \approx 0.3\,\frac{I_{\rm rad}}{v_{\rm exh}} = 0.3\,\sigma_{SB} T_{\rm rad}^{7/2} \sqrt{\frac{m_{\rm exh}}{k_B}} \tag{273}$$

For ICF with $T_{\rm rad} = 200 - 300$ eV and $m_{\rm exh} \geq m_p$, the pressure is $P_{\rm exh} \geq 30 - 140$ Mbar.

The efficiency of an ideal rocket (fraction of expended energy converted to kinetic energy of the final mass) is

$$\epsilon_{\rm rocket} \equiv \frac{\frac{1}{2} M_{\rm final} (\Delta v)^2}{\frac{1}{2}(M_{\rm initial} - M_{\rm final}) v_{\rm exh}^2} = \frac{(\Delta v / v_{\rm exh})^2}{\exp(\Delta v / v_{\rm exh}) - 1} = \frac{[\ln(M_{\rm initial}/M_{\rm final})]^2}{(M_{\rm initial}/M_{\rm final}) - 1} \tag{274}$$

This efficiency reaches a maximum of 0.65 at $\Delta v / v_{\rm exh} \approx 1.6$ or $M_{\rm initial}/M_{\rm final} \approx 5$. For an ideal rocket, no more energy is added to the exhaust once it leaves the rocket. However, for a radiation-driven ICF rocket, additional energy is absorbed by the exhaust even after it has left the capsule and cannot exert more force on the capsule. This lowers the efficiency considerably. For direct-drive ICF with a visible or near-UV laser wavelength, the maximum efficiency is 5-10%. For indirect drive, the X rays penetrate better through the exhaust to be absorbed at the capsule surface, so the rocket efficiency is 15-20%. Assuming a hohlraum efficiency of 20%, the overall efficiency is $\sim 4\%$ for indirect drive, near the lower limit of the efficiency for direct drive.

Just as multiple stages are used to attain higher final velocities in rockets, they could be used to reach higher implosion velocities in ICF. A multistage ICF capsule would have two or more concentric shells, with the outer shells more massive than the inner ones. An imploding outer shell would impart its momentum to the next inner shell; because of the lower mass of the inner shell, this would correspond to a higher velocity. While this approach could theoretically attain higher implosion velocities, the multishell structure would greatly exacerbate the Rayleigh-Taylor instabilities that plague ICF, potentially doing more harm than good.

Rayleigh-Taylor Instability

As discussed in Section 3.4, the Rayleigh-Taylor instability occurs when a heavy fluid layer is above a light fluid layer and is pulled "down" by gravity, centrifugal force, or another force. ICF capsules are prone to the Rayleigh-Taylor instability at two different points:

1. Early during implosion, the dense capsule shell is accelerated inward. Due to its inertia it wants to lag behind, and it is opposed only by the surrounding low-density ablated plasma. Thus perturbations at the surface of the dense capsule shell can grow into large instabilities.

2. In the later implosion phases, the solid DT shell decelerates as its inward inertial motion is opposed by the low-density but high-pressure DT plasma in the center. In this case, perturbations at the solid/plasma boundary can grow into serious Rayleigh-Taylor instabilities.

The instability growth rate determines how long the implosion can last before the instabilities become too severe, or equivalently how large an uncompressed capsule can be compared to its compressed radius. Assuming a constant acceleration a and initial capsule radius $R_{\rm init}$, the time $\tau_{\rm impl}$ required for the implosion is

$$\tau_{\rm impl} \;=\; \sqrt{\frac{2R_{\rm init}}{a}}\;. \tag{275}$$

Using Eq. (168) for the Rayleigh-Taylor instability growth rate γ, the number of e-foldings $N_{\rm e-fold}$ of the instability during the implosion time is

$$N_{\rm e-fold} \;=\; \gamma\,\tau_{\rm impl} \;=\; \sqrt{k\,a\,\tau_{\rm impl}^2}\;. \tag{276}$$

Instabilities with sizes comparable to the final compressed dimensions are of greatest concern, as they could seriously disrupt the final compressed state of the capsule. By choosing an appropriate instability wavenumber $k \sim 1/(2r_{hs})$ and using Eq. (275), one can rewrite Eq. (276) as

$$C_r \;\equiv\; \frac{R_{\rm init}}{r_{hs}} \;\sim\; N_{\rm e-fold}^2\;, \tag{277}$$

in which the convergence ratio C_r is defined as the ratio of the initial capsule radius to the final hot spot radius. If the maximum tolerable number of instability e-foldings is 5-6, the maximum convergence ratio is $C_r \sim 25 - 36$. This agrees with the results of more detailed calculations.

Constraints are also imposed on the uniformity of the acceleration. A local difference δa in the initial inward acceleration will result in a perturbation δr in the final compressed radius:

$$\delta r \;\approx\; \frac{1}{2}\delta a\;\tau_{\rm impl}^2 \tag{278}$$

Combining Eqs. (278) and (275) yields the maximum permissable deviation δa for the acceleration or δv for the implosion velocity:

$$\frac{\delta a}{a} \;\approx\; \frac{\delta v}{v_{\rm impl}} \;\approx\; \frac{\delta r}{R_{\rm init}} \;\approx \frac{1}{C_r}\,\frac{\delta r}{r_{hs}}\;. \tag{279}$$

If the perturbation were comparable to the final compressed size, it would disrupt the compressed fuel. It would also mean that a significant amount of the input energy had been wasted as kinetic energy of the final perturbation instead of compression energy for the entire fuel mass. Limiting the maximum perturbation to $\delta r < r_{hs}/4$ and assuming $C_r \sim 30$ gives

$$\frac{\delta a}{a} \;\approx\; \frac{\delta v}{v_{\rm impl}} \;<\; 1\%\;. \tag{280}$$

This tolerance is so tight because the perturbation size is compared to the compressed radius, which is ∼30x smaller than the initial capsule radius. Hohlraum radiation is typically much more uniform than direct beam energy, and thus indirect drive is better able to meet this requirement.

Ignition

External energy is used to heat only the central $\sim 2\%$ of the ICF fuel mass to fusion temperatures, since heating all of the fuel would require too much energy input. If fusion reactions can be ignited in the central hot spot, they should heat and cause fusion in the rest of the fuel. The requirements for igniting the hot spot may be determined by comparing the input and loss energies. There are two sources of input heat energy, compressive energy provided from the external driver and internally generated fusion energy that is deposited within the fuel. There are also two important loss mechanisms, bremsstrahlung radiation and electron-mediated heat conduction.

The power $P_{\rm in}$ per volume V put into the DT fuel by the implosion process may be found from the implosion velocity and the pressure p within the fuel:

$$\frac{P_{\rm in}}{V} \;=\; \frac{p\,dV/dt}{V} \;=\; \frac{p\,A\,v_{\rm impl}}{V} \;=\; \frac{3p\,v_{\rm impl}}{r} \;=\; 2.3\times10^8 \frac{\rho_{\rm g/cm^3}\,T_{keV}\,v_{\rm impl,\,cm/sec}}{r_{\rm cm}}\;\frac{\rm W}{\rm cm^3}\,. \qquad (281)$$

If a volume of fuel has $\rho r > 0.3$ g/cm^2, α particles produced by DT reactions will leave essentially all of their energy $E_\alpha = 3.5$ MeV in the volume, adding a power P_α to further heat the fuel:

$$\frac{P_\alpha}{V} \;=\; n_D n_T \langle\sigma v\rangle_{DT} E_\alpha \;=\; 8\times10^{33}\rho^2_{\rm g/cm^3}\langle\sigma v\rangle_{\rm cm^3/sec}\;\frac{\rm W}{\rm cm^3} \qquad \text{for } (\rho r)_{\rm h.s.} > 0.3\ {\rm g/cm^2} \quad (282)$$

Bremsstrahlung radiation losses may be calculated by rewriting Eq. (33) as

$$\frac{P_{\rm brem}}{V} \;=\; 3.0\times10^{16}\rho^2_{\rm g/cm^3}\sqrt{T_{keV}}\;\frac{\rm W}{\rm cm^3}\,. \qquad (283)$$

Radiation scattering can occur in ICF plasmas just as in stars. At the temperatures of interest, $T \geq 10$ keV, Thomson scattering off electrons dominates over scattering off ions. Using Eq. (221) with $\rho \approx 2.5 m_p n_e$, one finds that scattering of radiation within the fuel becomes important for

$$\rho r \;\geq\; \frac{2.5 m_p}{\sigma_{\rm Thomson}} \;\approx\; 6.3\ {\rm g/cm^2} \qquad (284)$$

Thus for typical hot spots with $\rho r \sim 0.3$ g/cm^2, bremsstrahlung radiation is essentially free to escape from the hot spot, and Eq. (283) may be used to calculate the bremsstrahlung power loss for the hot spot. However, complete fuel capsules typically have $\rho R \sim 6$ g/cm^2, so accurate calculations must include the effects of internal radiation scattering.

Electron heat conduction at the edge of the hot spot may be calculated by using Eq. (93) and estimating $|dT/dr| \equiv f_e T/r$, where $f_e \approx 0.5$ is an experimentally determined constant:

$$\frac{P_{\rm cond}}{V} \;=\; \frac{A}{V}\kappa_e\left|\frac{dT}{dr}\right| \;=\; \frac{6.4 f_e 24\pi\epsilon_o^2 (k_B T)^{7/2}}{r^2\sqrt{m_e}e^4\ln\Lambda} \;=\; 8\times10^{12}\,\frac{T^{3.5}_{keV}}{r^2_{\rm cm}}\;\frac{\rm W}{\rm cm^3}\,. \qquad (285)$$

From Eqs. (283) and (285), electron heat conduction will be the dominant loss mechanism when

$$P_{\rm cond} \;>\; P_{\rm brem} \qquad \leftrightarrow \qquad T \;>\; 15.5\,(\rho r)^{2/3}_{\rm h.s.,\ g/cm^2}\ {\rm keV} \qquad (286)$$

Equation (286) is satisfied at temperatures typical of DT fusion, $T \geq 10$ keV, and values of hot-spot ρr large enough to confine the α particle energy, $\rho r \approx 0.3$ g/cm^2.

Equations (281) and (282) show that α heating will dominate over implosion-driven heating for

$$P_\alpha \;>\; P_{\rm in} \qquad \leftrightarrow \qquad (\rho r)_{\rm h.s.,\ g/cm^2} \;>\; 0.3\ {\rm g/cm^2} \qquad (287)$$

Finally, the dominant energy gain and dominant energy loss may be compared. If $T = 10$ keV and

$$P_\alpha \;>\; P_{\rm cond} \qquad \leftrightarrow \qquad (\rho r)_{\rm h.s.,\ g/cm^2} \;>\; 0.3\ {\rm g/cm^2}\,, \qquad (288)$$

self-sustaining fusion reactions will occur in the hot spot and propagate outward into the rest of the fuel pellet, heating all of the fuel to reaction temperatures by α heating.

6.3 Requirements for ICF Energy Gain

By comparing the fusion energy produced by an ICF capsule with the energies needed to compress and heat the capsule, the fundamental requirements for energy gain can be determined.

Equation (269) estimated the ρR required for ICF. A more detailed analysis gives the amount of fusion as a function of any ρR. For $n_D = n_T = n_i/2$, fusion reactions consume ions at a rate

$$\frac{dn_D}{dt} \;=\; -n_D n_T \left\langle \sigma v \right\rangle_{DT} \qquad \Longrightarrow \qquad \frac{dn_i}{dt} \;=\; -\frac{1}{2} n_i^2 \left\langle \sigma v \right\rangle_{DT} \tag{289}$$

By assuming that $\langle \sigma v \rangle_{DT}$ and the density are approximately constant over the plasma volume and the confinement time $\tau_{\rm conf}$, Eq. (289) can be integrated to obtain

$$\frac{1}{n_{if}} \;-\; \frac{1}{n_{io}} \;=\; \frac{\left\langle \sigma v \right\rangle_{DT} \tau_{\rm conf}}{2} \;, \tag{290}$$

where n_{io} is the initial ion density and n_{if} is the final ion density.

One can define the fraction of the fuel that is burned up:

$$f_{\rm burn} \;\equiv\; \frac{\Delta n_i}{n_{io}} \;=\; \frac{n_{io} - n_{if}}{n_{io}} \qquad \Longrightarrow \qquad n_{if} \;=\; n_{io}(1 - f_{\rm burn}) \tag{291}$$

Substituting this expression for n_{if} into Eq. (290) gives an expression for the fuel burnup:

$$f_{\rm burn} \;=\; \frac{n_i \tau_{\rm conf}}{n_i \tau_{\rm conf} + 2/\left\langle \sigma v \right\rangle_{DT}} \;=\; \frac{\rho R}{\rho R + 6\sqrt{2.5 m_p k_{_B} T}/\left\langle \sigma v \right\rangle_{DT}} \;\approx\; \frac{(\rho R)_{\rm g/cm^2}}{\rho R + 6 \text{ g/cm}^2} \quad \text{for 20 keV DT} \tag{292}$$

Equation (292) used Eq. (268) and $\rho \approx 2.5 m_p n_i$. It shows that $\rho R \geq 6$ g/cm^2 is required to burn up at least 50% of the fuel, confirming the earlier estimate in Eq. (269).

In DT fusion, 0.375% (17.6 MeV) of the particle rest mass is converted to energy, so the yield is

$$E_{\rm yield} \;=\; 0.00375 f_{\rm burn} M c^2 \;=\; 3.38 \times 10^{11} f_{\rm burn} M_{\rm g} \text{ J} \;=\; 80 f_{\rm burn} M \text{ t} \tag{293}$$

from $M_{\rm g}$ grams of DT, where 1 t$= 4.2 \times 10^9$ J is an energy equivalent to the detonation of one ton of high explosive. Thus a little mass gives a big bang, which is good news for bombs but bad news for ICF. To prevent a capsule explosion from destroying an ICF reactor, the capsule mass must be kept very small. Assuming the largest explosion that can be contained in a reactor is approximately 1/4 t$\approx$ 1 GJ, for 50% burnup the maximum capsule size from Eq. (293) is $M_{\rm max} \approx 6$ mg.

A typical power plant size of 1 GW electric would require a gross fusion power of ~ 3 GW, assuming a thermal conversion efficiency of $\sim 1/3$ and neglecting all input and loss powers. If the yield per capsule is ≤ 1 GJ, an ICF reactor must detonate at least three capsules every second.

Holding ρR constant at the value in Eq. (269) needed for fusion, the fuel mass may be written as

$$M \;=\; \frac{4}{3}\pi R^3 \rho \;=\; \frac{4}{3}\pi \frac{(\rho R)^3}{\rho^2} \;. \tag{294}$$

Therefore, achieving the ρR required for fusion while keeping the pellet mass as small as possible requires maximizing the density or compression. To attain $\rho R = 6$ g/cm^2 with a pellet mass $M \leq 6$ mg, Eq. (294) shows that the compressed density must be $\rho \geq 400$ g/cm^3.

To be as efficient as possible, the fuel should first be compressed to the necessary density (while being kept as cold as possible), *then* heated to fusion temperatures. If the fuel were heated before or during compression, the added thermal pressure of the particles would oppose the compression and reduce the maximum attainable density. As was shown for stars, when matter is compressed sufficiently, its electrons become degenerate, thereby acquiring a relatively high Fermi energy E_F. Using $n_e = n_i \approx \rho/(2.5 m_p)$, the Fermi energy from Eq. (230) may be written as

$$E_F \;=\; \frac{\hbar^2}{2m_e}\left(\frac{3\pi^2}{2.5 m_p}\rho\right)^{2/3} \;=\; 14 \rho_{\rm g/cm^3}^{2/3} \text{ eV} \;. \tag{295}$$

The average energy per degenerate electron is $0.6E_F$, so compression to high densities requires supplying that much energy to each electron. Since the total number of electrons is $N_e = N_i = M/(2.5m_p)$, the energy required for compression is

$$E_{\rm compress} \;=\; 0.6E_F\,\frac{M}{2.5m_p} \;=\; 3\times10^5\rho_{\rm g/cm^3}^{2/3}M_{\rm g}\ {\rm J}\ . \tag{296}$$

For a compressed density $\rho = 400$ g/cm^3, Eq. (295) gives $E_F = 760$ eV. Therefore, the fuel temperature must be kept significantly below this value if the fuel is to remain Fermi-degenerate during compression. Realistically, the electrons will have a finite temperature that opposes compression, and some energy will go to the ions, so Eq. (296) is a minimum bound on the compression energy.

After compression, the ions (and inevitably the electrons) must be heated to a fusion temperature T, which requires an input energy

$$E_{\rm heat} \;=\; f_{\rm heated}(N_i+N_e)\frac{3}{2}k_BT \;=\; \frac{M}{2.5m_p}3k_BT \;=\; 1.15\times10^8\ f_{\rm heated}\ M_g\ T_{keV}\ {\rm J} \tag{297}$$

in which $f_{\rm heated}$ is the fraction of the fuel that must be initially heated by input energy. If the reaction is self-sustaining, the initial reactions will then heat the rest of the fuel to fusion temperatures.

For $\rho = 400$ g/cm^3, limiting the heating energy to $E_{\rm heat} \le E_{\rm compress}$ limits the fraction of the fuel that can be heated to 10 keV to $f_{\rm heated} = 1.4\%$. Heating much more of the fuel would drastically increase the required energy input. Thus in ICF, one strives to create a central hot spot that contains only 1-5% of the total pellet mass.

Using Eqs. (296) and (297), the total energy required to compress a 6-mg DT capsule to $\rho = 400$ g/cm^3 and heat $\sim 3\%$ of its mass to 10 keV is ~ 0.3 MJ. Assuming a 5% maximum efficiency for coupling driver energy to pellet implosion, the minimum required driver energy is ~ 6 MJ. If additional energy is necessary to heat more of the fuel or to overcome instabilities, the required driver energy could be much higher. In the 1980s, the Halite-Centurian underground nuclear tests used fission bomb X-rays (currently the only driver of sufficient energy) to ignite ICF capsules. The limited information available in unclassified sources suggests that capsules needed to absorb at least 20 MJ to ignite [14], which would correspond to a 400 MJ driver assuming 5% overall coupling efficiency. Even for a relatively high driver efficiency of 30%, operating the driver would require ~ 1.3 GJ, far more than the $0.3 - 0.4$ GJ of electrical energy produced per capsule.

Another consideration is the peak fusion power that must be withstood and converted by the inner walls of a reactor. As found earlier, an ICF reactor with 1 GW electric output must detonate at least three 1-GJ capsules per second. Each detonation would release most of its 1 GJ of energy as neutrons and X-rays during a time $\tau_{\rm conf} \sim \tau_{\rm fus} \approx 5\times10^{-11}$ sec, as given by Eq. (267) for DT at 20 keV. This represents a cumulative duration of 1.5×10^{-10} sec for all three detonations each second. In contrast, a magnetic fusion reactor of the same size could operate on a continuous or nearly continuous basis, spreading the 3 GJ of energy out evenly over the second. Thus the inner walls of an ICF reactor must withstand a peak power $\sim 7\times10^9$ higher than a magnetic fusion reactor.

It is instructive to consider ICF with D-^{3}He fuel, which is cleaner than DT but harder to burn. Using Eq. (292), 50% burnup of D-^{3}He at a representative temperature of 50 keV requires $\rho R = 74$ g/cm^2. The fusion yield is roughly the same as for DT, so the maximum capsule fuel mass is still 6 mg. Achieving the required ρR with this mass requires a compressed density of $\rho = 1.7\times10^4$ g/cm^3 according to Eq. (294). Including a factor of $(3/2)^{2/3}$ in Eq. (296) to account for the different fuel mass per electron, the required compression energy is 1.6 MJ. Allowing a comparable amount of energy in order to heat the hot spot, the total absorbed target energy is ~ 3 MJ. If the driver-target coupling efficiency is 5%, the minimum required driver energy is 60 MJ.

The most efficient drivers currently contemplated are heavy ion accelerators with efficiencies of $\sim 30\%$, so ~ 200 MJ would be required to run the driver for D-^{3}He. After converting the fusion energy to electricity (either thermally or by directly converting the charged particles to electricity), each fusion capsule would produce at most several hundred MJ. This energy must supply the driver, make up for bremsstrahlung and other losses, and still have enough left over to make this a worthwhile energy generation method. Yet the minimum driver energy would consume a sizeable fraction of this output. Thus there is little margin to increase the driver energy if that proves necessary in order to heat more of the fuel or minimize instabilities. While the situation would improve with larger capsule sizes, increasing the size significantly beyond the 1 GJ maximum yield that has been assumed here would probably destroy the ICF reactor. Therefore, ICF with advanced fuels would be marginal at best and may not even be able to break even.

To summarize, ICF does not appear promising for power generation because of the following reasons:

- **Minimum implosion energy.** The Halite-Centurian experiments indicate that ICF capsules may need to absorb as much as 20 MJ to ignite [14], as opposed to the 0.3 MJ theoretical minimum predicted by Eqs. (296) and (297) for ideal conditions. This could require a driver with an input energy > 1.3 GJ, exceeding the fusion output energy.
- **Advanced fuels.** ICF with advanced fuels like D-^{3}He would require even more energy.
- **Targets.** A daunting engineering requirement of ICF reactors is an automated system to reprocess lithium breeder material into precisely fabricated DT targets, then inject and carefully position the targets in the reactor chamber, all with a throughput of several per second.
- **Port access and shielding.** It would be very difficult to protect the target injection port and driver beam injection ports from blast damage while still being able to use them, especially with several injections and several detonations per second.
- **First wall.** Any fusion reactor must have inner walls that absorb and convert the fusion energy, use neutrons to breed tritium if necessary, and do not ablate into the plasma or otherwise interfere with the fusion process. Because the peak output power is $\sim 7 \times 10^9$ higher in ICF than in a continuous magnetic fusion reactor of the same time-averaged output power, design and operation of these walls would be particularly challenging for ICF.
- **Cost.** The National Ignition Facility is estimated to cost $4 billion (and still rising!) and will have 0.6 MJ of driver energy [14]. An ICF power plant would need a much larger driver and additional equipment like a high-throughput automated target cycling system, rendering it far more expensive than other power plants that electric utilities could build.

While ICF is probably not suitable for power generation, it could be useful for nuclear weapons development. Since the U.S. no longer conducts test explosions of nuclear weapons, ICF could be used for subscale tests of new weapon designs. As has been noted, ICF and nuclear bombs share a great deal of physics in common. The similarity could be extended by adding fissile material to an ICF target. Although the masses involved are far less than the usual critical mass for fission, significant reactions might be attained with enough compression and/or fusion neutrons [17]. (This potential performance-enhancing strategy is not an option for ICF reactors, as it could greatly contribute to the radioactivity and the blast.) ICF might also be useful for measuring basic materials properties at weapon-like conditions [17]. Of course, such subscale tests would not be as good as full-scale tests for evaluating new weapons designs, but they may be the only option. An additional application that is sometimes cited is predicting the readiness of existing weapons in the stockpile, though there does not appear to be a convincing physics basis for this assertion.

7 Magnetic Confinement Fusion

Fusion-temperature plasmas at ICF densities create too much pressure to be confined by any man-made approach. To contain plasmas and circumvent some of the problems of ICF, one must decrease the plasma pressure by lowering the density, typically to $n_i \sim 10^{15}$ cm^{-3} [Eq. (142)]. Because a plasma would rapidly cool if it contacted material walls, it must be confined by force fields. Confinement by electromagnetic wave pressure would require too much input power, and static electric fields could only contain one particle species (ions or electrons), while encouraging the other to escape [2]. One is thus led to use magnetic fields to confine plasmas. This section will cover both open and closed magnetic field geometries that have been considered for fusion plasmas. Engineering considerations associated with magnetic fusion reactors will also be presented briefly.

7.1 Open Magnetic Field Geometries

As explained in Sections 1.4 and 2.3, particles spiral tightly around magnetic field lines, so a longitudinal magnetic field can confine a cylindrical plasma [Fig. 8(a)]. However, particles freely move along the field lines and escape from the ends of the cylinder. By using a weak field B_o in the middle and a stronger field B_m at the ends, the magnetic mirror effect can be employed to reflect particles at each end back into the plasma, as shown in Figs. 6 and 28.

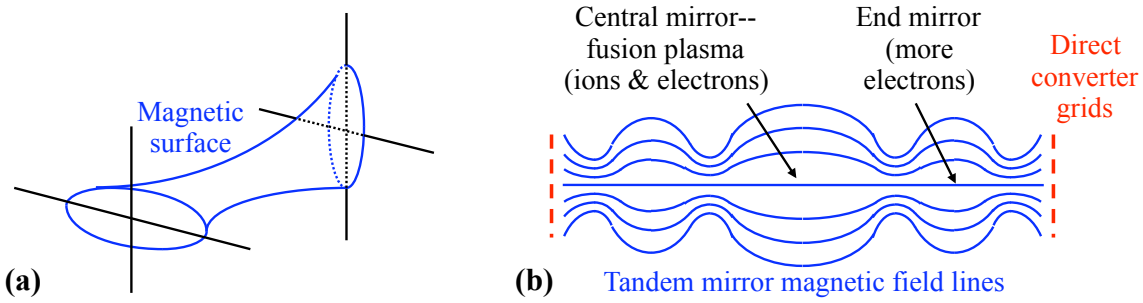

Figure 28. Magnetic mirror confinement fusion system. (a) By compressing one end of the mirror field in the vertical direction and compressing the other end in the horizontal direction, the magnetic field lines can be made to curve inward, while still being stronger at the ends than in the middle. This minimum-B configuration prevents the flute instability from occurring. **(b)** End mirrors on either side of a central mirror catch particles (predominantly electrons) that escape from a central mirror. The potential difference between the end mirrors and central mirror reduces particle losses. When particles escape from the end mirrors, high voltage grids convert their kinetic energy directly to electrical energy.

Because the mirror field lines in Fig. 6(a) curve outward, the system is susceptible to flute instabilities, as discussed in Section 3.4. To avoid this problem, the geometry can be altered so that the field lines curve inward yet are still stronger at the ends than in the middle [Fig. 28(a)].

As shown in Fig. 6(b), particles whose velocities fall within the loss cone can readily escape from each end of the mirror field. If there were no collisions between particles, particles within the loss cone would escape and all other particles would be permanently trapped in the mirror. Collisions do occur, though, continually scattering more particles into the loss cone on a time scale of order τ_{col}, which is taken as τ_{ii} for ions and τ_{ei} for electrons. More detailed calculations by Sivukhin [7] indicate that particles escape by being scattered into the loss cone on a timescale

$$\tau_{\text{mirror}} \approx 0.8 \ln\left(\frac{B_m}{B_o}\right) \tau_{col} . \tag{298}$$

This confinement time is indeed of order τ_{col} and only logarithmically increases with the mirror ratio B_m/B_o. Electrons escape long before they acquire much energy from ions ($\tau_{\text{mirror, e}} \approx 0.8 \ln(R_m/R_o)\tau_{ei} \ll \tau_{ie}$), so if only the ions are heated, in principle the electrons could remain cool and energy losses due to their escape could be minimized. In contrast, ions escape more slowly but carry much more energy. Using Eqs. (72) and (298) for $\ln\Lambda = 20$ and $B_m/B_o = 10$, one finds

$$\begin{aligned} n_i\tau_{\text{mirror, i}} &\approx 4.0\times10^{11} \ln\left(\frac{B_m}{B_o}\right) \frac{T_{i,\,keV}^{3/2}}{Z^4 \ln\Lambda} \sqrt{\frac{m_i}{m_p}} \ \text{sec/cm}^3 = 4.6\times10^{10} \frac{T_{i,\,keV}^{3/2}}{Z^4} \sqrt{\frac{m_i}{m_p}} \ \text{sec/cm}^3 \\ &= \begin{cases} 7\times10^{12} \ \text{sec/cm}^3 & \text{for} \quad 20 \text{ keV D+T } (m_i \approx 2.5 m_p) \\ 2\times10^{13} \ \text{sec/cm}^3 & \text{for} \quad 50 \text{ keV D+D} \\ 2\times10^{13} \ \text{sec/cm}^3 & \text{for } 100 \text{ keV D+}^3\text{He } (m_i \approx 2.5 m_p;\ Z_{\text{effective}} \approx \sqrt{2}) \end{cases} \end{aligned} \tag{299}$$

These results fall well short of the Lawson criteria in Eq. (68) for net fusion power production. In order to reduce the end losses, researchers have added a small mirror field to each end of the central mirror, creating a **tandem mirror** as shown in Fig. 28(b). Because electrons escape more quickly than ions from the central mirror, an electrostatic potential difference develops between the central mirror and end mirrors. By adjusting the potential difference and maintaining sufficient particle densities in the end mirror, researchers have attempted to minimize the effects of end losses [4]. Grids with voltages $\sim k_B T/e$ have also been employed at the ends to directly convert the kinetic energy of escaping particles to electricity, as illustrated in Fig. 28(b).

As explained in Section 4, anisotropic velocity distributions can lead to instabilities. This occurs in mirror systems because the loss cone is depleted of particles, and it can disrupt the plasma or aggravate particle losses beyond the values calculated here [4]. Due to the problems with velocity-space instabilities and the difficulty of sufficiently reducing particle losses at the ends, research into mirror confinement fusion was cut back in the U.S. around 1990.

To avoid end losses, several mirrors can be connected end-to-end to create a closed torus, called the **ELMO bumpy torus** [9]. Unfortunately, the magnetic constrictions at each mirror point cause bad curvature of the plasma/field boundary and thus flute instabilities. Researchers have proposed tricks such as created hot electron rings inside the plasma to prevent these instabilities, but it is probably simplest to consider more straightforward toroidal systems like those in the next section.

While mirror fields are roughly cylindrical with the magnetic field lines escaping at each end, researchers have also considered **cusp** magnetic fields that are generally polyhedral in shape and have more than two points at which the magnetic field lines escape. These approaches suffer from the same problems as magnetic mirrors, except they are even more severe [4].

7.2 Closed Magnetic Field Geometries

To avoid large particle losses along magnetic field lines, the field lines are usually bent into a circle to form a closed toroidal magnetic field B_t [Fig. 29(a) and (b)]. Section 2.4 showed that a poloidal magnetic field B_p is necessary too in order to prevent charge separation and large $\mathbf{E} \times \mathbf{B}$ particle drift losses [Fig. 29(b) and (c)]. Yet as noted in Eq. (155), MHD stability requires $B_t/B_p > R/a$, so the poloidal magnetic field must not be too large compared to the toroidal field. Toroidal plasmas also require a vertical magnetic field B_z to hold the plasma in equilibrium against the hoop and tire tube forces, as explained in Section 3.1 [Fig. 13, Fig. 29(c) and (d)]. B_z is generally produced by external vertical field coils above and below the torus.

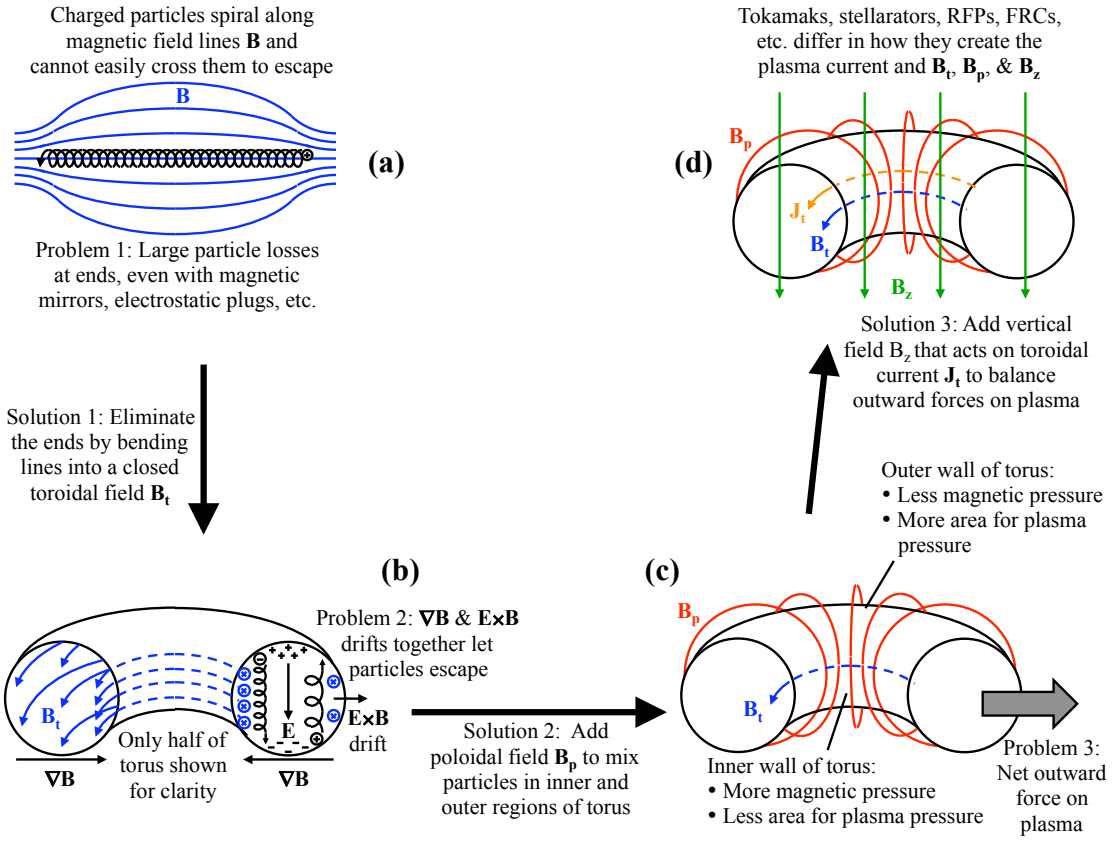

Figure 29. Magnetic confinement, which begins as a simple idea, is inevitably forced by fundamental physical laws to become very complex, with requirements for three different magnetic fields as well as a plasma current.

This requirement for an externally produced B_z is an example of a more general principle: a plasma cannot be confined solely by magnetic fields created by plasma current–the confining magnetic fields must be at least partially created by current-carrying coils outside the plasma. This is another form of the virial theorem. It can be proved by integrating the MHD equilibrium equation (138) over a volume enclosing the plasma [9], just as volume integration of the stellar equilibrium equation (213) yielded the stellar virial theorem (238).

Four major toroidal approaches are considered below: the tokamak, stellarator, reversed field pinch, and field reversed configuration. The key difference among them is how they produce B_t and B_p.

Tokamak

In a tokamak [Fig. 30(a)], external poloidal coils create a toroidal field $B_{\mathrm{t,\,int}}$ inside the plasma and $B_{\mathrm{t,\,ext}}$ outside the plasma, while induced toroidal plasma current creates an external poloidal field $B_{\mathrm{p,\,ext}}$. The toroidal current can be induced by using the plasma torus as the secondary coil in a transformer. Passing a time-varying current through the primary coil of the transformer induces a time-varying toroidal current in the plasma. Because the plasma current and accompanying poloidal field are inherently transient, such tokamaks cannot be operated continuously. For continuous operation, it has been proposed to use the bootstrap current (Section 2.4) or fire electromagnetic waves or neutral particle beams into the plasma to maintain a steady-state toroidal current, but these techniques need further development.

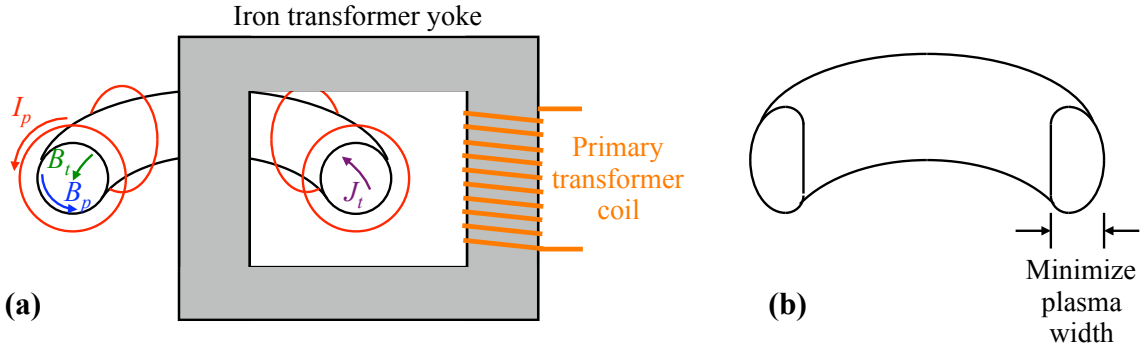

Figure 30. Tokamak. **(a)** B_t is created by poloidally arranged coils carrying current I_p. B_p is produced by an internal toroidal plasma current J_t. By using the toroidal plasma as the secondary winding of an iron transformer yoke and passing a time-varying current through the primary winding, a time-varying J_t is induced in the plasma. Vertical field coils [Fig. 10(c)] are also required but not illustrated here. **(b)** Actual toroidal plasmas often have a D-shaped cross section. This minimizes the width of the plasma and the problems caused by the magnetic gradient across that width. It also puts most of the plasma near the inner plasma/magnetic field boundary, which has the right curvature to avoid the flute instability.

From Eq. (139), the plasma pressure p at the plasma boundary must satisfy the condition

$$p + \frac{B^2_{\mathrm{t,\,int}}}{2\mu_o} = \frac{B^2_{\mathrm{t,\,ext}}}{2\mu_o} + \frac{B^2_{\mathrm{p,\,ext}}}{2\mu_o} \tag{300}$$

Assuming that $B_{\mathrm{t,\,int}}$ and $B_{\mathrm{t,\,ext}}$ are not very different, one finds the poloidal β value

$$\beta_p \equiv \frac{p}{B^2_{\mathrm{p,\,ext}}/2\mu_o} \approx 1\,. \tag{301}$$

Actually $\beta_p \approx 0.5$ is more typical, due to small differences between $B_{\mathrm{t,\,int}}$ and $B_{\mathrm{t,\,ext}}$.

Whereas B_p is simply created by plasma current, B_t must be produced by external field coils, so the toroidal value β_t is more relevant than β_p. β_t may be estimated from β_p and Eq. (155):

$$\beta_t \equiv \frac{p}{B^2_{\mathrm{t,\,ext}}/2\mu_o} = \beta_p \left(\frac{B_p}{B_t}\right)^2 = \beta_p \left(\frac{a}{R}\right)^2 \frac{1}{q_s^2} \tag{302}$$

$\beta_t \leq 5\%$ for typical values of $\beta_p \approx 0.5$, $a/R \leq 1/3$, and $q_s > 1$. Recall from Eq. (141) that $P_{\text{fus}} \propto \beta^2$. The low β and the intense cyclotron radiation losses due to the large B_t in the plasma make it very difficult for tokamaks to burn D+^{3}He or possibly even D+D fuel; D+T is more feasible.

Throughout our analyses we assume a circular plasma cross section for simplicity, but it is actually often D-shaped [Fig. 30(b)]. By reducing the width of the cross section, one minimizes the difference in B_t between the inner and outer edges of the plasma and the problems that difference can cause. The D shape also puts most of the plasma near the inner plasma/magnetic field boundary, which is concave and thus stable against flute instabilities (Section 3.4), unlike the outer boundary.

Stellarator

In tokamaks, external poloidal coils create the toroidal magnetic field, while internal toroidal plasma current produces the poloidal magnetic field. In **stellarators**, **heliotrons**, and **torsatrons** (Fig. 31), the external coils are altered into a helix, with components of their current flow in both the poloidal and toroidal directions. Thus the external coils create both the toroidal and poloidal magnetic fields, and it is not necessary to induce a plasma current. For this reason, stellarators and their cousins permit straightforward steady-state operation, which is an advantage over tokamaks.

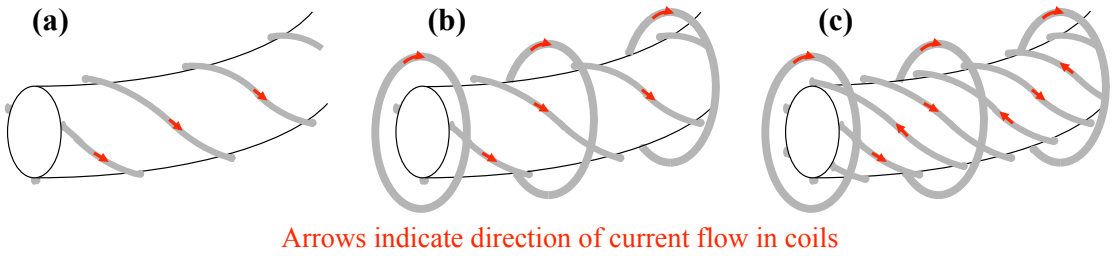

Figure 31. (a) Torsatron. (b) Heliotron. (c) Stellarator. Only a short section of the torus is shown. Each configuration has more coils than the previous one, but the common characteristic of all three configurations is that external coils carry both poloidal and toroidal current to create the necessary toroidal and poloidal magnetic fields.

Torsatrons only have helical coils carrying current in one direction [Fig. 31(a)], heliotrons have those helical coils plus poloidal coils [Fig. 31(b)], and stellarators have helical coils carrying current in both directions as well as poloidal coils [Fig. 31(c)]. Having fewer coils makes a fusion reactor simpler and allows the plasma to occupy more of the reactor's volume. However, having more coils permits greater control over the poloidal and toroidal magnetic fields if adjustments are needed.

While stellarators and their cousins use external coils instead of plasma current to create the poloidal field, the resulting magnetic fields resemble those in tokamaks. Therefore, the β limit is the same as that calculated for tokamaks. Moreover, neoclassical diffusion of particles still applies, although the equation for neoclassical diffusion in the banana regime must be modified because the particle orbits assume a different shape [4].

Reversed field pinch

Plasma current is generally electrons moving along the magnetic field lines. In a tokamak, the field lines are relatively straight ($q_s > 1$) and the current is primarily toroidal. Yet in a **reversed field pinch** (RFP), the internal field lines and hence the plasma current assume a spiral shape, so that the current has a significant poloidal component as well as a toroidal one [Fig. 32(a)]. This poloidal plasma current produces a toroidal magnetic field B_t that opposes that created by the external poloidal coils. Near the center of an RFP plasma, the internally produced B_t actually overcomes the externally created one. Thus the total B_t points in one direction near the edge of an RFP plasma and in the other direction near the plasma's center, as shown in Fig. 32(b). Because RFPs (like tokamaks) require induced plasma current, their operation is inherently pulsed.

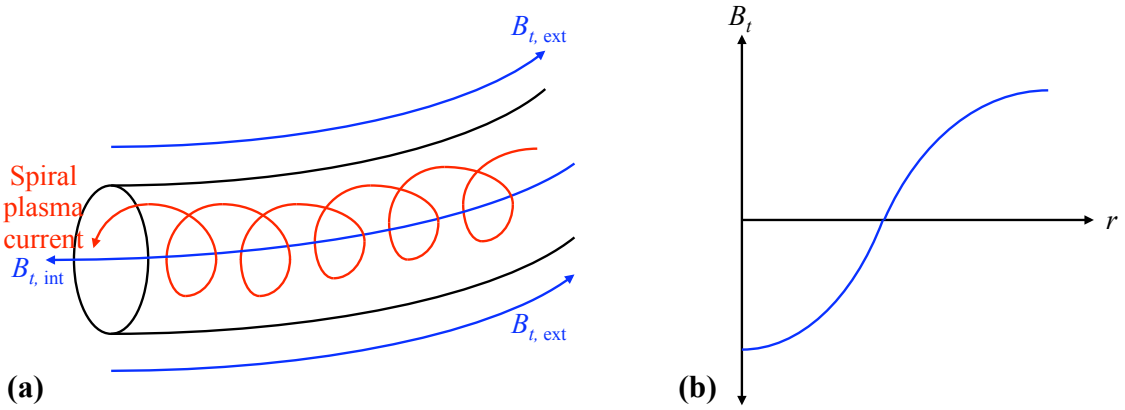

Figure 32. Reversed field pinch. **(a)** Particles following the tightly spiraling magnetic field lines carry a plasma current with a large poloidal component, producing an internal toroidal field that opposes the toroidal field of the external coils. **(b)** The sum of the internally and externally created toroidal fields is a field that points one way inside the plasma and the other way outside the plasma.

Whereas tokamaks cannot have more plasma current than the Kruskal-Shafranov limit [Eq. (154) without violating $q_s > 1$ and becoming unstable, the whole idea of RFPs is to produce tight spiral field lines with $q_s < 1$. Therefore the Kruskal-Shafranov limit is irrelevant and RFPs can use as much plasma current as is desired for Ohmic heating. In lieu of the $q_s > 1$ condition, MHD stability is ensured by exploiting the strong shear in the toroidal magnetic field and by adding a conducting shell around the plasma (see Section 2.3 and [9]). Due to their creative use of plasma currents and internally generated magnetic fields, RFPs can achieve values of β as high as $\sim 30\%$.

Field reversed configuration

In a **field reversed configuration** (FRC), a plasma is confined in a magnetic mirror field, and a ring of strong plasma current is induced [Fig. 33(a)], creating a poloidal field that helps confine a torus of plasma [Fig. 33(b)]. The corresponding toroidal field is produced by passing a current axially through the mirror plasma, and the vertical field needed to hold the torus in equilibrium is simply the mirror field. FRCs are sometimes called **spheromaks** when the mirror is short and roughly spherical as in Fig. 33. Like RFPs, FRCs make extensive use of plasma-current-created magnetic fields and might attain $\beta \geq 30\%$. Whether they are steady state or pulsed depends on how the current ring is produced.

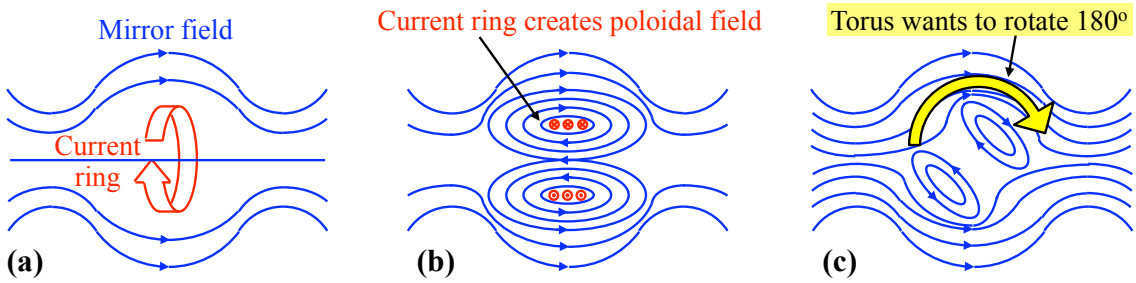

Figure 33. Field reversed configuration (FRC). (a) A plasma is confined in a mirror field, and a ring of plasma current is induced. **(b)** The current ring produces a poloidal field that confines a torus of plasma. **(c)** Because the magnetic field of the FRC torus points in the opposite direction as the mirror field, FRCs are prone to the tilting instability, in which the torus rotates by 180^o, straightening out the field lines and allowing the toroidal plasma to escape.

The greatest difficulty for FRCs is creating the current ring. In the original **Astron** FRC design [2, 3], a relativistic electron beam was injected and trapped in the mirror to form a current ring, called the E-layer. Severe problems with E-layer formation, radiation losses from the E-layer, and stability necessitated a new approach. In newer FRC designs, the current ring is created by applying a strong rotating magnetic field that drags plasma electrons around the circumference of the plasma. Unfortunately, the superposition of this strong applied magnetic field generally makes the plasma-current-created field lines open up and release particles from the torus. Furthermore, since plasmas tend to screen out applied magnetic fields, the rotating field cannot penetrate very deeply, so FRCs cannot be scaled up to large diameters and hence large fusion power levels. In a **dipole** FRC, the ring is actually a current-carrying ring of superconducting material levitated within the plasma. Because the levitation is very tricky and superconductors revert to normal conductors when exposed to high temperatures and radiation, dipole reactors face several unique difficulties. **Multipole** reactors, which use several levitated superconducting rings to favorably modify the magnetic fields inside the plasma, would multiply these difficulties.

Another problem is the **tilting instability**. The magnetic field through the FRC ring points in the opposite direction as the externally created magnetic mirror field [Fig. 33(b)]. Like a weather vane pointing the wrong way in the wind, the FRC ring desperately wants to rotate by 180^o [Fig. 33(c)]. Since this would open up the self-created FRC magnetic field lines and release the toroidal plasma, it cannot be permitted. Keeping the FRC torus balanced and pointing in the right direction requires active feedback stabilization, for example by hitting the torus with waves or neutral particle beams from one side or another as required. A different way to view this problem is that whereas tokamaks, stellarators, and RFPs have hardware on the central axis of the toroidal plasma that physically prevents the torus from flipping over, FRCs do not and so are prone to flipping.

7.3 Engineering Considerations

Even if the plasma physics cooperates, making a practical fusion reactor still involves many engineering challenges. For example, if tritium is used as fuel, it must be replenished by surrounding the reactor with a lithium-6-containing blanket that undergoes reaction (60) when struck by fusion neutrons. New tritium that is bred in the blanket must be chemically extracted.

Fusion energy deposited as heat in the blanket must be converted to electrical power output via a gas turbine or similar method. Alternatively, direct electric conversion has been proposed for reactions such as (58) that impart most of the fusion energy to charged particles. Unfortunately, a plasma confinement magnetic field that lets $\sim 3-14$ MeV charged fusion products escape to reach a direct converter would generally also allow an intolerable fraction of $\sim 50-100$ keV plasma particles to escape. Moreover, electric grids at voltages of $\sim 2-14$ MV that could receive most of the energy from the fusion products usually short out due to unpreventable electrical arcing at such high voltages. Folks have proposed other direct converters, such as a modified linear accelerator (Section 8.1) in which charged fusion products impart their energy to an electromagnetic wave, but these converters are still a long way from becoming real.

Fresh fuel must be injected across the magnetic field lines as neutral particle beams or pellets. Particles that escape from the confining magnetic field or are ablated off the first wall need to be scooped up by a magnetic divertor, a special field near the physical first wall surrounding the plasma. Valuable fuel ions like tritium may need to be purified from this renegade population and reinjected into the plasma.

Methods must be provided for heating the plasma to fusion temperatures T. Ohmic heating, using the I^2R power dissipated by driving a current I through a plasma of resistance R, is the most common technique for initially heating a plasma. However, electron runaway and plasma resistance that decreases like $T^{-3/2}$ prevent Ohmic heating from exceeding $T \sim 1$ keV. To reach the higher temperatures necessary for fusion, one must then use other heating methods, such as adiabatic compression of the plasma with the magnetic fields [Eq. (134)], electromagnetic wave heating, or injection of neutral or charged particle beams.

Inner reactor components such as the first wall surrounding the plasma would be exposed to very large fluxes of neutrons, charged particles, electromagnetic radiation, and heat. The wall material must withstand this bombardment without sputtering many of its atoms into the plasma or being structurally degraded. Realistically the wall will probably need to be periodically replaced, so the wall material must not be activated by the fusion neutrons to form long-lived radioactive waste.

Although superconducting coils would minimize power losses in the magnets, it is very challenging to maintain superconductors near the plasma in such an environment. The coils must also be structurally supported against the enormous magnetic forces they create.

8 Particle Accelerators

Another important application of plasma physics is particle accelerators. This section will examine some of the main methods of accelerating and focusing charged particle beams.

8.1 Particle Acceleration Methods

All accelerators use an electric field to accelerate charged particles. However, different types of accelerators produce the electric field in different ways, accelerate particles either continuously or by a series of impulses, and employ either circular or linear geometries.

Van de Graaff and Cockcroft-Walton accelerators

Van de Graaff and Cockcroft-Walton accelerators are simple, early designs that use very high voltages to accelerate either electrons or ions. In a Van de Graaff accelerator, friction from sliding belts builds up electrostatic charge on metal domes, creating high voltages. In contrast, a Cockcroft-Walton accelerator uses a high-voltage alternating current circuit of such low frequency that the particles are accelerated to their maximum energy before the direction of the electric field reverses; since a particle beam can only be accelerated during part of the circuit's cycle, this method can only produce pulsed particle beams. Cockcroft-Walton accelerators are often used as a first stage for much larger accelerators. High-voltage discharges limit the maximum practical energy of Van de Graaff and Cockcroft-Walton accelerators to $\sim 5 - 15$ MeV.

Betatron

A betatron is a type of accelerator used for producing high-energy electrons, or beta particles. As shown in Fig. 34(a), the electrons have momentum p and follow a circular cyclotron orbit of radius

$$r_c \;=\; \frac{p}{eB(r_c)} \;\approx\; \frac{E_{\rm eV}}{3\times 10^8 B_T} \text{ meters} \quad \text{for relativistic particles } (E \;\approx\; pc) \tag{303}$$

in a perpendicular magnetic field $B(r)$ that can vary with radial position. Note that the electron cyclotron radius from Eq. (39) has been rewritten here in terms of the electron momentum.

By varying the magnetic flux passing through the cyclotron orbit, an accelerating electric field E is induced around the orbit. Using Faraday's law in integral form, with the line element dl along the orbit and the area element dA through the orbit, the induced electric field may be found:

$$\oint E\, dl \;=\; -\oint \frac{dB}{dt} dA \qquad \Longrightarrow \qquad 2\pi r_c E \;=\; -\pi r_c^2 \frac{d\,\langle B\rangle}{dt}\,, \tag{304}$$

in which $\langle B\rangle$ is the area-averaged magnetic field passing through the orbit.

The electron momentum changes due to the electric field, which may be rewritten using Eq. (304):

$$\frac{dp}{dt} \;=\; -eE \;=\; e\,\frac{r_c}{2}\,\frac{d\,\langle B\rangle}{dt}\,. \tag{305}$$

The electron orbit travels through a toroidal vacuum chamber. To avoid hitting the walls, the electrons must remain in the same cyclotron orbit as their energy increases. To keep r_c constant, the magnetic field $B(r_c)$ at the electron orbit must increase as the electron momentum increases. Using Eq. (303), this condition on $B(r_c)$ may be expressed:

$$\begin{aligned} B(r_c) \;=\; \frac{p}{er_c} \quad &\Longrightarrow \quad \frac{dB(r_c)}{dt} \;=\; \frac{1}{er_c}\frac{dp}{dt} \;=\; \frac{1}{2}\,\frac{d\,\langle B\rangle}{dt} \\ &\Longrightarrow \quad 2\frac{dB(r_c)}{dt} \;=\; \frac{d\,\langle B\rangle}{dt} \qquad \textbf{Betatron equilibrium condition} \end{aligned} \tag{306}$$

Thus the average field $\langle B\rangle$ inside the orbit must increase twice as fast as the field $B(r_c)$ at the orbit. This is accomplished by shaping the pole pieces [Fig. 34(a)] so that B (and hence its rate of increase) is larger inside the orbit than at the orbital radius. Betatrons can accelerate electrons up to ~ 300 MeV. Relativistic cyclotron radiation losses make higher energies impractical [19].

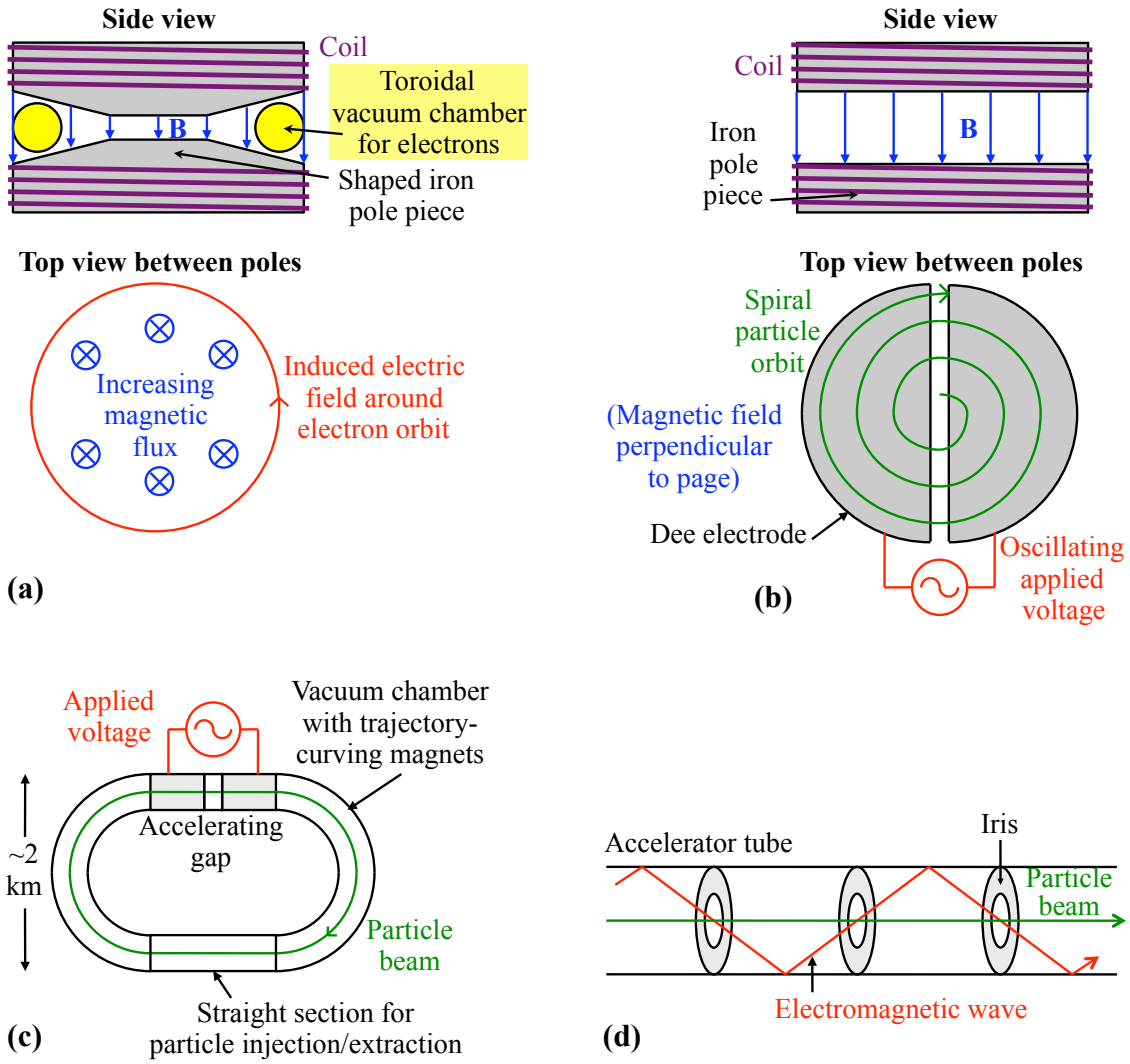

Figure 34. Particle accelerators. **(a)** In a betatron, electrons follow a circular orbit in a magnetic field. Changing the magnetic flux passing through the orbit induces an accelerating electric field around the orbit. The increasing magnetic field keeps the orbital radius constant despite the increasing particle energies. The iron pole pieces are shaped to provide a stronger magnetic field inside the orbit than at the orbital radius. **(b)** In a cyclotron, an accelerating electric field is applied each time the particles pass between two D-shaped electrodes. Particles are allowed to spiral outward as their energy increases. **(c)** In a synchrotron, an accelerating electric field is applied each time the particles cross an electrode gap. Magnetic sections bend the particle trajectories into a closed orbit. Straight, magnetic-field-free sections are useful for injecting or extracting particles. By allowing a large orbital radius and adjusting the electric and magnetic fields as particles are accelerated, energies of > 1 TeV can be obtained. **(d)** In a linear accelerator, particles travel down the center of a long, straight tube. There is a traveling or standing electromagnetic wave in the tube, and a series of irises in the tube makes the wave ricochet back and forth off the walls instead of passing straight down the tube. The ricocheting slows the waves longitudinal velocity to match the particle velocity and also makes the wave have an electric field component in the longitudinal direction, suitable for accelerating the particles.

Cyclotron

In a cyclotron, shown in Fig. 34(b), particles follow circular orbits in a perpendicular magnetic field B, as in a betatron. However, instead of being created by magnetic induction, the accelerating electric field is applied between two "D"-shaped electrode **dees** that together encompass the orbits. The particles travel together in a synchronized group, and the applied voltage between the dees alternates at the cyclotron frequency of the particles,

$$\omega_c = \frac{qB}{\gamma m}, \tag{307}$$

where $\gamma = 1/\sqrt{1 - v^2/c^2}$ is a relativistic factor depending on the particle velocity v. Thus the electric field always has the right sign to accelerate the particles crossing the gap.

Unlike in a betatron, the perpendicular magnetic field is held constant, and orbiting particles are allowed to spiral outward as their energy increases. If the particles remain nonrelativistic, $\gamma \approx 1$ and particles at different energies have the same cyclotron frequency. Therefore, as long as the particles stay in phase with the alternating electric field, particles with a broad range of energies may be accelerated simultaneously in a cyclotron. Low-energy particles can be continually injected near the center (at the right phase of the alternating electric field, of course) and high-energy particles can be continually removed at the outer edge.

Unfortunately, when particles begin to approach relativistic energies, γ increases and the high-energy particles' cyclotron frequency is no longer in tune with the alternating electric field. This limits the maximum particle energy to ~ 30 MeV for protons. The corresponding limit for electrons is ~ 15 keV due to their much smaller rest mass, so cyclotrons are generally used only for ions.

To achieve higher energies, one can accelerate batches of ions all having approximately the same energy. As a batch is accelerated and its energy becomes relativistic, the frequency of the alternating electric field is adjusted to remain tuned to the current cyclotron frequency of the ion batch. The maximum energy of such a **synchrocyclotron** is then limited only by the practical difficulty of building a magnet that covers the entire area from the center out to the cyclotron radius corresponding to the maximum ion energy. In practice, this limit is ~ 700 MeV for protons.

Synchrotron

In a **synchrotron** [Fig. 34(c)], as in a synchrocyclotron, particles are accelerated in monoenergetic batches. Moreover, particles are accelerated by voltage applied across one or more gaps between electrodes encompassing part of the particle orbit; the frequency and phase of the applied voltage is synchronized to coincide with the arrival of the particle batch at each gap, and that frequency can be adjusted as the particles gain energy, thereby compensating for relativistic effects.

However, the magnetic field in a synchrotron increases as the particles gain energy, so the particle orbit maintains a fixed cyclotron radius instead of spiraling outward as in a synchrocyclotron. Therefore, one can use a series of small magnets along the fixed particle orbit instead of one giant magnet that covers the whole orbit. Being limited by neither relativistic effects nor magnet size, synchrotrons can accelerate protons to energies of over 1 TeV (10^{12} eV) and are used for the ultra-high-energy accelerators at Fermilab and CERN. Synchrotrons can also accelerate electrons, although cyclotron radiation losses become prohibitive at electron energies greater than ~ 10 GeV.

From Eq. (303), a synchrotron with 1 TeV particles and a 5 T magnetic field must have a radius of almost 700 m, so the largest synchrotrons hog a lot of real estate. As shown in Fig. 34(c), synchrotrons are actually even larger because they usually also contain some straight, magnetic-field-free regions in which particles can be easily injected or extracted. Smaller accelerators are used to impart moderate energies to particles before they are injected into a synchrotron.

Linear accelerator

Whereas most other accelerators use a magnetic field to bend particle trajectories into a circle or spiral, linear accelerators just don't bother. Linear accelerators still need an electric field to accelerate the particles, though. In this case, the electric field belongs to an electromagnetic wave propagating down a long conducting tube through which the particles also pass, as in Fig. 34(d). Typically the electromagnetic wave is in the microwave frequency range ($f > 300$ MHz).

The tube has a series of irises that prevent the electromagnetic wave from traveling straight down the tube, forcing it instead to ricochet back and forth off the tube's walls in order to fit through the central hole in each iris. The particle beam is kept focused to pass through the irises. The irises serve a dual purpose: (1) Since the electromagnetic wave moves at an angle across the tube, its electric field has a component in the longitudinal direction that can accelerate the particles. (2) The irises reduce the effective longitudinal velocity of the electromagnetic wave from c to match that of the particles for efficient acceleration. Further down the accelerator tube where the particles have a higher velocity, the spacing between the irises increases to adjust the wave velocity accordingly.

A traveling wave linear accelerator continuously accelerates particles that keep pace with the wave and are timed to experience the accelerating part of the wave's cycle. Alternatively, waves traveling in opposite directions can be superimposed to yield a standing electromagnetic wave with strong oscillating electric fields at fixed, spatially periodic antinodes. Such a standing wave accelerator gives impulses to particles that arrive at each antinode during the accelerating part of the cycle.

8.2 Particle Beam Focusing and Maintenance

The particles in accelerators and beams must be herded to arrive at the desired place and time. Phase stability ensures their arrival at the correct time for an accelerating electric field, while betatron oscillations, electrostatic lenses, and magnetic lenses provide spatial focusing. The Brillouin limit is the maximum unneutralized charged particle density that a magnetic field can maintain.

Phase stability

In many accelerators, the electric field oscillates with time. It is vital for the particles to encounter the electric field during the correct part of its oscillation in order to be accelerated instead of decelerated. Keeping all the particles in sync with the electric field is called **phase stability**.

Figure 35(a) shows the force imparted to particles that encounter different phases ϕ of the electric field's cycle. A particle that encounters one of the equilibrium points $\phi = 0$ or $\phi = \pi$ of the cycle feels no accelerating or decelerating force. **Synchronous** particles have a velocity such that they always encounter the same phase of the electric field (the time between encounters equals the period of the electric field) and can keep that velocity if they are at one of the equilibrium points.

However, the $\phi = 0$ equilibrium is stable, while the $\phi = \pi$ one is unstable. If a particle at $\phi = 0$ slows down for some reason, it will lag behind and encounter an accelerating electric force. This acceleration will boost the particle until it actually leads a bit in phase. Then it will encounter a decelerating electric field and slow down again. Therefore, particles near $\phi = 0$ undergo stable oscillations in phase about the equilibrium point. In contrast, particles near the $\phi = \pi$ equilibrium that lag behind experience a field that decelerates them further, and particles that get ahead encounter a field that accelerates them further ahead, so the $\phi = \pi$ equilibrium is unstable.

The natural frequency of phase oscillations about the stable equilibrium point can be derived. As a simple example, consider a traveling wave linear ion accelerator of moderate energy, so that the particles are nonrelativistic and are accelerated continuously, not in impulses. The particles and the electromagnetic wave travel at some velocity, and the particles have a relative longitudinal position

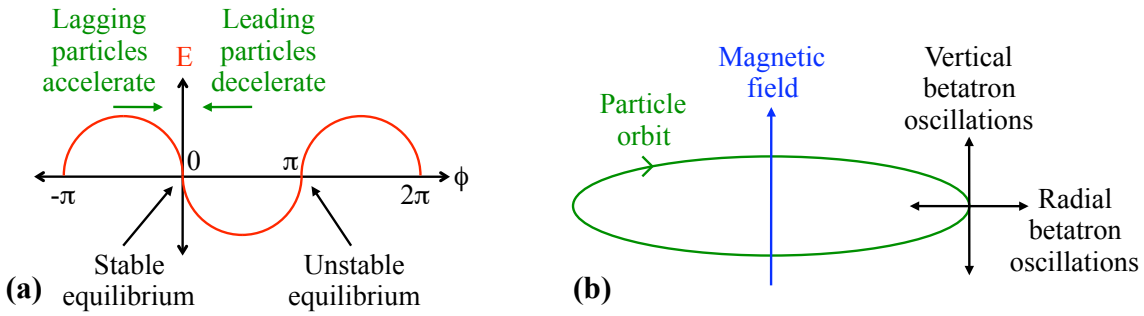

Figure 35. Phase stability and betatron oscillations. (a) Particles that always arrive when a time-varying electric field is zero ($\phi = 0$ or π) experience no acceleration and are at equilibrium points. Particles near $\phi = 0$ that lag behind are accelerated toward the equilibrium point, while those that get ahead are decelerated toward the equilibrium, so $\phi = 0$ is stable. In contrast, $\phi = \pi$ is not. **(b)** Particles in circular accelerators can undergo oscillations in the vertical position or radius of their orbit. Spatial variations in the magnetic field determine whether the oscillations are stable or unstable.

Δz or phase ϕ with respect to a stable equilibrium point in the wave. Denoting the electric field as $E_o \sin\phi$, Newton's second law for particles of mass m and charge q is

$$m\frac{d^2(\Delta z)}{dt^2} \;=\; -qE_o\,\sin\phi \;\approx\; -qE_o\phi \qquad \text{for small } \phi \tag{308}$$

If the wave has a period T, angular frequency ω_s, and velocity v_s (also the velocity of synchronous particles), the phase and relative position of the particles are related by

$$\phi \;=\; 2\pi\frac{\Delta z}{v_s T} \;=\; \frac{\omega_s}{v_s}\,\Delta z \tag{309}$$

Taking the second time derivative of Eq. (309) and using Eq. (308) yields

$$\frac{d^2\phi}{dt^2} \;=\; \frac{\omega_s}{v_s}\,\frac{d^2(\Delta z)}{dt^2} \;=\; -\frac{\omega_s q E_o}{v_s m}\,\phi \tag{310}$$

Equation (310) describes simple harmonic oscillations of the phase with angular frequency

$$\omega \;=\; \sqrt{\frac{\omega_s q E_o}{v_s m}}\,. \tag{311}$$

This is the frequency at which nearly synchronous particles oscillate back and forth between lagging and leading the synchronous particles. Although it was obtained for nonrelativistic, continuously accelerated particles, similar results can be derived for relativistic particles and/or impulse acceleration [19]. These systems all exhibit similar phase stability, such that nearly synchronous particles undergo small oscillations in phase about the stable synchronous phase position.

Because synchronous particles experience no electric field, to accelerate particles one must gradually adjust the frequency/wavelength of the electric field so that the synchronous velocity v_s steadily increases. Particles that have been synchronous suddenly find themselves lagging behind and experience an accelerating electric field. Conversely, by gradually lowering v_s, the kinetic energy of charged particles (such as fusion products) can be directly converted to electrical energy.

Betatron Oscillations

Particles in a circular accelerator must be stable with respect to vertical or radial perturbations of their positions [Fig. 35(b)], so that they oscillate about the equilibrium values $z = 0$ and $r = r_c$ instead of drifting further from those values. This condition is called **weak focusing**, and the oscillations are called **betatron oscillations**. To find the requirements for weak focusing, assume that the vertical magnetic field B_z varies with radial position according to a field index n:

$$B_z \;=\; B_o \left(\frac{r}{r_c}\right)^{-n} \tag{312}$$

Ampère's law relates the radial component B_r of the magnetic field to the vertical one (neglecting currents and time-varying electric fields):

$$\nabla \times \mathbf{B} \;=\; 0 \qquad \Longrightarrow \qquad \frac{\partial B_r}{dz} \;=\; \frac{\partial B_z}{dr} \tag{313}$$

B_r may be integrated up from Eq. (313), using Eq. (312) and the boundary condition $B_r|_{z=0} = 0$:

$$B_r \;=\; z\,\frac{\partial B_z}{dr} \;=\; -n\,\frac{z}{r_c}\,B_o \tag{314}$$

Using Eq. (314) and $\gamma = 1/\sqrt{1 - v^2/c^2}$, Newton's second law for the vertical $\mathbf{v} \times \mathbf{B}$ force is

$$\begin{aligned} \gamma m \frac{d^2 z}{dt^2} \;&=\; q v_\theta B_r \;=\; -n\,\frac{q v_\theta B_o}{r_c}\,z \;, \qquad \text{or} \\ \frac{d^2 z}{dt^2} \;&=\; -n\omega_c^2\,z \qquad\qquad \textbf{Vertical betatron oscillations} \end{aligned} \tag{315}$$

where the cyclotron frequency $\omega_c \equiv qB/\gamma m \;=\; v_\theta/r_c$ has been used. Equation (315) describes small-amplitude, simple harmonic oscillations at a natural angular frequency $\sqrt{n}\,\omega_c$ about the equilibrium orbital plane $z = 0$. If the field index n is negative, this frequency becomes imaginary and the perturbation in vertical position will grow. Thus $n > 0$ is required for vertical stability. In physical terms, if $n < 0$, B_r will point the wrong way and the Lorentz force $B_r \times v_z$ will accelerate errant particles further away from $z = 0$ instead of returning them toward $z = 0$.

Small radial oscillations may be examined using $x \equiv r - r_c$ and a Taylor expansion for B_z,

$$B_z \;\approx\; B_o + \left.\frac{\partial B_z}{dr}\right|_{r_c} x \;=\; B_o\left(1 - n\frac{x}{r_c}\right) \;. \tag{316}$$

Newton's second law for the centrifugal and $\mathbf{v} \times \mathbf{B}$ forces in the radial direction is

$$\gamma m \frac{d^2 r}{dt^2} \;=\; \gamma m \frac{v_\theta^2}{r} - q v_\theta B_z \tag{317}$$

Using Eq. (316) and $\frac{1}{1+x/r_c} \approx 1 - \frac{x}{r_c}$ for $x/r_c \ll 1$, Eq. (317) may be rewritten in terms of x:

$$\frac{d^2 x}{dt^2} \;=\; \frac{v_\theta^2}{(x + r_c)} - \frac{q v_\theta B_z}{\gamma m} \;\approx\; \frac{v_\theta^2}{r_c}\left(1 - \frac{x}{r_c}\right) - \frac{q v_\theta B_o}{\gamma m}\left(1 - n\frac{x}{r_c}\right) \tag{318}$$

$$\approx\; -(1-n)\omega_c^2\,x \qquad\qquad \textbf{Radial betatron oscillations} \tag{319}$$

The lowest-order terms in Eq. (318) cancelled each other, as expected from the definition of cyclotron motion. Equation (319) describes oscillations in radius about the equilibrium value r_c at an angular frequency $\sqrt{1-n}\,\omega_c$. The condition $n < 1$ is required for this frequency to be real and radial oscillations to be stable. Physically, if $n > 1$, B_z falls off too quickly with increasing radius;

a particle that wanders out to a larger radius would encounter a much weaker B_z and hence have a much larger cyclotron orbital radius, reinforcing the perturbation. Similarly, a particle that moves to a smaller radius would find a much stronger B_z and acquire an even smaller cyclotron radius.

Combining the requirements for vertical and radial stability yields

$$0 < n < 1 \qquad \textbf{For stability against vertical and radial betatron oscillations} \qquad (320)$$

Particle beams can be cooled to reduce transverse momentum such as underlies betatron oscillations or to reduce the spread of energies in a packet of particles [19]. Cyclotron radiation is strongly dependent on particle energy, so it decelerates faster particles much more and reduces the spread in electron beams. While ion beams do not radiate enough to use this method, they can be cooled by temporarily adding electrons to the beam, letting the electrons soak up excess energy from the ions, and then removing the electrons. In stochastic cooling, one continually monitors the particle beam distribution and uses applied fields to manipulate it as desired, much like Maxwell's demon.

Electrostatic lenses

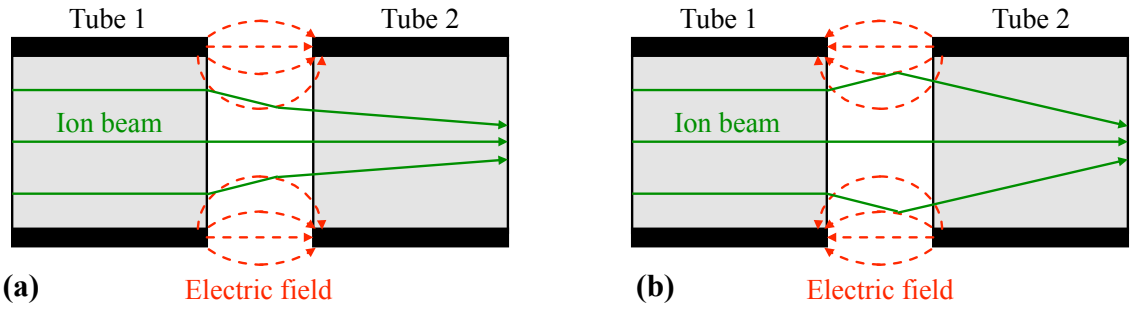

Figure 36. Electrostatic immersion lens. A voltage difference is applied between two conducting tubes, creating an electric field in the gap between the tubes. Charged particles passing from one tube to the other are focused **(a)** if the electric field is accelerating and also **(b)** if the field is decelerating.

Electric fields can be used as a lens to focus beams of charged particles. Figure 36 shows a common type, an **electrostatic immersion lens**. Two conducting tubes are separated by a gap; a voltage is applied across the gap, and charged particles are focused as they travel from the first tube into the second. Electric field lines that span the gap curve toward the interior of the tubes, and the direction of the electric field depends on the sign of the applied voltage. If particles maintained the same radial position r and longitudinal velocity v_z, the radial component of the electric field near the end of the gap would exactly negate the effect of the radial electric field near the beginning of the gap on the charged particles, and there would be no lens effects. However, focusing arises because r and v_z change as a particle crosses the gap.

If the electric field accelerates particles crossing the gap, the curved field lines will deflect particles inward near the beginning of the gap and outward near the end. Because the particles near the end of the gap have a smaller r and larger v_z than those near the beginning, the final outward deflection will be smaller than the initial inward deflection. Thus an accelerating gap focuses particles.

If the electric field at the gap decelerates particles, the field lines will deflect particles outward near the beginning and inward near the end of the gap. Particles near the end of the gap have a larger r and smaller v_z, making the final inward deflection larger, so decelerating gaps also focus particles.

Because of spatial variations in the electric field and particle trajectories, the focal length of an electrostatic immersion lens must be calculated numerically [19]. Similar focusing effects also occur when particles cross gaps with applied electric fields in particle accelerators.

Magnetic lenses

Magnetic fields can also be used as a lens for charged particles. The most common type is a **magnetic quadrupole lens**, illustrated in Fig. 37(a). Particles pass through a tube in the z direction, shown perpendicular to the page. Four current-carrying coils are evenly spaced around the tube, creating a magnetic field that enters through two opposite coils and leaves through the other two coils. As illustrated in Figs. 37(a) and (b), the quadrupole creates a magnetic field within the tube with a B_x component proportional to y and a B_y component proportional to x,

$$B_x = B_o\frac{y}{a} \qquad\qquad B_y = B_o\frac{x}{a} \tag{321}$$

where B_o is a characteristic field strength and a is the characteristic length over which $\mathbf{B}$ varies. This produces $\mathbf{v}\times\mathbf{B}$ forces on particles passing through the lens with velocity v_z in the z direction:

$$F_x = -qv_zB_y = -qv_zB_o\frac{x}{a} \tag{322}$$

$$F_y = +qv_zB_x = +qv_zB_o\frac{y}{a} \tag{323}$$

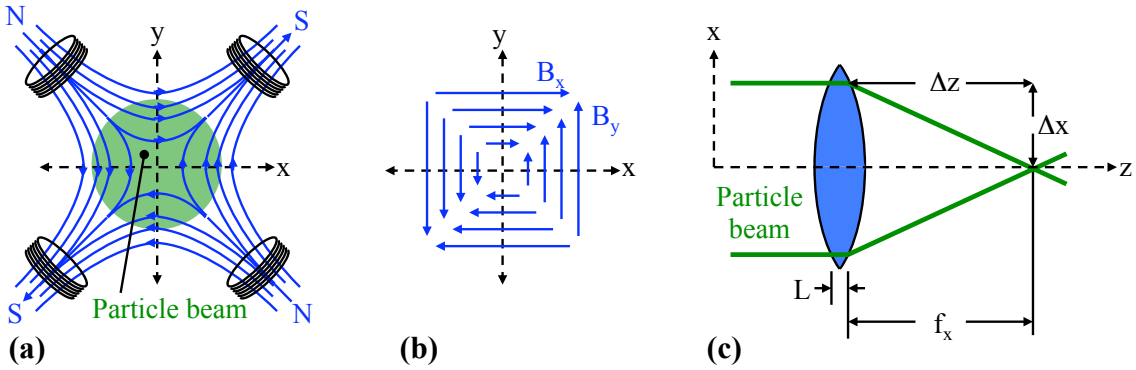

Figure 37. Magnetic quadrupole lens. (a) A particle beam travels perpendicular to the page, and the quadrupole field is created by four coils evenly spaced around the beam. The field lines enter through two opposite coils and leave through the other two. **(b)** The magnetic quadrupole field has a component B_x that is proportional to y and a component B_y that is proportional to x, where the axes are the same as those in (a). **(c)** In this side view, the magnetic quadrupole lens is illustrated schematically as an optical lens of thickness L. A beam with parallel particle trajectories in the z direction is brought to a focus with respect to the x direction at a focal length f_x beyond the lens.

Equation (322) indicates that a particle that has some position $x > 0$ and is moving in the z direction experiences a magnetic force that moves the particle toward $x = 0$, so the lens focuses particles in the x direction [Fig. 37(c)]. In contrast, Eq. (322) shows that a particle at some position $y > 0$ feels a magnetic force that pushes it even further from $y = 0$, so the lens defocuses in the y direction. Gauss's law prevents the design of a magnetic lens that simultaneously focuses in both the x and y directions. Nonetheless, two magnetic quadrupole lenses can be used together to simultaneously focus in both directions, as will be demonstrated shortly.

To find the focal length f of a lens with forces (322) - (323), Newton's second law for a particle with relativistic mass γm is written in terms of the particle's z position instead of time, $dt \to dz/v_z$:

$$\frac{d^2x}{dz^2} = \frac{1}{v_z^2}\frac{d^2x}{dt^2} = \frac{1}{v_z^2}\frac{F_x}{\gamma m}$$

$$= -\frac{qB_o}{\gamma m v_z a}\,x \equiv -k^2 x \qquad\qquad k \equiv \sqrt{\frac{qB_o}{\gamma m v_z a}} \tag{324}$$

$$\frac{d^2y}{dz^2} = +\frac{qB_o}{\gamma m v_z a}\,y \equiv +k^2 y \tag{325}$$

The force of the magnetic lens extends over some effective lens length L in the z direction. Assuming a thin lens, $L \ll f$, greatly simplifies the math, since then the x and y positions of a particle (and hence the forces F_x and F_y) remain approximately constant while the particle is passing through the lens, $0 < z < L$. For this simple case, Eq. (324) may be integrated over the lens length,

$$\left.\frac{dx}{dz}\right|_{z=L} - \left.\frac{dx}{dz}\right|_{z=0} = -k^2 L x \tag{326}$$

If a particle at $x > 0$ has a trajectory slope $dx/dz|_{z=0} = 0$ before the lens, as shown in Fig. 37(c), Eq. (326) indicates that its trajectory slope after the lens will be

$$\left.\frac{dx}{dz}\right|_{z=L} \equiv -\frac{\Delta x}{\Delta z} = -k^2 L x \tag{327}$$

From Eq. (327) and Fig. 37(c), the particle will cross the x axis ($\Delta x = x$) after traveling a distance $\Delta z = 1/(k^2 L)$ beyond the lens. Thus the focal length f_x for focusing in the x direction is

$$f_x = +\frac{1}{k^2 L} \tag{328}$$

The focal length in the y direction is similar but negative because of the defocusing:

$$f_y = -\frac{1}{k^2 L} \tag{329}$$

Now consider a **doublet** of two successive quadrupole lenses (lens 1 and lens 2), such that:

- Lens 1 focuses in the x direction ($f_{x1} > 0$) and defocuses in the y direction ($f_{y1} < 0$).
- Lens 2 defocuses in the x direction ($f_{x2} < 0$) and focuses in the y direction ($f_{y2} > 0$).

Using the formula from optics for successive thin lenses separated by a distance d, and assuming $f_{x2} = -f_{x1}$, the net focal length $f_{x\,\mathrm{net}}$ in the x direction for the doublet is

$$\frac{1}{f_{x\,\mathrm{net}}} = \frac{1}{f_{x1}} + \frac{1}{f_{x2}} - \frac{d}{f_{x1} f_{x2}} \quad , \quad \text{or}$$

$$f_{x\,\mathrm{net}} = +\frac{f_{x1}^2}{d} \tag{330}$$

Therefore, the net effect of one lens that focuses and one lens that defocuses in the x direction is still focusing in the x direction. Likewise, the lenses have a net focusing effect in the y direction.

Magnetic quadrupole lenses are often thick lenses, $L \sim f$, necessitating more complicated versions of Eqs. (328)-(330). Nonetheless, the basic principles which have been illustrated here still apply.

Accelerators such as synchrotrons commonly use many successive magnetic lenses to maintain a tightly focused beam. This strategy is called **strong focusing**, in contrast to the weak focusing that betatron oscillations naturally cause in circular accelerators.

Brillouin limit

Unlike fusion plasmas, particle accelerator beams generally contain particles that all have the same sign of charge. To maintain the beam, the electric repulsion among the charges must be opposed by an external force, such as that provided by a magnetic field. The maximum density of unneutralized charged particles that can be confined by a magnetic field is called the **Brillouin limit**.

To derive the Brillouin limit, consider a cylindrical beam of radius r containing particles of charge q and mass m, as shown in Fig. 38. The particles are confined by an axial magnetic field, $\mathbf{B} = B\hat{\mathbf{z}}$. For simplicity, we can assume a uniform density n for the particles. From the Poisson equation, $\nabla \cdot \mathbf{E} = qn/\epsilon_o$, the particles' charge creates an electric field E_r at the outer edge of the beam:

$$E_r = \frac{qnr}{2\epsilon_o} . \tag{331}$$

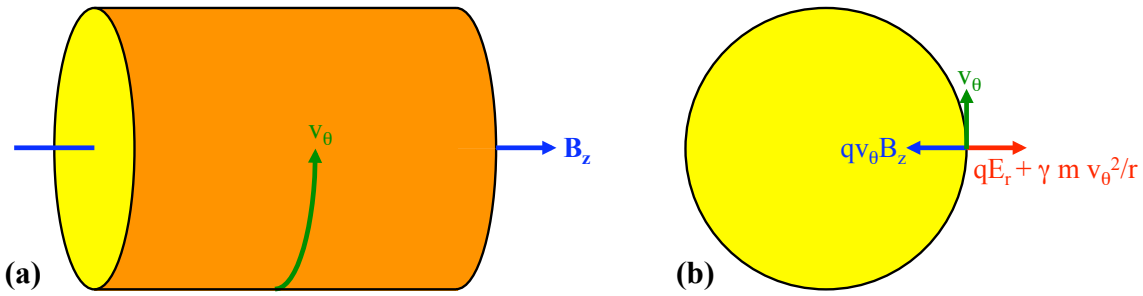

Figure 38. Brillouin density limit. Shown is a cross section through a cylindrical plasma in an axial magnetic field Bz that is perpendicular to the page. All the plasma particles have the same charge q and relativistic mass γm. A repulsive radial electric field E_r or force qE_r exists at radius r within the beam. For particles with angular velocity v_θ, there is also an outward centrifugal force $\gamma m v_\theta^2/r$ and an inward Lorentz force $qv_\theta B_z$. The Brillouin limit is the maximum plasma density for which the magnetic Lorentz force can overcome the outward forces and confine the plasma.

Due to cyclotron motion, particles rotate around the beam at a velocity v_θ. Particles at the edge of the beam experience an inward Lorentz force $qv_\theta B$, outward centrifugal force $\gamma m v_\theta^2/r$, and outward repulsive electrical force qE_r. For the beam to be in equilibrium, these forces must balance:

$$\begin{aligned} qv_\theta B &= \frac{\gamma m v_\theta^2}{r} + qE_r \\ &= \frac{\gamma m v_\theta^2}{r} + \frac{q^2 nr}{2\epsilon_o} \end{aligned} \tag{332}$$

Writing the angular velocity in terms of the cyclotron frequency $v_\theta = ar\omega_c = arqB/\gamma m$, where a is some number, and using Eq. (307) and the relation $1/\epsilon_o = c^2\mu_o$, Eq. (332) may be rewritten as

$$\gamma m c^2 n = 4(a - a^2)\,\frac{B^2}{2\mu_o} \tag{333}$$

Because the r dependence cancels out, this result applies to particles at any radius within the beam. The righthand side of Eq. (333) has a maximum value of $B^2/2\mu_o$ for $a = 1/2$, or for particles that rotate at half the cyclotron frequency. Using this fact, Eq. (333) may be simplified to

$$\gamma m c^2 n \le \frac{B^2}{2\mu_o} \qquad \text{or} \tag{334}$$

$$n \le 2.65 \times 10^9\, \frac{m_p}{\gamma m}\, B_T^2 \ \text{cm}^{-3} \qquad \textbf{Brillouin density limit} \tag{335}$$

Equation (334) means the energy density of the confined plasma (rest and kinetic energy) cannot exceed the energy density of the confining magnetic field. Although this was derived for the geometry in Fig. 38, it applies to unneutralized particles confined by any magnetic field. Equation (335) shows that for nonrelativistic deuterons without any electrons, even a strong 20 T magnetic field can only confine a maximum deuteron density of 5×10^{11} cm^{-3}. The fusion power density varies as n_i^2 and at this ion density is much too low for a fusion reactor. Therefore, fusion plasmas need electrons to neutralize the ions' charge and allow the density to exceed the Brillouin limit.

Accelerators with the highest energies generally collide two particle beams with equal but opposite momenta so that all of the kinetic energy goes into reactions. Equation (334) limits the beam densities and hence reaction rates in such systems. Higher reaction rates can be achieved by colliding a Brillouin-density-limited beam with a stationary solid or liquid target ($n \sim 10^{23}/\text{cm}^3$). However, conservation of momentum prevents such collisions from using the kinetic energy as efficiently as beam-beam center-of-mass collisions.

References

[1] F. F. Chen, *Introduction to Plasma Physics and Controlled Fusion. Volume 1: Plasma Physics* (2nd ed., Plenum Press, 1984). This introductory textbook is a model of clarity and physical insight. While Vol. 2 on fusion reactors has never been published, the last chapter of the one-volume first edition (1974) covers that ground briefly but clearly.

[2] S. Glasstone and R. H. Lovberg, *Controlled Thermonuclear Reactions* (Van Nostrand, 1960);

[3] D. J. Rose and M. Clark, Jr., *Plasmas and Controlled Fusion* (MIT Press, 1961). Even though parts of Glasstone & Lovberg and Rose & Clark are now somewhat out of date, these books do what more modern texts fail to do: give an orderly, unified presentation of the physics and engineering required to create a fusion reactor. The books are excellent and have much in common, yet they are complementary. Glasstone & Lovberg presents wonderful physical intuition but sometimes fails to back it up with a proper mathematical derivation, and on the other hand Rose & Clark sometimes makes the math more complicated than necessary.

[4] K. Miyamoto, *Plasma Physics for Nuclear Fusion* (revised ed., MIT Press, 1989). No other book provides as many details about as many aspects of plasma physics and fusion. However, the wholesale regurgitation (without digestion) of complicated derivations from the literature and the lack of an organized approach to carefully introduce successive concepts make this book more of a reference work than an educational textbook.

[5] T. H. Rider, *Fundamental Limitations on Plasma Fusion Systems Not in Thermodynamic Equilibrium* (Ph.D. thesis, MIT, 1995) and *Physics of Plasmas* **4**, 1039-1046 (April 1997). This demonstrates that virtually all fusion reactors that attempt to use clean fuels such as p+^{11}B, p+^{6}Li, or ^{3}He+^{3}He cannot produce net power. Reactors with plasmas that are highly non-Maxwellian or otherwise far from thermodynamic equilibrium are also toast. The work presents useful background information on fusion cross sections, bremsstrahlung, Fokker-Planck collision operators, and other plasma physics topics. The references are useful too.

[6] E. M. Lifshitz and L. P. Pitaevskii, *Physical Kinetics* (Pergamon Press, 1981). As usual for the Landau and Lifshitz series, the treatment is mathematical yet very solid.

[7] M. A. Leontovich (ed.), *Reviews of Plasma Physics* (Consultants Bureau, 1965 onward). This series of Russian books covers various topics in plasma physics that are not adequately treated in standard textbooks. The articles on transport by S. I. Braginskii (Vol. 1) and D. V. Sivukhin (Vol. 4) are particularly noteworthy.

[8] P. Helander and D. J. Sigmar, *Collisional Transport in Magnetized Plasmas* (Cambridge University Press, 2002). This textbook is a detailed treatment of an area of plasma physics that is slighted in most other textbooks.

[9] J. Freidberg, *Ideal Magnetohydrodynamics* (Plenum Press, 1987). This is virtually the only complete textbook devoted to MHD. It provides detailed analysis of the equilibrium and stability of a number of cylindrical and toroidal plasma systems.

[10] M. Schwarzschild, *Structure and Evolution of the Stars* (Dover, 1958). Although it is rather old, this book covers most of the physics of stars and is wonderfully clear and concise, so it makes an excellent introduction to stellar physics.

[11] R. Kippenhahn and A. Weigert, *Stellar Structure and Evolution* (Springer-Verlag, 1990). This text is more up-to-date and complete than Schwarzschild, though not as well-written.

[12] S. L. Shapiro and S. A. Teukolsky, *Black Holes, White Dwarfs, and Neutron Stars* (Wiley, New York, 1983). This aptly named text covers its subject clearly yet thoroughly.

[13] J. D. Lindl, *Inertial Confinement Fusion* (Springer-Verlag, 1998). This is the official bible of declassified information on the U.S. ICF program.

[14] C. E. Paine, M. McKinzie, and T. B. Cochran, *When Peer Review Fails* (Natural Resources Defense Council, www.nrdc.org/nuclear/nif2, 2000). This critique of how the U.S. ICF program has been run contains some good points and useful numbers.

[15] C. Sublette, *Nuclear Weapons Frequently Asked Questions* (www.fas.org/nuke/hew/Nwfaq, 1997). This is the most thorough unclassified source of physics details on nuclear weapons.

[16] C. Hansen, *Swords of Armageddon* (CD-ROM, 1995). This compiles a massive amount of information on the history of nuclear weapons and some information on their physics.

[17] A. Gsponer and J.-P. Hurni, *Fourth Generation Nuclear Weapons* (6th ed., International Network of Engineers and Scientists Against Proliferation, 1999). This discusses the physics of ICF, nuclear bombs, and speculative designs for miniaturized nuclear weapons.

[18] S. Glasstone and P. J. Dolan, *Effects of Nuclear Weapons* (3rd ed., U.S. Government Printing Office, 1977). The name says it all. Unfortunately it doesn't cover weapon designs, though.

[19] S. Humphries, Jr., *Principles of Charged Particle Acceleration* (Wiley, 1986) and *Charged Particle Beams* (Wiley, 1990). Textbooks on particle accelerators are relatively scarce, but these two volumes do a good job of covering particle acceleration, focusing, and beam maintenance.